RECLAMATION

Managing Water in the West

Hydraulic Laboratory Report HL-2004-04

Hydraulic Model Study of the Enlarged Outlets at Folsom Dam

1:17 Scale Sectional Model

U.S. Department of the Interior
Bureau of Reclamation
Technical Service Center
Water Resources Research Laboratory
Denver, Colorado

December 2004

REPORT DOCUMENTATION PAGE

Form Approved
OMB No. 0704-0188

PLEASE DO NOT RETURN YOUR FORM TO THE ABOVE ADDRESS.

1. REPORT DATE *(DD-MM-YYYY)*	2. REPORT TYPE	3. DATES COVERED *(From - To)*
28-12-2004	Technical	Jan - Dec 2004

4. TITLE AND SUBTITLE

Hydraulic Model Study of the Enlarged Outlets at Folsom Dam: 1:17 Scale Sectional Model

5a. CONTRACT NUMBER

5b. GRANT NUMBER

5c. PROGRAM ELEMENT NUMBER

6. AUTHOR(S)

Frizell, K. Warren

5d. PROJECT NUMBER

5e. TASK NUMBER

5f. WORK UNIT NUMBER

7. PERFORMING ORGANIZATION NAME(S) AND ADDRESS(ES)

U.S. Department of the Interior, Bureau of Reclamation
Water Resources Research Laboratory
PO Box 25007
Denver, CO 80225

8. PERFORMING ORGANIZATION REPORT NUMBER

HL-2004-04

9. SPONSORING/MONITORING AGENCY NAME(S) AND ADDRESS(ES)

Corps of Engineers
Sacramento District

10. SPONSOR/MONITOR'S ACRONYM(S)

11. SPONSOR/MONITOR'S REPORT NUMBER(S)

12. DISTRIBUTION/AVAILABILITY STATEMENT

Available from:
National Technical Information Service, Operations Division, 5285 Port Royal Road, Springfield, Virginia 22161
http://www.ntis.gov

13. SUPPLEMENTARY NOTES

Prepared in cooperation with the U.S. Army Corps of Engineers, Sacramento District.

14. ABSTRACT

A 1:17 scale physical sectional model of the enlarged outlet works at Folsom Dam was built and tested at Reclamation's Water Resources Research Laboratory in Denver Colorado. This model featured detailed representations of the upper (9.33-ft by 14-ft) and lower (9.33-ft by 12-ft) enlarged gate designs (by Reclamation) along with hydraulic features including air vents and manifolds, intakes and conduits for the new larger gates (by COE) a 50-ft-wide section of spillway, and an 85-ft-wide section of stilling basin (both exisiting).

15. SUBJECT TERMS

Folsom Dam, outlet works, high-pressure slide gates, cavitation, air venting, pressure coefficients, sectional model,

16. SECURITY CLASSIFICATION OF:			17. LIMITATION OF ABSTRACT	18. NUMBER OF PAGES	19a. NAME OF RESPONSIBLE PERSON
a. REPORT	b. ABSTRACT	c. THIS PAGE			Clifford A. Pugh
UL	UL	UL	SAR	80	19b. TELEPHONE NUMBER *(Include area code)* 303-445-2151

Hydraulic Laboratory Report HL-2004-04

Hydraulic Model Study of the Enlarged Outlets at Folsom Dam

1:17 Scale Sectional Model

K. Warren Frizell

U.S. Department of the Interior
Bureau of Reclamation
Technical Service Center
Water Resources Research Laboratory
Denver, Colorado

December 2004

Mission Statements

The mission of the Department of the Interior is to protect and provide access to our Nation's natural and cultural heritage and honor our trust responsibilities to Indian Tribes and our commitments to island communities.

The mission of the Bureau of Reclamation is to manage, develop, and protect water and related resources in an environmentally and economically sound manner in the interest of the American public.

Acknowledgments

Portions of laboratory testing were performed by Caroline Rees (LCA-1006), Connie DeMoyer (D-8560) and Jerry Fitzwater (D-8560). The principal craftsmen for the model construction were Neal Armstrong and Jason Black (D-8561). Technical review of this document was performed by the Hydraulic Design Team assembled by the Corps of Engineers and included: Robert Vrchoticky, Sacramento District COE, Charlie Mifkovic, Consultant for the COE, Henry Falvey, Consultant for the COE, and John Hite, Waterways Experiment Station, COE. Reclamation Peer review was performed by Clifford Pugh (D-8560).

Hydraulic Laboratory Reports

The Hydraulic Laboratory Report series is produced by the Bureau of Reclamation's Water Resources Research Laboratory (Mail Code D-8560), PO Box 25007, Denver, Colorado 80225-0007. At the time of publication, this report was also made available online at **http://www.usbr.gov/pmts/hydraulics_lab/pubs/HL/HL-2004-04.pdf**

Disclaimer

No warranty is expressed or implied regarding the usefulness or completeness of the information contained in this report. References to commercial products do not imply endorsement by the Bureau of Reclamation and may not be used for advertising or promotional purposes.

This work was funded by the Corps of Engineers, Sacramento District under a cooperative design process for the outlet works rehabilitation at Folsom Dam.

TABLE of CONTENTS

TABLE of FIGURES

1. Background.

Folsom Dam is on the American River about 20 miles northeast of Sacramento, California, figure 1. The dam was designed and built by the Corps of Engineers (COE) and transferred to Reclamation for operation and maintenance in 1956. The dam is a concrete gravity structure 340 ft high and impounds a reservoir of a little more than one million acre-ft.

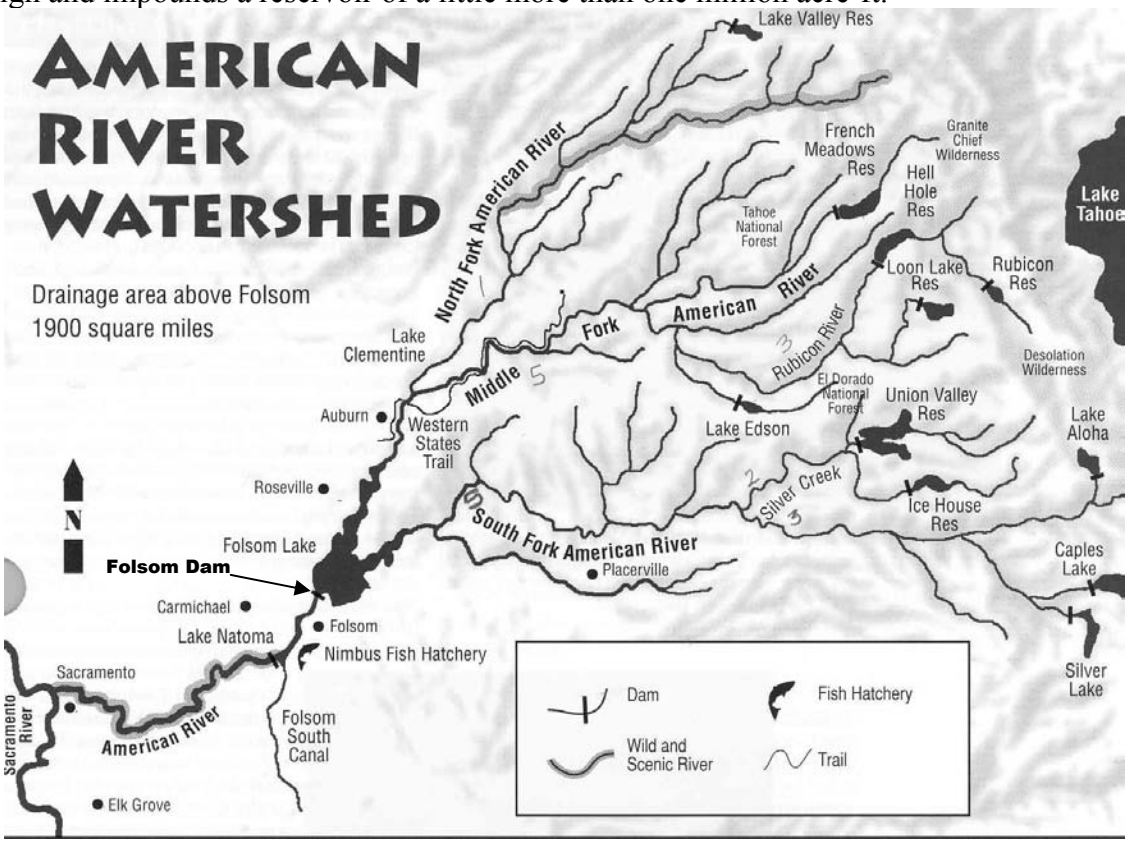

Figure 1: Location map of Folsom Dam with the American River watershed.

The dam features two tiers of four outlets each, controlled by 5- by 9-ft slide gates. The outlets consist of rectangular conduits of formed concrete passing through the dam and exiting on the face of the service spillway. As a result of legislation approved in 1999, the Corps of Engineers secured funding to begin studies and designs that include an enlargement of the outlets at Folsom Dam. The main design goal for the enlargement project is to provide a discharge capacity of 115,000 ft^3/s at a reservoir elevation of 418.0 ft (spillway crest elevation). A preliminary study showed that in order to provide this discharge with 8 gates, a uniform gate size of 9.33- by 16.25-ft was required. This enlargement was an increase in gate area of 237-percent. The significant increase in water discharge would also lead to an increase in the air demand. A new air intake manifold and delivery system would be required to provide adequate air to ensure cavitation-free operation and proper hydraulic performance. The enlarged outlets follow a similar profile to the present conduits, exiting on the face of the service spillway. To insure hydraulic performance, physical modeling of the improvements was conducted at the Bureau of Reclamation's Denver laboratory facilities in 2000-2001, Appendix A.

With the hydraulic model study nearing completion, additional studies indicated that the

9.33- by 16.25-ft size gates may not be entirely appropriate for installation at an existing dam with the particular features of Folsom Dam. In December 2001, a gate sizing study was completed recommending ten gates, 6 upper gates 9.33- ft by 14-ft, and 4 lower gates 9.33- ft by 12-ft. The two additional gates on the upper level would be constructed one each in Monoliths 12 and 17 and be placed at a skewed angle of 3.5 degrees so that the outlets exit very near each sidewall of the existing service spillway in the half-monoliths and are angled toward the center of the stilling basin. The skew is due to structural space requirements between the inlet and the monolith joint. The new gates that replace the existing lower tier gates will retain the same gate numbers and the upper gates will be numbered 5-10, from right to left looking downstream. The new arrangement was studied at Reclamation's Denver laboratory in two models. This report describes the testing of the 1:17 model, a section through the spillway encompassing one upper and one lower gate plus a section of the service spillway and stilling basin.

The primary objectives of the physical model study are to insure that 115,000 ft^3/s can be released through the outlet works at a reservoir elevation of 418 ft without producing damaging cavitation or undue surging in the outlets, that the air vents are functioning with subsonic flow, that combined outlet works and spillway releases can be made without outlet operating limitations, and that the stilling basin functions without damage.

2. Physical Hydraulic Model.

2.1 General.

A sectional Froude-based model at a scale of 1:17 provided design data for verification of discharge capacity, air demand, optimal conduit dimensions downstream from the gate, and most effective air delivery geometry. The model investigated the hydraulic losses and pressures associated with the new bell mouth entrance and the performance of the eyebrow flow deflector over each of the outlet openings. In addition, pressure forces in the stilling basin were investigated. Figure 2 shows a plan view with the extents of the model overlaid on the full spillway.

The model used the existing head box from the previous modeling of the 9.33- ft by-16.25 ft gates, capable of modeling reservoir elevations up to elevation 466.0 ft. A section of the dam including one upper and one lower level outlet along with two half-spillway bays was included. The outlets exit onto the spillway chute that terminates in the stilling basin. An expanded width of stilling basin was modeled due to the difficulties with maintaining tailwater elevations in the previous model. Tailwater levels were adjusted with variable width slats at the downstream end of the model, just downstream of the stilling basin endsill. Several features of the model were constructed of clear acrylic or clear PVC to enable good visualization. These included: the intake bell mouths, the outlet conduits and gate frames, the air vent piping and manifold, one sidewall of the spillway and one side of the stilling basin wall. Other features of the model were constructed from marine-grade plywood, high-density polyurethane foam (spillway crest and

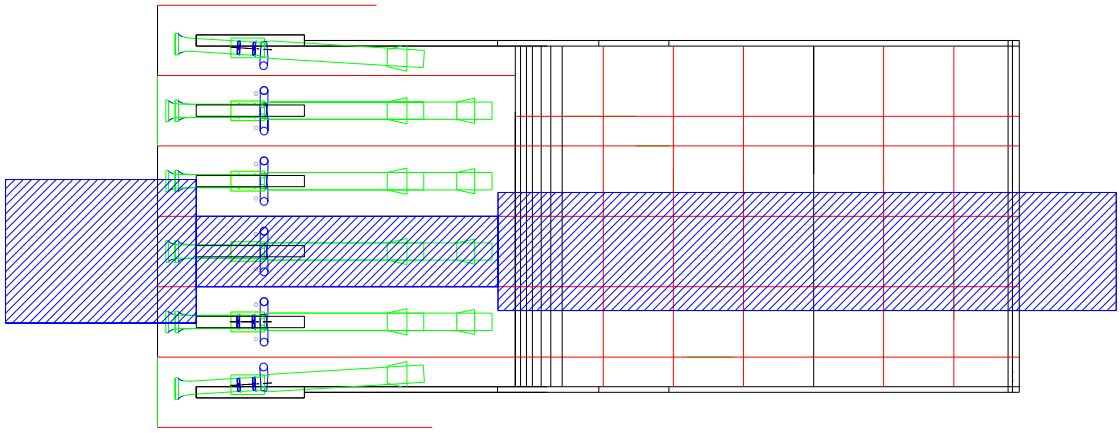

Figure 2: Plan view showing the sectional model extents overlaid on the spillway and stilling basin. 1:17 model bounds are shown in hatched blue.

piers), and aluminum. Piezometer taps were located on the bell mouth entrance surfaces and at numerous locations on the outlet conduits and gate frames. Water columns and/or pressure transducers were used to measure pressures. Pressures were also measured along the centerline of the stilling basin section with tailwater elevations determined near the exit of the box. Calibrated venturi meters measured water discharges to the model. These meters are indicated by a mercury manometer and are generally within about 0.25-percent of the actual flow over the full range of the meter. Air discharges were measured with a thermal anemometer that was traversed through the vent piping. One hundred readings were collected over the period of about 1 min to attain the average point values at 5 locations across the pipe diameter. These average point readings were then averaged and combined with the vent area to compute an average air discharge. Meter readings were adjusted for actual barometric pressure. A section of the model is shown in figure 3.

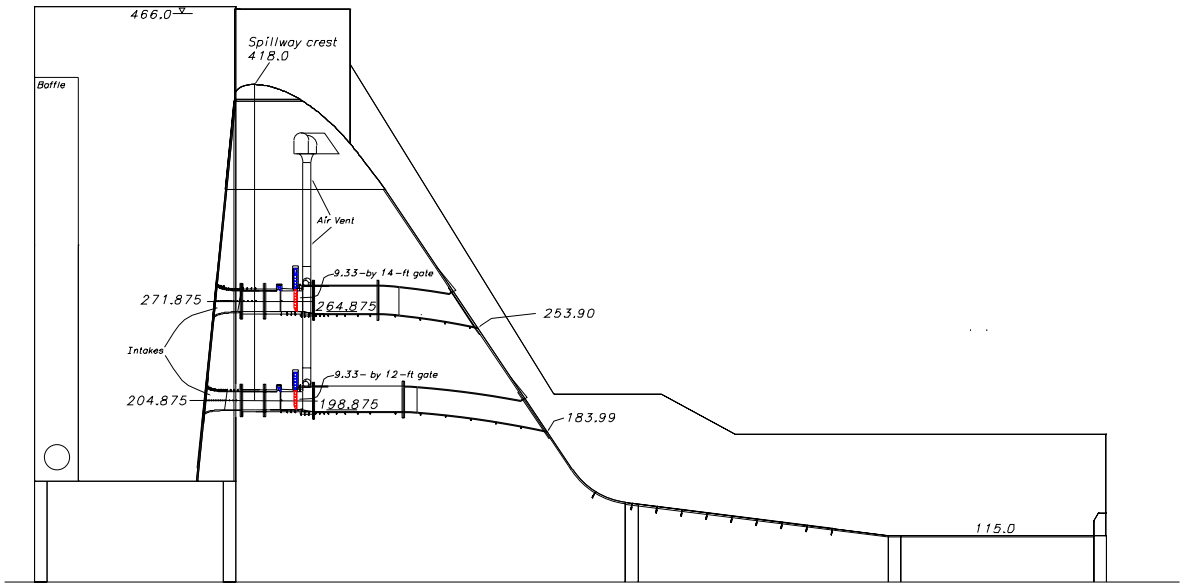

Figure 3: Sectional view of the 1:17 scale model features, model slide gates in red.

2.2 Similitude.

This structure represents a complex modeling challenge, as there are free surface flows, pressurized flows, and airflows to simulate. Hydraulic models are typically built following scaling laws based on the importance of certain dominating forces in the type of flows that are present. In the case for the outlet flows at Folsom Dam, gravitational, viscous, and surface tension forces are all important to correctly predict information critical to the design. Typically scaling is accomplished by evaluating dimensionless parameters developed by ratioing the inertial forces to the force important in the simulation, mentioned previously. It is not possible to perfectly satisfy Froude, Reynolds, and Weber number scaling concurrently in the model/prototype when using water as the modeling fluid, so experience must be used to properly select the model scale. The basic similitude is based on equal Froude numbers in the model and the prototype. This scaling equates the Froude numbers in the model and prototype, equation 1.

$$\frac{V_m}{\sqrt{g_m L_m}} = \frac{V_p}{\sqrt{g_p L_p}} \quad (1)$$

where: V is velocity
g is the gravitational constant
L is a length scale
m and p are model and prototype respectively.

Froude scaling is generally used where gravitational forces are important, as in most free surface flows. Typically Reynolds scaling would be used in pressure conduits, such as the sections from intake leading up to the gate. Although satisfying both Froude and Reynolds scaling is not possible for this study, previous modeling experience provides guidelines concluding that the viscous forces will not be important as long as the Reynolds number in the model is greater than some minimum criteria, eq. 2.

$$R = \frac{VL}{\nu} \quad (2)$$

where: ν is the kinematic viscosity
L is the equivalent diameter.

This minimum value generally is considered to be the minimum Reynolds number for fully turbulent flow. In terms of local velocity and depth or thickness, this value is somewhere on the order of 10^5 (Wood 1991). Some researchers have shown that the scale effects due to Reynolds number effects may exist well past this minimum value for certain phenomena, so some care is still required in interpretation of data. Most of the flows of interest in this study will have a model Reynolds number greater than 10^6 and with the short lengths of closed conduit, friction losses should be relatively unimportant.

Similitude of air demand is dependent on the ability of the model flows to overcome surface tension effects. The Weber number (eq. 3) is the parameter that has been used to relate model to prototype performance of air demands.

$$W = \frac{\rho V^2 L}{S} \quad (3)$$

where: ρ is the liquid density,
S is the surface tension coefficient (air and water)
L is the trajectory length.

Pinto (1982) has shown that scale effects are minimized in modeling spillway aeration slots when the Weber number based on a computed jet length is ≥ 500. Speerli (1999) has shown a similar value for use in predicting aeration in bottom outlets. At the 1:17 scale, the Weber number is greater than 500 for the entire range of gate openings, including openings as low as 0.25 ft.

Predicted design discharges in the model were 9.84 ft^3/s for the lower level outlet at elevation 418.0 ft, and 9.54 ft^3/s for the upper level outlet at elevation 418.0 ft, yielding a combined

discharge of 19.38 ft^3/s. This corresponds to a prototype release of 23,095 ft^3/s for the model and represents a total prototype release of 115,100 ft^3/s for all (10) the outlets.

3. Testing and Results.

3.1 Bell Mouth Intakes.

Initially the goal of the model testing was to finalize components of the flow passage geometry such that additional design work could proceed. This included evaluation of the compound elliptical entrance curves. The combined elliptical curves should have a lower cavitation potential than the simple ellipses that were tested in the first model (figure 4 and Appendix A). Data collected previously indicated that there was a possibility for cavitation to occur in the lower outlets at full open conditions and high reservoir heads. The design goal for the new intake curves is that they should allow for unrestricted use of the outlets under all conditions. In order to further investigate cavitation potential, maximum gate openings were evaluated for pool elevations of 418 and 466 ft as well as for some random gate openings and pool elevations. Data were taken for single outlet releases and dual outlet releases. Pressure data was collected using piezometers (0.0625 in diameter) along the top centerline and side centerline (see Appendix B for locations) as well as at a couple locations near the top corner, in order to confirm the shape of the pressure coefficient curve. The piezometers were connected to the same pressure transducer used to measure the reservoir elevation, so a simple subtraction made it possible to measure and calculate the head drop. This transducer was a Sensotec Model GM, differential pressure cell with a 10 lb/in^2 range (see Appendix B for calibration information and uncertainty estimates).

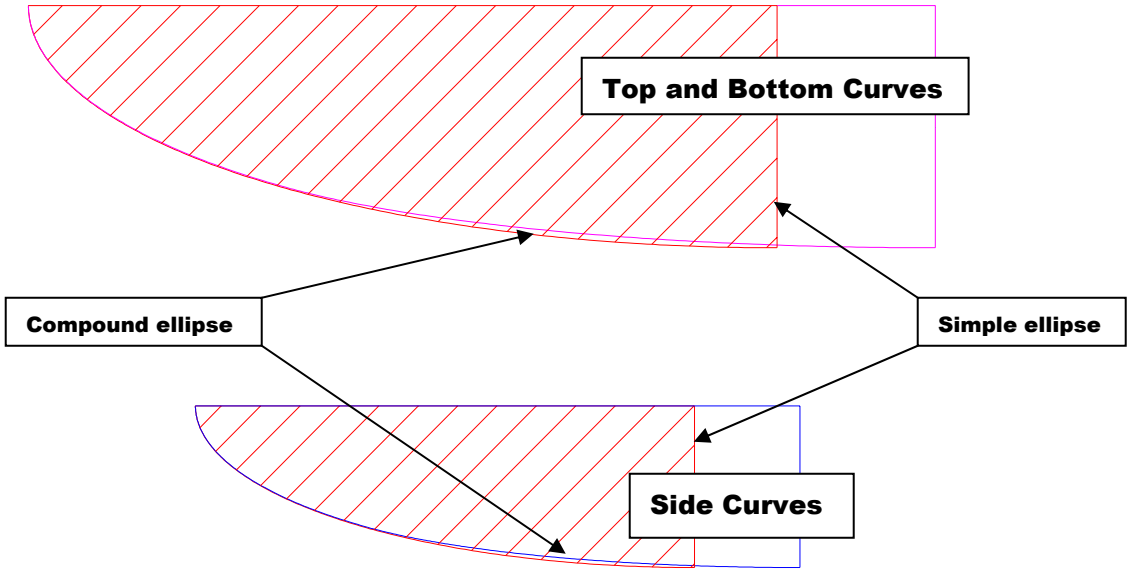

Figure 4: Comparison between the simple ellipse and the combined elliptical curves.

The parameter of interest in these tests is the pressure drop coefficient *C*, defined in the Corps of Engineer's (COE) Hydraulic Design Criteria. This coefficient is given by equation 4.

$$C = \frac{H_D}{\left(\frac{\overline{V}^2}{2g}\right)} \tag{4}$$

where: H_D is the head drop from the pool
$\overline{V}$ is the mean velocity in the conduit, d.s. from the intake.

The data are presented for the upper and lower tiers in the form of this pressure drop coefficient versus a dimensionless length ratio *L/D* where *L* is the distance along the conduit and *D* is the dimension of the conduit in the direction concerned. Results are shown in figure 5a and 5b.

This pressure drop coefficient can be used to assist in the evaluation of the cavitation potential of the inlet curves. We can look at the dimensionless form of the Bernoulli equation to derive the pressure coefficient (also known as the Euler Number),

$$C_p = \frac{P - P_o}{\rho V_o^{\,2} / 2}, \tag{5}$$

where: P is the pressure along the surface
P_o is a reference pressure
ρ is the water density
V_o is a reference velocity.

This parameter is very similar to the pressure drop coefficient defined in equation 4. The value of this parameter is constant at any point along a streamlined boundary as long as the minimum pressure on the boundary remains greater than vapor pressure. If we write Bernoulli's equation from the reservoir to the downstream conduit, eq. 6,

$$H_{res} = (1 + K_e)\frac{V^2}{2g} + \frac{P_o}{\gamma} \tag{6}$$

where: K_e is the inlet loss coefficient (0.02 for the Folsom Inlet).

With a couple of substitutions, we can get

$$C_p = (1 + K_e) - C \tag{7}$$

If the pressure at the location of the minimum Euler number drops to vapor pressure, then the pressure at that point cannot decrease any further. By replacing the surface pressure in equation 5 with the vapor pressure, this new expression defines the reference conditions that will correspond to the onset of cavitation. The resulting parameter is called the cavitation index,

$$\sigma = \frac{P_o - P_v}{\rho V_o^2 / 2} \tag{8}$$

where: P_o is a reference pressure
P_v is the vapor pressure of water
ρ is the density of water
V_o is the reference velocity.

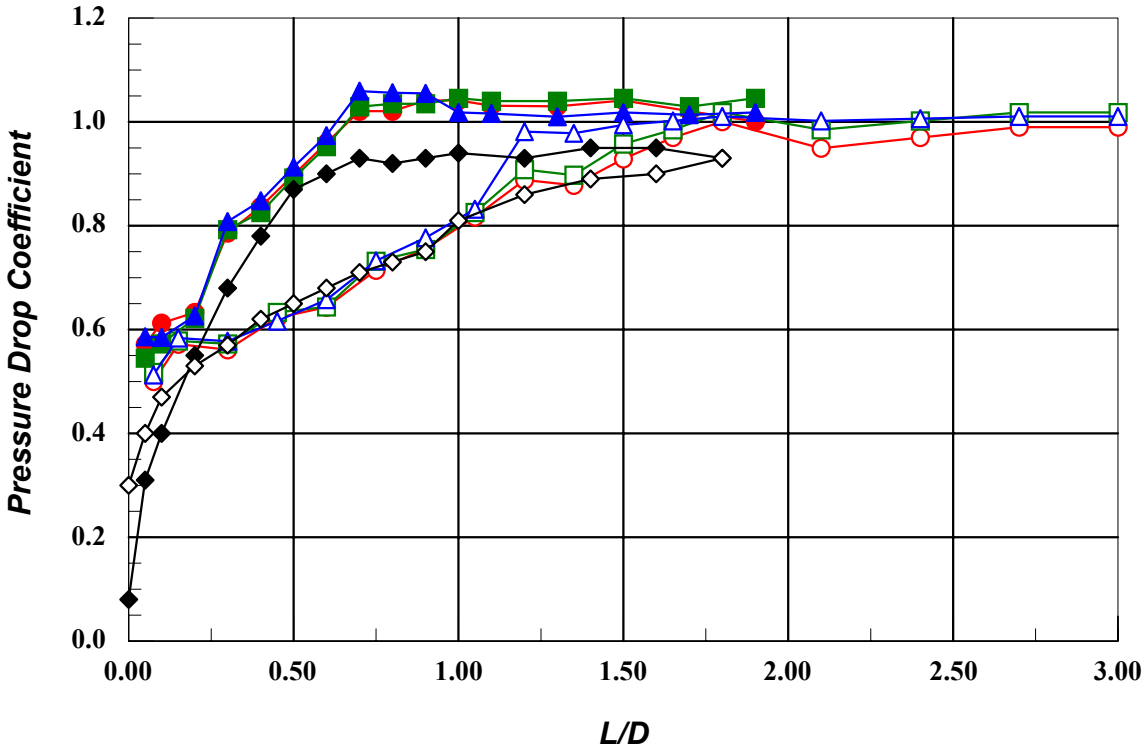

(a) Upper Tier

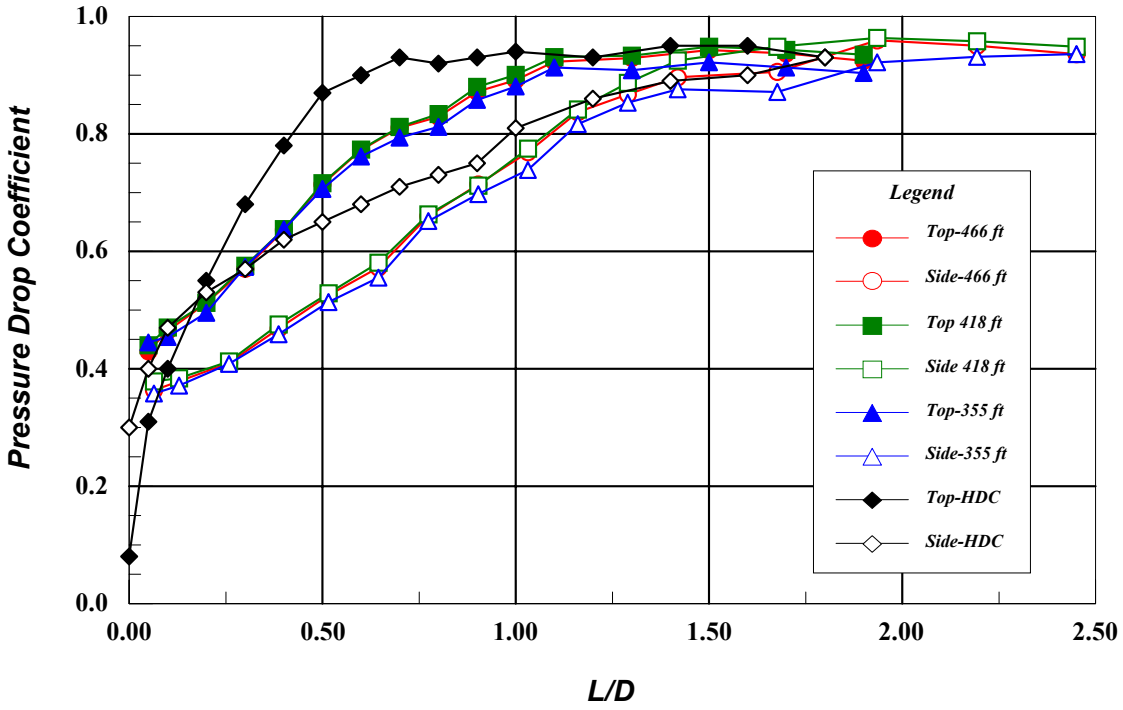

(b) Lower Tier

Figure 5: Pressure drop coefficient for intake bell mouth combined elliptical curves. Legend refers to both a and b.

The above treatment results in $\sigma = -(C_p)_{min}$ (eq. 8 = -[eq. 5]). You can then use pressure measurements taken along the surface to predict whether cavitation will be present. If we use the reservoir elevation as the reference pressure and the velocity in the conduit downstream from the inlet as the reference velocity, we can calculate the cavitation index based on the average pressure drop coefficient measured in the model (figs. 5 a & b). If the value of these flow-based sigmas drops below the value of the pressure coefficient, then cavitation inception will occur at that location along the curve. This technique was used to develop figures 6a and 6b. The figures show that the sigma values never approach the $-C_{pmin}$ values; hence no cavitation is to be expected through any of the operating conditions for the shape alone. Application of the superposition principle should allow designers to adopt finish criteria such that cavitation will not occur. Henry Falvey performed analyses to look at cavitation due to singular irregularities within the intake curves, i.e. joint or form offsets, holes, etc. He used the data from the model as well as the velocity predictions from the mathematical model (Flow-3D) to apply the superposition principle and assess the cavitation potential in the inlets.

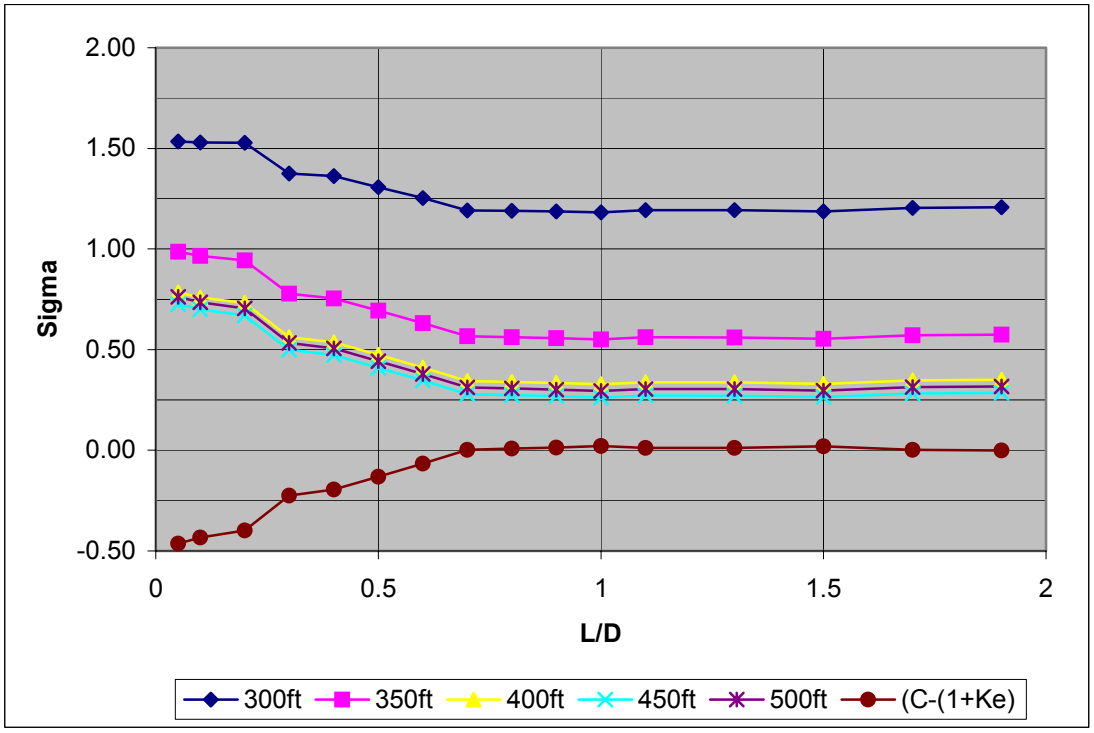

a) Upper conduit, cavitation index and -C_{pmin}.

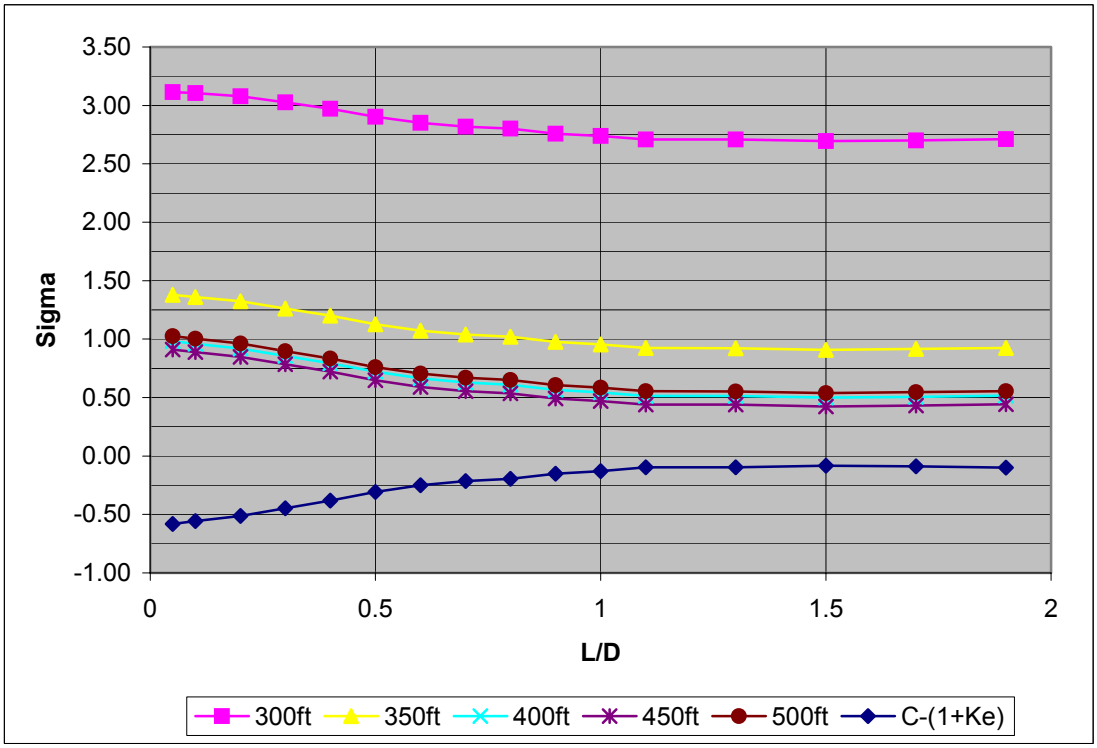

b) Lower conduit, cavitation index and -C_{pmin}.

Figure 6: Cavitation index for a range of head conditions at full gate.

The two new upper outlets while of a similar size to the others, have a skewed alignment, 3.5-degrees angled in toward the center line of the stilling basin. There has been some concern that even though the model results did not show problems with the straight intakes, these skewed intakes have a tighter radius curve on the inner side curves, and also present a compound angle when interfaced with the sloping dam face at the entrance. Results from the 1:36 model (in progress) have not shown any reason for alarm, however there has been discussion regarding the relative accuracy of these measurements and whether the error bands for the model results would be wide enough to result in possible problems. Due to these reasons, we initiated a 3-dimensional computer model of the intake area only. The idea being that if we could get good agreement on the pressure drop coefficient data for a straight entrance between the 1:17 model and the computer model, then we would have the confidence to accept the computer model results for the skewed intake and forego any further physical model testing.

3.1.1 3-Dimensional Hydrodynamic Model.

Computational fluid dynamics is becoming more commonplace for standalone solutions and in support of physical modeling measurements. There are a number of commercially available codes for use on a variety of hydraulic-related problems. Reclamation's Water Resources Research Lab is currently using FLOW-3D® by Flow Science, Inc. FLOW-3D® is a finite difference, free surface, transient flow modeling system that was developed to solve the Navier-Stokes equations, in three spatial dimensions.

The finite difference equations are based on a fixed Eulerian mesh of non-uniform rectangular control volumes using the Fractional Area/Volume (FAVOR) method. Free surfaces and material interfaces are defined by a fractional volume-of-fluid (VOF) function. FLOW-3D® uses an orthogonal coordinate system as opposed to a body-fitted system.

Geometry was input into FLOW-3D® using a stereo lithography file generated from AutoCad, figure 7. Input to the computer model included the full gate flow for a reservoir elevation of 465 ft. Several iterations of the problems were run, each one at an increased mesh density. In addition to making the grid finer, adjustments were also made to the original stereo lithography file, making the flow surfaces less faceted and smoother. FLOW-3D® supports nested grids and that feature was used in these problems. In the straight conduits, the areas farthest away from the intake were meshed with a spacing of about 1.6 ft, resulting in 645,120 cells. The inner mesh had a spacing of about 0.8 ft and 517,888 cells. The final run took just under 47 hours of CPU time. The skewed intake was run at a slightly tighter mesh. The outer mesh spacing was about 0.8 ft for a total of 1,730,560 cells while the inner mesh spacing was 0.4 ft, resulting in 1,340,416 cells. The computational time for the final run of the skewed intake took almost 245 hours of CPU time.

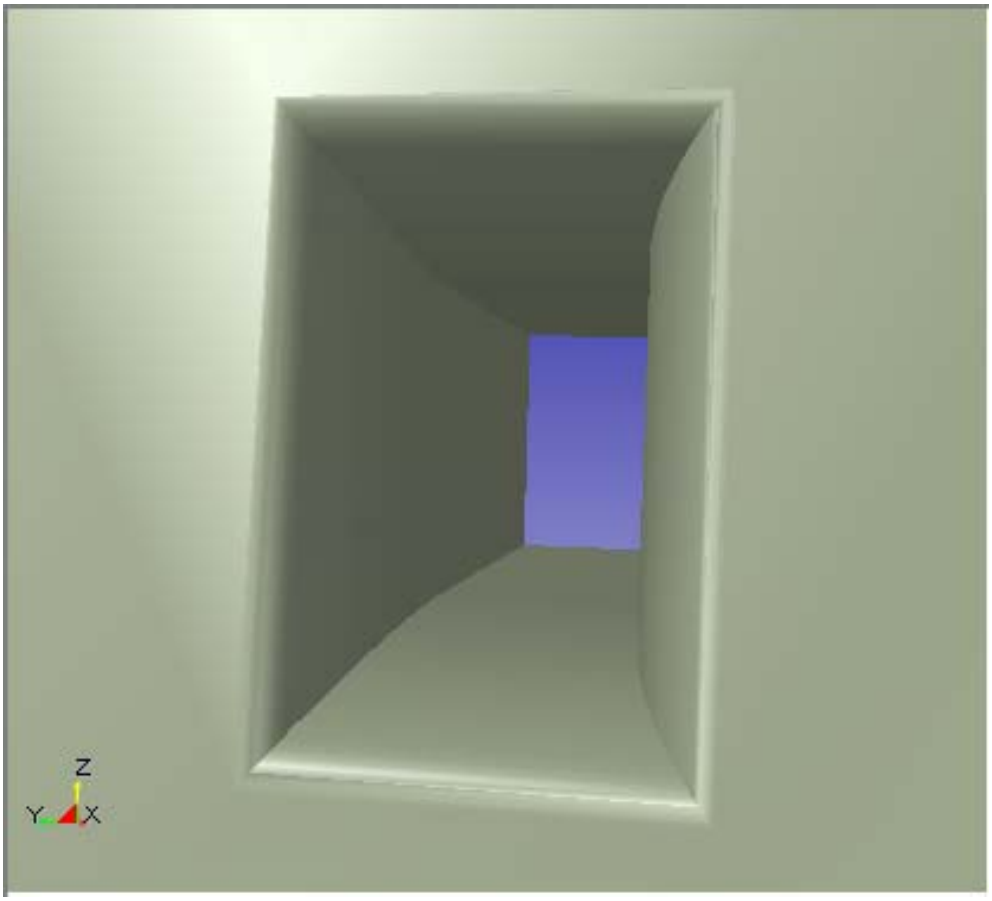

Figure 7: Stereo lithography solid generated by AutoCad, used to input geometry into Flow-3D.

Each of the models included free surface, renormalized group model for turbulence, wall shear, monotonicity preserving, second order advection, and line implicit successive over relaxation in the x, y and z directions. Figure 8 shows 2D planar velocity contours for the straight intake.

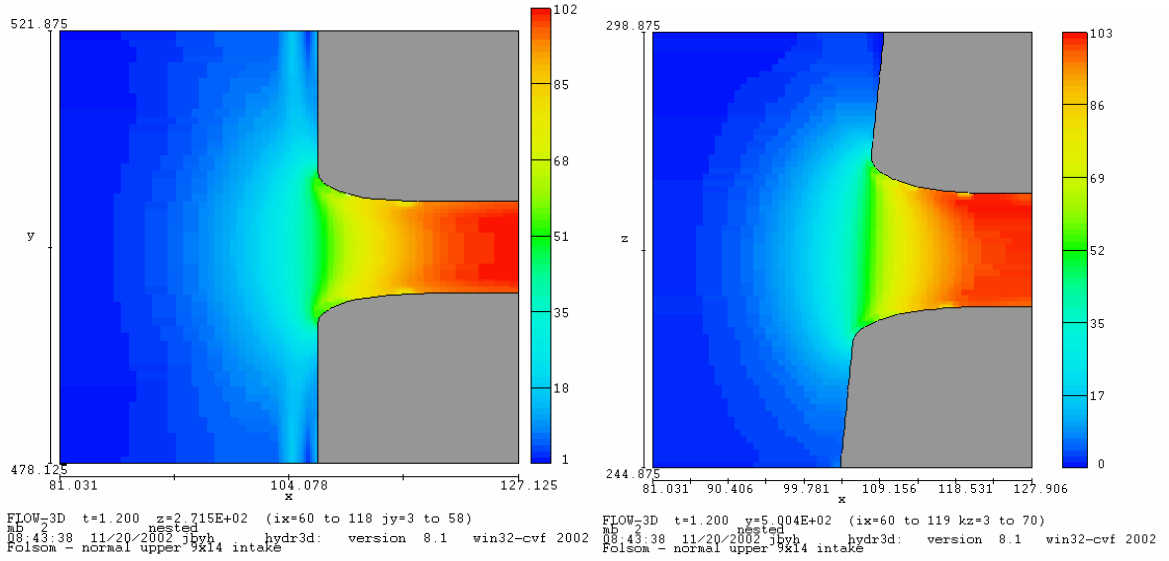

Figure 8: 2D planar velocity slices for an upper straight outlet full open at res. elevation 465 ft.

In order to get surface pressures along the intake, probe locations are input into the model that corresponded to the piezometer locations in the physical model. At the end of the run, the steady-state pressures are output and then the pressure drop coefficient can be calculated, figure 9.

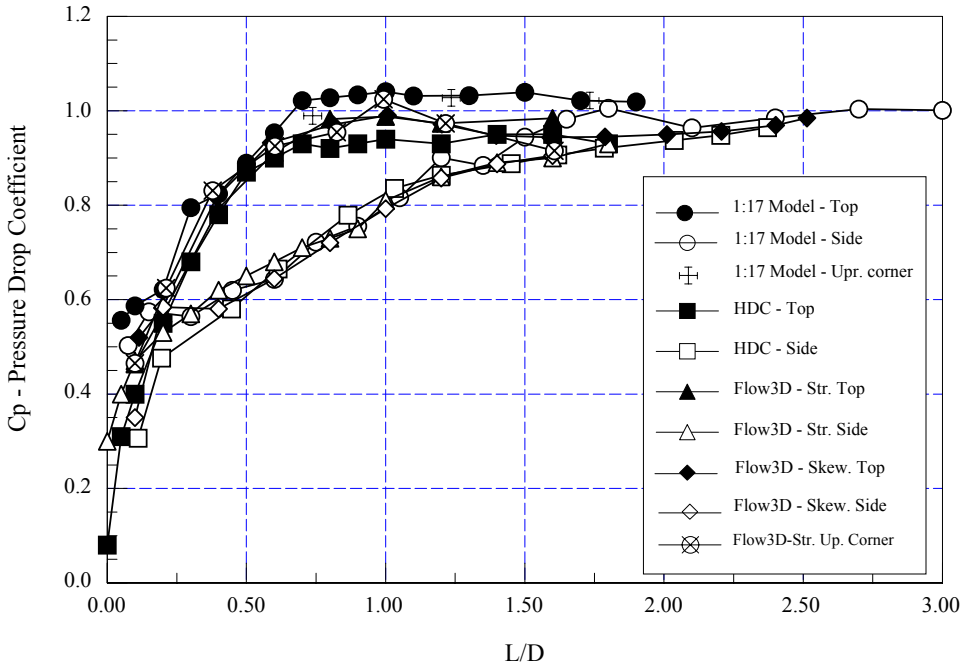

Figure 9: Comparison between 1:17 model data, Flow-3D results, and the COE Hydraulic Design Criteria data for pressure drop coefficients on a combined elliptical intake.

The agreement between the 1:17 physical model results and the Flow-3D output was very good for the straight intakes. This good agreement instilled confidence to accept the data from the computer model for the skewed intake design as well. The input data file for Flow-3D is included in Appendix C.

3.2 Flow surfaces downstream from gate.

Developing flow geometry downstream from the gate was also a critical step. The initial design contained shallow angle ramps just downstream from the regulating gate based on results from the study of the 9.33- by 16.25-ft gates. Those initial studies showed a discharge reduction due to these ramps. In order to evaluate the effects of the ramps on water and air discharges as well as overall hydraulic performance, conditions with no ramps, floor ramp only, and floor and sidewall ramps were tested at gate openings of 20-, 60-, and 100-percent for both the upper and lower regulating gate. Figure 10 shows a sketch of the ramps. In addition, it is possible to retract the gate an additional 2.5 in, even with the crown elevation on the downstream side of the bonnet. This opening will be referred to as 102% throughout this document. Discharge, airflow through the vents, and pressures downstream from the gates were collected for each gate opening. The previous model had a sudden offset of 1.5 ft on the invert and sidewalls downstream of the gates. However, structural concerns related to gate anchorage required the use of a structural wedge to form the offset rather than a sudden offset. The structural wedges are

offset 2 inches below the gate invert and 3.5 inches on the sidewalls and are installed over a length of 7.5 ft. yielding a total offset at the end of the wedges of 1.5 ft from the upstream conduit surfaces. Tests were conducted at pool elevation 418 feet for gate openings of 20-, 60- and 100-percent. Data from the no ramp condition is shown in table 1 and figure 11. A 3-inch high, 3.7 ft long, floor ramp was then added directly downstream from the gate and identical measurements were collected, Table 2 and figure 12. Finally 1.5-inch-high by 3.7-ft-long sidewall ramps were added and the measurements repeated, Table 3 and figure 13. Each of the figures features four graphs, (a) the upper tier alone, (b) the lower tier alone, (c) the upper tier data with both upper and lower conduits operating, and (d) the lower tier data with both conduits operating.

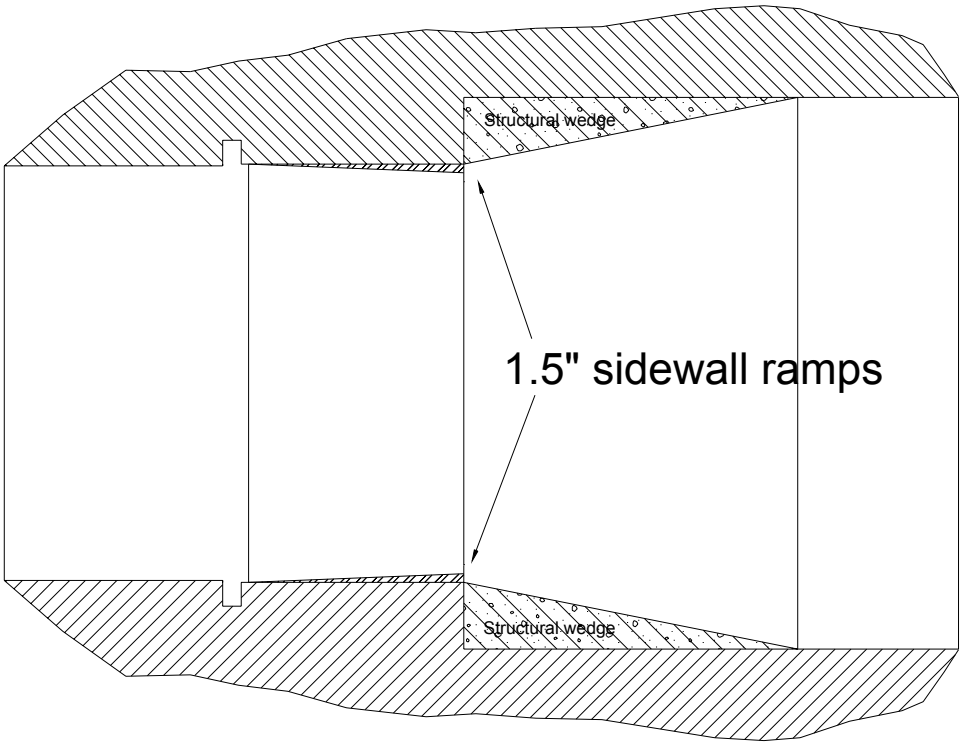

Sketch of sidewall ramps

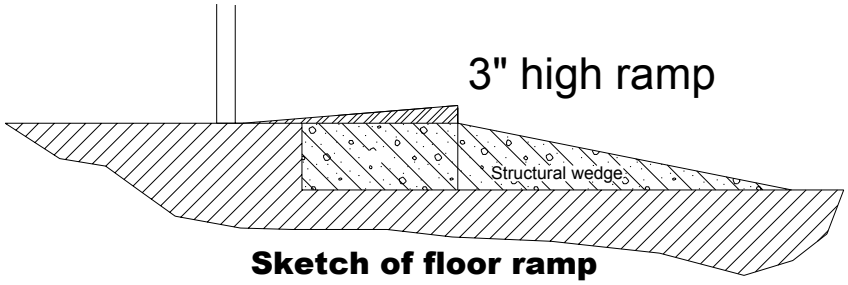

Sketch of floor ramp

Figure 10: Initial ramp design for downstream of regulating gates.

Table 1: Water and air discharge for the no ramp condition

Gate (percent)	Lower Q_w (ft^3/s)	Lower Q_a (ft^3/s)	Lower β Q_a/Q_w	Upper Q_w (ft^3/s)	Upper Q_a (ft^3/s)	Upper β Q_a/Q_w

0	0	0	0	0	0	0
20	2015	1003	0.50	1997	755	0.38
60	5968	1643	0.28	5932	1079	0.18
100	11428	2615	0.23	11794	1806	0.15
102	12779	2984	0.23	12523	-	-

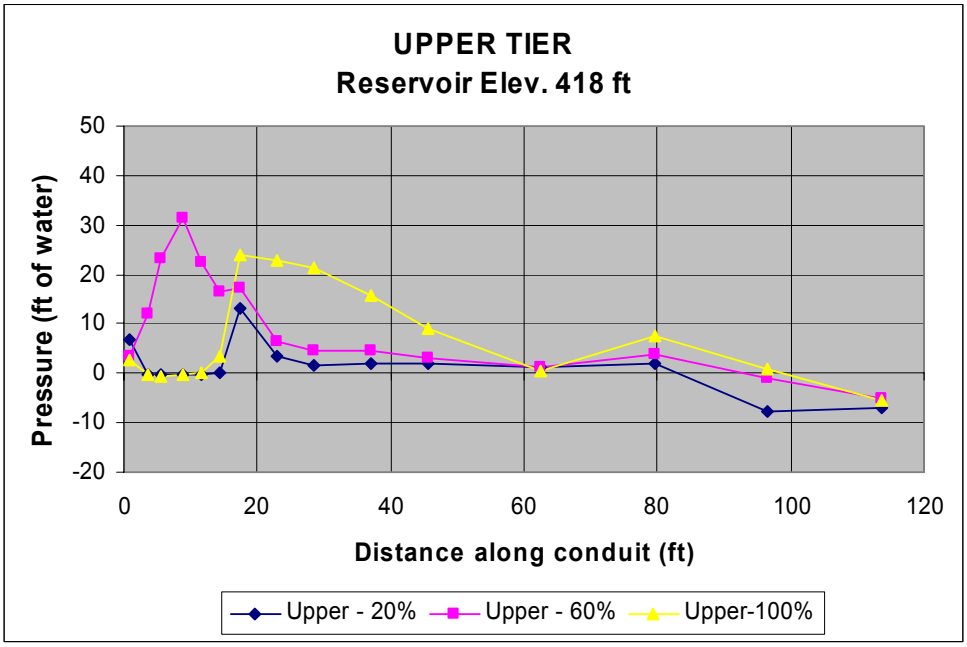

(a)

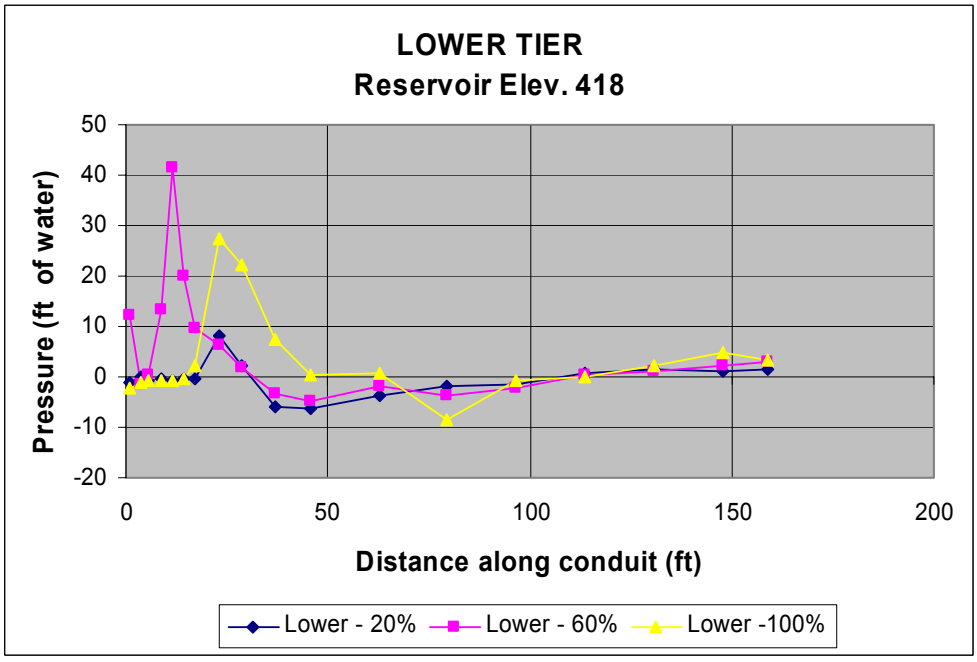

(b)

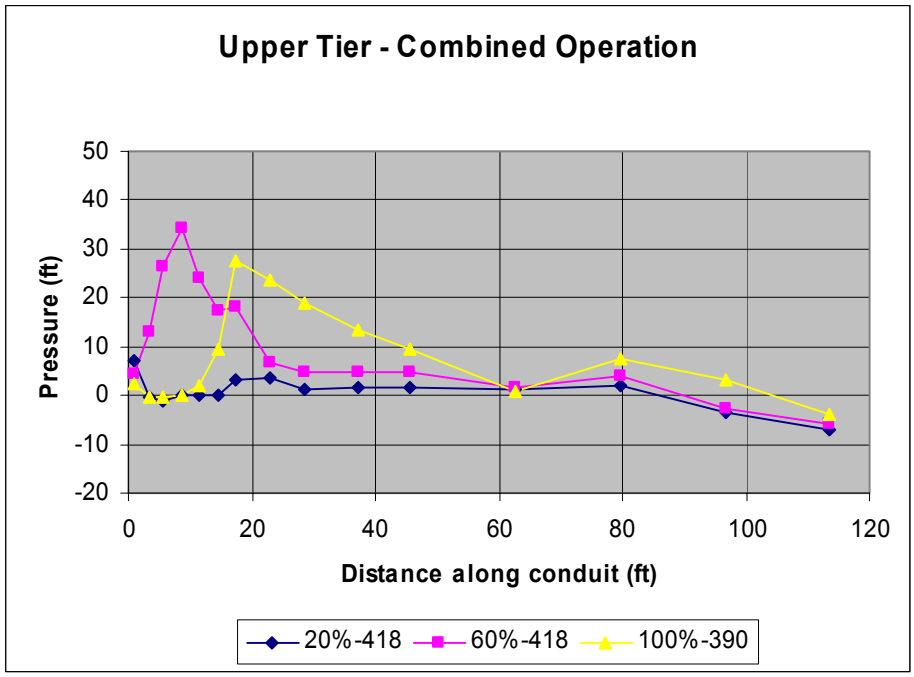

(c)

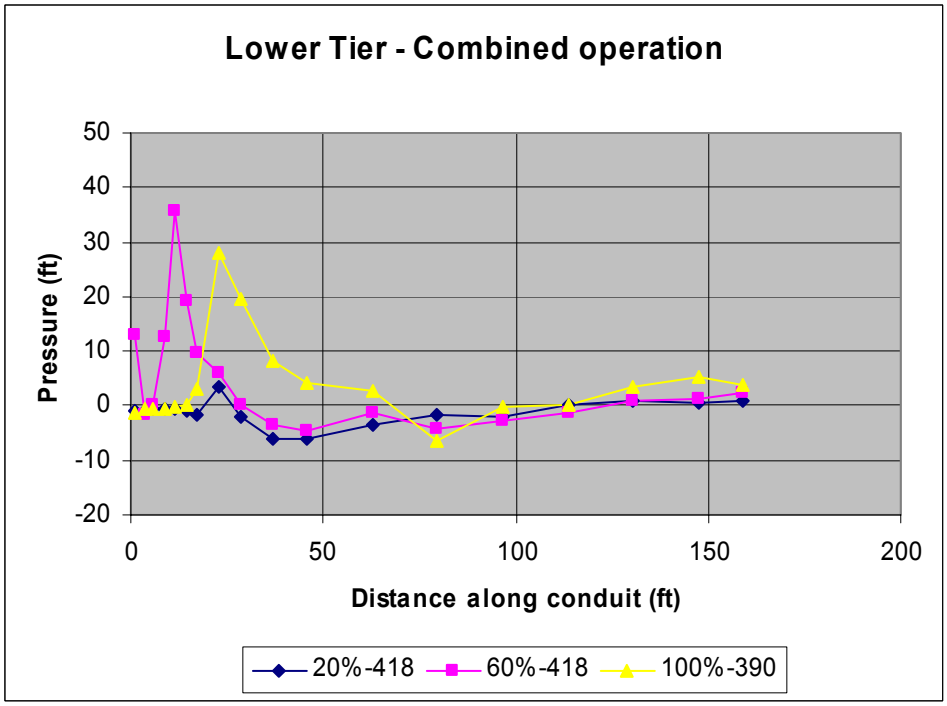

(d)

Figure 11: Pressures downstream from the regulating gate for the no ramp condition.

Table 2: Water and air discharge for the floor ramp only condition.

Gate (percent).	Lower Q_w (ft^3/s)	Lower Q_a (ft^3/s)	Lower β Q_a/Q_w	Upper Q_w (ft^3/s)	Upper Q_a (ft^3/s)	Upper β Q_a/Q_w
0	0	0	0	0	0	0
20	1934	1093	0.57	1961	975	0.50
60	5933	1295	0.22	5743	1029	0.18
100	11692	1907	0.16	11498	1289	0.11
102	12564	-	-	12133	-	-

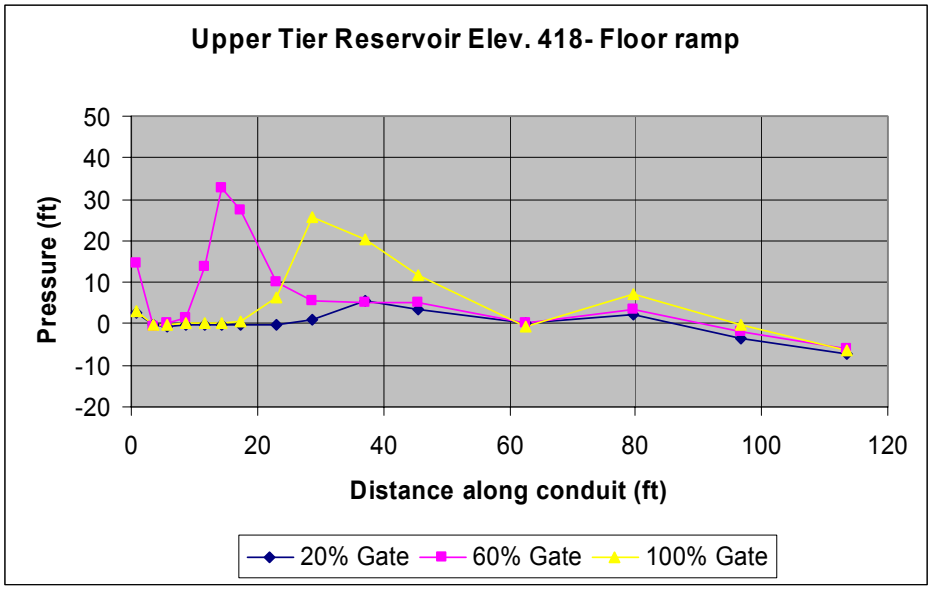

(a)

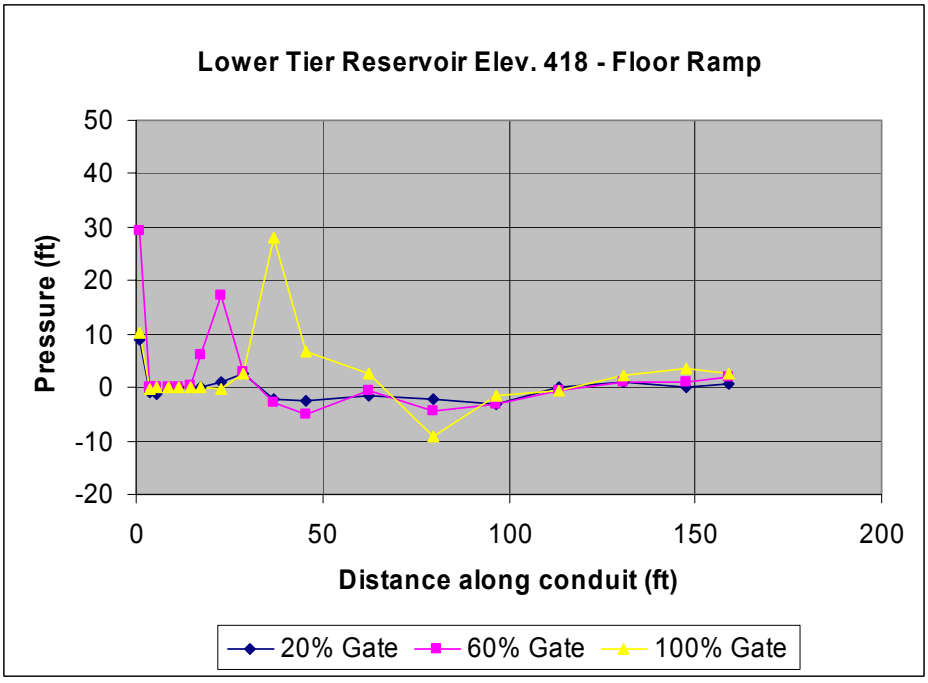

(b)

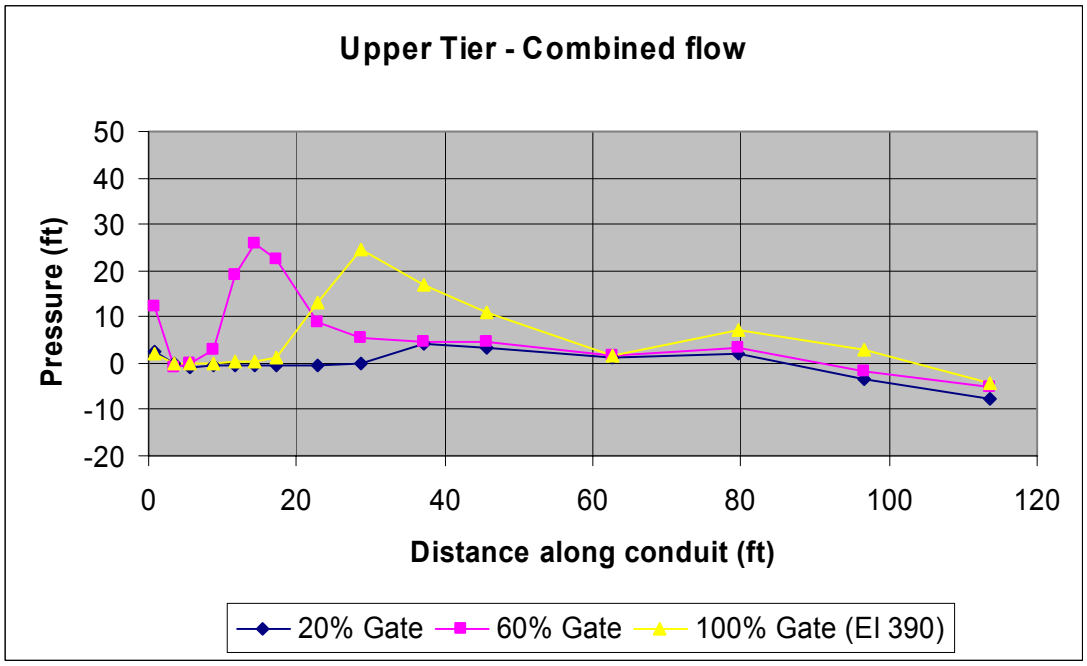

(c)

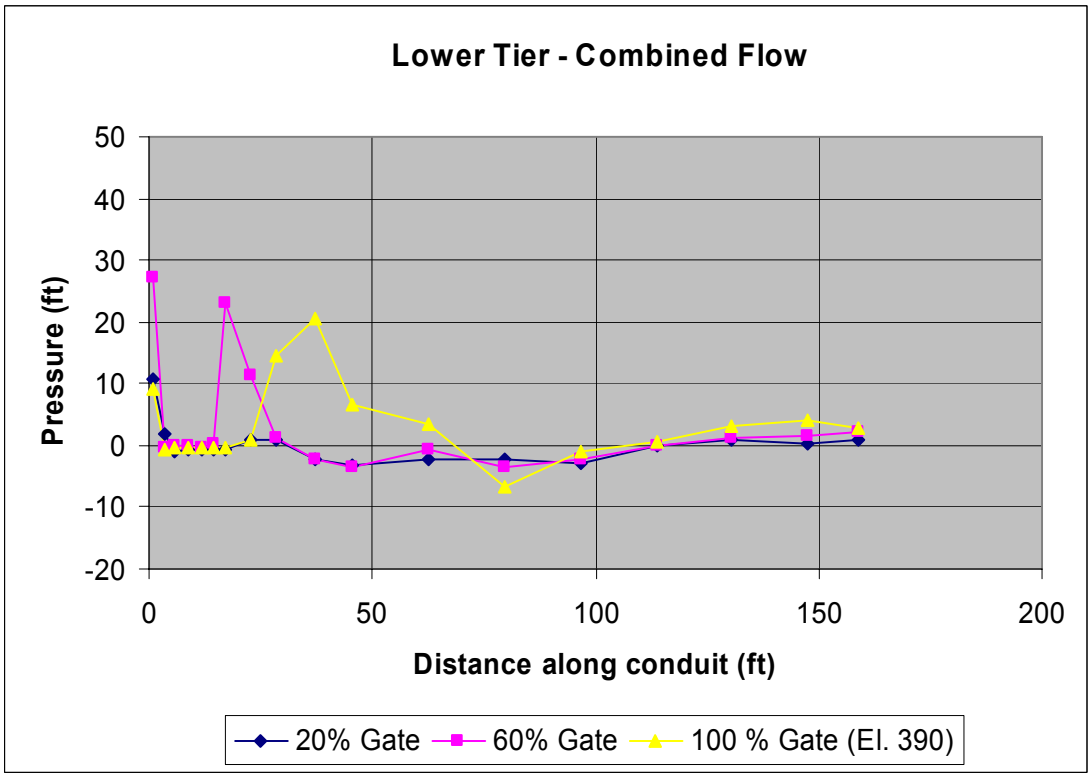

(d)

Figure 12: Pressures downstream from the regulating gate, floor ramp only condition.

Table 3: Water and air discharges for the floor and sidewall ramp condition.

Gate (percent)	Lower Q_w (ft^3/s)	Lower Q_a (ft^3/s)	Lower β Q_a/Q_w	Upper Q_w (ft^3/s)	Upper Q_a (ft^3/s)	Upper β Q_a/Q_w
0	0	0	0	0	0	0
20	1835	1132	0.62	1941	861	0.44
60	5739	1567	0.27	5758	1180	0.20
100	11356	3879	0.34	11396	2773	0.24
102	12267	4204	0.34	11902	2482	0.21

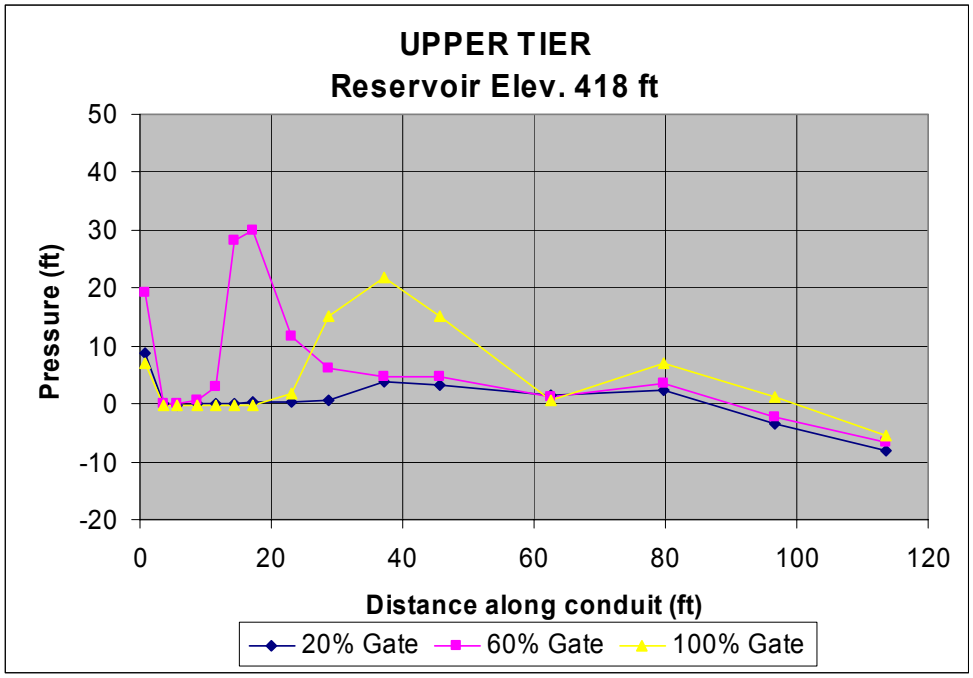

(a)

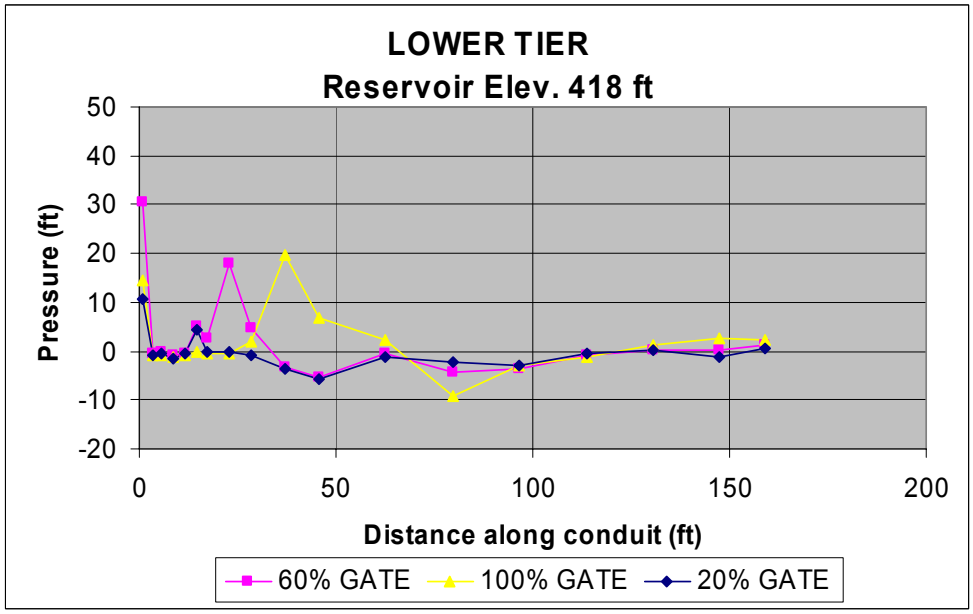

(b)

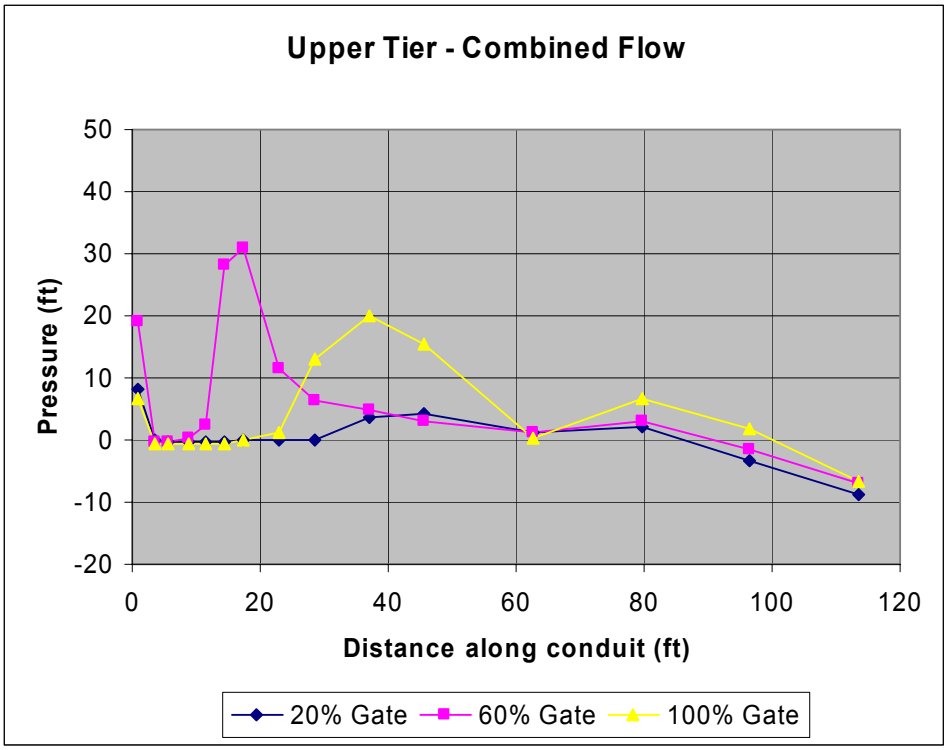

(c)

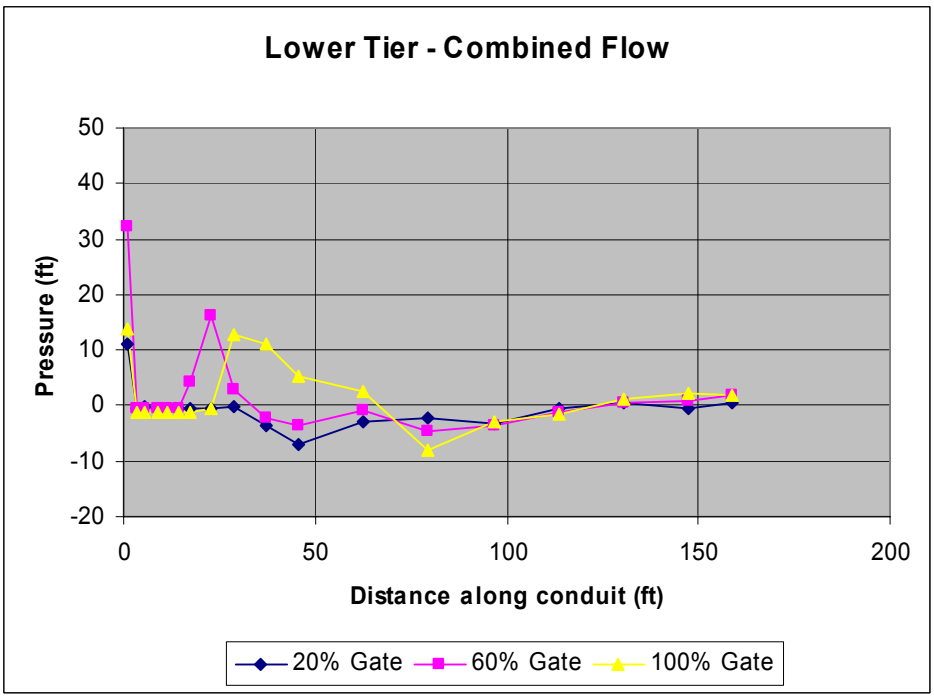

(d)

Figure 13: Pressures downstream from the regulating gate for the floor and sidewall ramp condition.

3.3 Vortex formation**.**

During the original study of the 9.33- by 16.25-ft gates, vortices were observed in both conduits under certain conditions. These vortices occurred at reasonably high reservoir heads and only formed with *full* gate openings. They would initially form and vent with air in the area downstream from the gate where the sides of the jet from the gate contacted the sidewalls of the conduit. Occasionally the vortex would travel upstream of the gate and sometimes all the way to the headbox. The vortex appeared very weak when it traveled into the headbox and would not travel up toward the water surface but would occasionally attach to the dam face or side wall of the headbox. The formation of these vortices was not fully understood but the small headbox size was figured to be a contributing factor, yielding increased asymmetric flow in the intakes resulting in increased vorticity.

Observations on the present model have been completed for the no ramp, floor ramp only, and floor + sidewall ramp conditions. Under all conditions, no vortex was observed in the lower tier outlet. However, in the upper tier, a similar vortex to that described in the previous study was observed. The vortex appears to originate downstream from the regulating gate, forming and venting with the free surface in the conduit. The vortex occasionally travels upstream from the gate but tends to be very consistent in the downstream conduit. Vortex formation generally occurred beginning at about reservoir elevation 330 ft continuing for the no ramp condition up to reservoir elevations above 425 ft. With installation of the floor ramp and sidewall ramps, no vortex activity was noticeable above reservoir elevation 410 ft. At no time did these vortices appear noticeable in the headbox. A set of radial flow vanes were constructed and placed in the headbox, see figure 14.

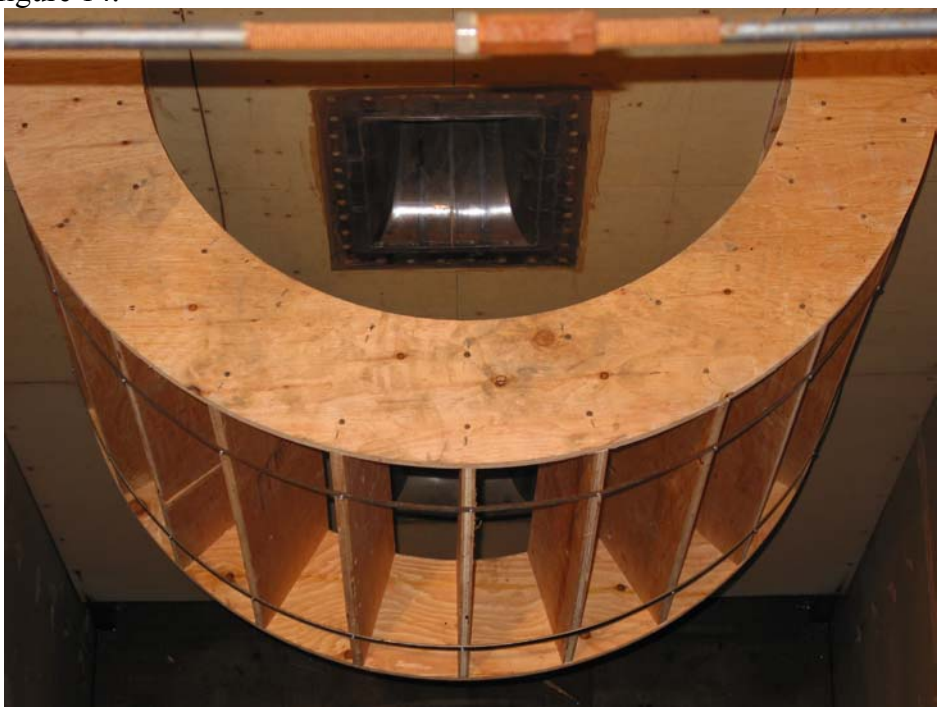

Figure 14: Radial straightening vanes installed in the model head box.

The placement of these vanes was an attempt to verify whether inlet flow conditions due to the

small headbox were influencing the vortex development. Tests were repeated with the flow vanes installed and no vortex formation was observed for the upper tier outlet for any head condition. Measurements of velocity with an acoustic Doppler velocimeter (ADV) were completed in the reservoir along the centerline of the upper intake for the conditions of having the radial vanes in place and removed. Although there were some differences, the resulting velocity fields did not clearly point to the conditions that would cause a vortex to form. At the velocity magnitudes present, very slight asymmetries were noted in the velocity distribution at the intake without the flow vanes. Maybe more importantly, increased turbulence and velocity fluctuations were present without the straightening vanes in place. It is also interesting that only a slight decrease in gate opening from the full position eliminates the visible vortex under all head conditions. This appears to be due to the change in the flow conditions downstream from the regulating gate in the area that the vortex gets its supply of air. While the circulation may still exist, its strength is not enough to maintain an air core.

In addition to the vortex described above, typical low submergence vortices are formed in the reservoir and occasionally pull air into the conduits when the crown of the conduit has only 5 to 10 ft of submergence. These vortices occur at these low submergence values for both upper and lower tier outlets. The reservoir conditions for the low submergence vortices in the lower intake were from 215 ft to 225 ft. In the upper intake, these reservoir conditions were from 284 ft to 295 ft.

3.4 Cavitation potential in outlet conduits.

Along with the concern over cavitation potential in the inlet curves, there are a couple of other areas that may have potential problems in the outlet conduits. The first area is the gate slots. The gate slots for both the guard gates and regulating gates are identical. They have a ***W/D*** of 0.66, figure 15. Both gates have the downstream conduit side walls offset 0.375 in from the upstream side walls. This offset is feathered back to the original dimension over the length between the guard gate and regulating gate (11 ft) and transitions into the sidewall aeration ramp downstream from the regulating gate. The upstream gate frame on the guard gate will extend about 7 ft upstream from the gate slot, there is 11 ft between gates, and the downstream gate frame will extend about 11 ft downstream from the regulating gate. This gate frame will incorporate all the ramps and wedges of the design within the steel-lined section.

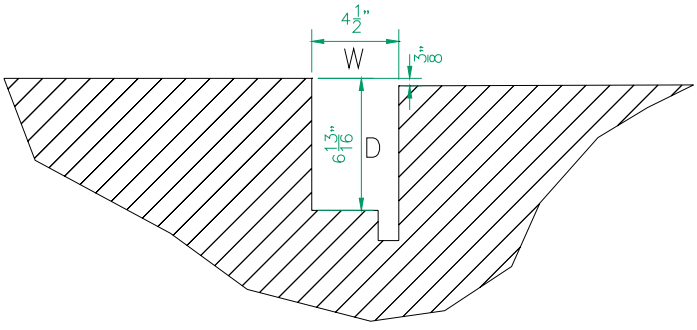

Figure 15: Cut away of gate slot showing W versus D.

Prior research on gate slot cavitation potential appears in Ball (1959), and the COE's

Hydraulic Design Criteria, Hydraulic Design Chart 212-1/2. Ball presents a chart that shows pressure characteristics for slots with offset downstream corners and constant rate converging downstream walls. Similar gate slot aspect ratios were tested (0.67); however the convergence of the downstream walls was more abrupt, at a 24:1 ratio (much less than the Folsom geometry, 350:1). Using the nomenclature of Ball, from data taken at a pressure tap on the centerline, 4.25 in downstream from the end of the gate slot, $(h_x - h_o)/h_v = -0.07$. Due to the slight differences in the convergence of the downstream sidewalls, we will choose this pressure coefficient to be -0.10. Evaluating the expression to find the reservoir elevation where minimum pressure downstream from the slot becomes subatmospheric quickly yields that it is not be possible with the expected conditions at Folsom. This was confirmed by the 1:17 scale model data, all data remained above atmospheric pressure for every case tested.

The cavitation potential along the invert flow surfaces in the outlets themselves can also be evaluated by calculating a flow sigma at the most negative pressures recorded. The lower conduit has a minimum pressure of about 14 ft below atmospheric pressure for a fully opened gate at reservoir elevation 466 ft. The mean velocity at this location is estimated to be about 90 ft/s, using visual observations of flow depth. This results in a flow sigma of 0.16. A value of this magnitude would lead a designer to provide protection either by adding aeration, or modifying the surface smoothness or profile. The gates do feature aeration ramps and large amounts of air have been measured entering the conduit, just downstream from the regulating gate. Aeration in the amounts added at this ramp, have been shown to prevent damage to downstream surfaces at many outlets and spillways all around the world. Even with aeration protection provided downstream from the gate, Reclamation guidelines would still recommend no offsets greater than 0.5 in, and slopes less than 1:8, (Falvey 1990).

3.5 Stilling Basin Pressures.

The significant increase in gate size has yielded a large increase in the outlet works flow capacity, resulting in a modified flow condition entering the stilling basin. Eleven piezometer taps were located on the invert of the stilling basin along the centerline of the model. These taps were located on the sloping section of the basin at an equal spacing of 17 ft beginning at Sta. 12+51. Upper and lower tiers individually as well as dual operation and spillway only flows for the 102-percent gate opening at reservoir elevation 418 ft were run for conditions of no tailwater, tailwater of 160 ft, and tailwater of 180 ft. The operation of a single upper outlet and tailwater elevation of 160 ft was of particular interest as it may be the worst case condition that could occur during construction. The tailwater condition of 180 ft is more or less the minimum condition that would be possible with multiple outlets in operation. The operations at tailwater levels of 180 ft typically yielded piezometric pressures of about 3 to 5 ft above the tailwater elevation. The critical case described above gave piezometric pressures of 10-17 ft above the tailwater depth, figure 16.

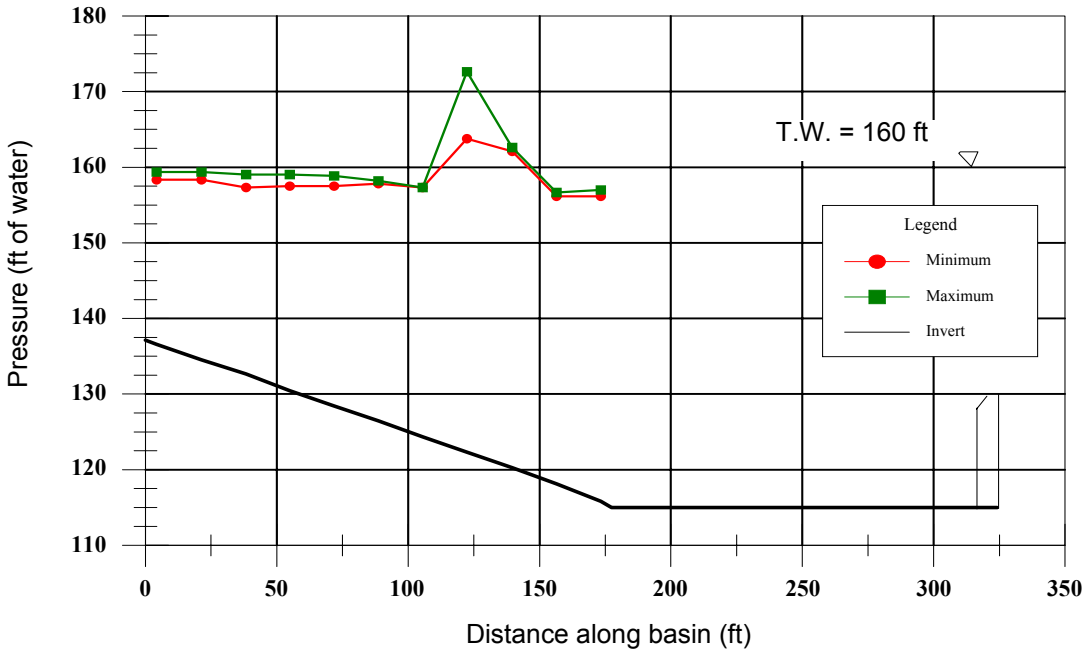

Figure 16: Example of piezometer pressures along the stilling basin centerline for a single upper outlet operation at minimal tailwater (early construction scenario).

Flush-mounted dynamic pressure transducers were added in a line parallel to the piezometers, figure 17. We used 4 Kistler Model 606A dynamic cells. These transducers were mounted in an aluminum plate that was installed flush with the surface of the plywood stilling basin, about 3 in off the centerline of the basin, centered at Sta. 13+70 (piezometer tap #8). These transducers are piezoelectric-based and yield only dynamic pressures with no static indication.

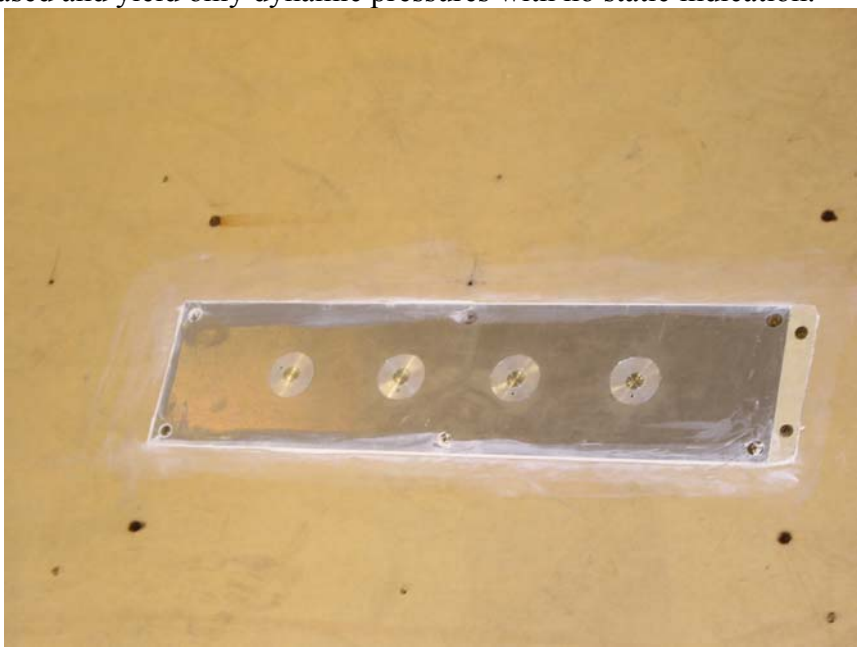

Figure 17: Plate with 4 flush-mounted dynamic pressure transducers, 3 inches between sensors and 3 inches off basin centerline.

The transducers were connected to charge amplifiers and then to a laptop computer via an IOTech Wavebook16 portable data acquisition system, figure 18. Initial data were collected at 200 Hz for a period of 6.4 minutes (26.4 minutes prototype). Two of the charge amplifiers were Kistler Model 5004 Dual Mode amplifiers and two were Bruel & Kjaer Type 2635. Since there were differences in the charge amplifiers, some initial tests were completed in order to optimize the setting to yield nearly identical amplified signals. The main adjustment on the Kistler amplifiers was the selection of the length of time constant; short, medium, or long. This was essentially a selection between quasistatic measurements and dynamic measurements. For the range used in these measurements, the short time constant was 0.01s and it filtered using a 16 Hz cutoff frequency, the medium time constant was 1 s with a lower cutoff frequency of 0.16 Hz, and the long time constant was >1000s with essentially a cutoff near DC. The B&K amplifiers had only an adjustable lower cutoff frequency of 0.2 Hz or 2 Hz. This information lead to setting the Kistler amplifiers on the medium time constant and the B&K amplifiers on the 0.2 Hz lower cutoff frequency. In addition, the frequency of the data collection was evaluated. A data sample at 1000 Hz was collected. The minimum and maximum pressures were noted along with the probability distribution of the sample. Digital filtering was then applied, adjusting the upper cutoff frequency at 500 Hz, 400 Hz, 300 Hz, 200 Hz, 100 Hz, and 50 Hz. The maximum peaks were greatly affected by this filtering. With filtering of 300 Hz or higher, the maximum peaks remained unchanged, however at smaller frequency values the maximum peaks were clipped, yielding much lower values, especially at the 50 Hz level. This data lead to resetting the data collection rate to 500 Hz in order to assure that the peak magnitudes would be recorded. Data sets were 3.33 min in length (13.7 min prototype) in order to allow easy analysis. Several extended length samples were collected in order to evaluate the affect of length of time series on measured maxima.

Figure 18: Charge amplifiers and data acquisition system for recording dynamic pressures in the stilling basin.

The most critical condition is one that may be encountered during the construction period where a single upper outlet may be required to discharge full open at reservoir elevation 418 ft, into minimum tailwater (~160 ft). In order to define the effect of the tailwater on dynamic pressures, we ran this test flow with no tailwater, tailwater at 160 ft, and tailwater at 180 ft. Descriptive statistics from the data files for each of these cases are shown in Table 4.

Table 4: Descriptive statistics for dynamic pressure fluctuations in the stilling basin.

		Dynamic Pressure (ft)			
		A	B	C	D
No TW	Min – Max	-82 to 282	-97 to 263	-80 to 224	-91 to 183
	Std. Dev.	26.2	24.2	25.7	25.2
	Piezometric	75	75	75	75
TW=160 ft	Min – Max.	-58 to 79	-48 to 87	-54 to 146	-55 to 135
	Std. Dev.	13.2	12.4	15.6	16.6
	Piezometric	62	62	62	62
TW=180 ft	Min – Max.	-19 to 39	-28 to 42	-44 to 113	-35 to 153
	Std. Dev.	3.4	4.2	6.5	7.8
	Piezometric	51	51	51	51

The data in Table 4 and photos in figure 19, indicate that the location of the maximum pressure moves downstream as the tailwater increases. This is probably due to a combination of the deflection of the jet by the water surface in the basin and perhaps some density/buoyancy effects of the aerated jet once it enters the basin. Observations indicate there is substantial spread of the jet at the time it enters the basin with the width of the jet at 20-30 ft, and a longitudinal spread of 50-80 ft. Samples of the time series for each of the cases detailed in the table above appear in figure 20. In order to get the total pressure, the dynamic pressure must be added to the piezometric pressure for that condition. In order to be somewhat conservative, we have reported the maximum piezometric pressure from the taps (#7, 8, and 9) surrounding the transducer plate.

In addition, the transducers were spread out longitudinally to capture pressure fluctuations acting over entire slabs of the stilling basin. The common size of a slab is 50-ft square. Transducers were again placed on a single line, but at a spacing of 50 ft prototype, corresponding to the joint lines. Data collection was similar. Data were acquired at 1000 Hz for a period of slightly less than 5 minutes prototype. Figure 21 shows data for this transducer arrangement for upper conduit only, lower conduit only, combined conduits, lower conduit plus spillway discharge, and spillway discharge only. Pressures plotted are the piezometric pressure at each location with bars showing the maximum and minimum pressures collected at each site. The frequency content of impact versus spillway (hydraulic jump) pressure fluctuations appears to be slightly more broadband with direct impact and very low frequency (< 1 Hz) with the hydraulic jump.

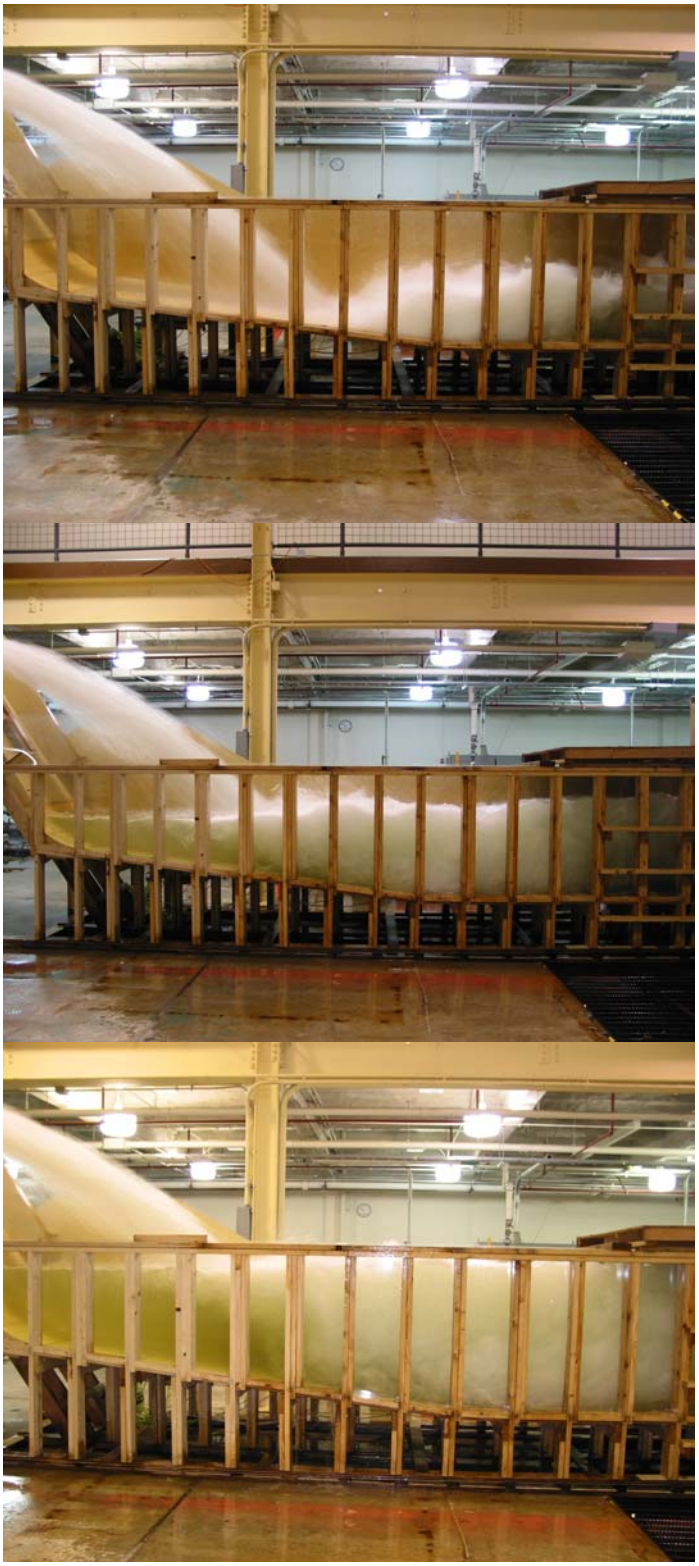

a.) Upper tier, full open, reservoir elevation = 418 ft, No tailwater

b) Upper tier, full open, reservoir elevation = 418 ft, TW= 160 ft.

c) Upper tier, full open, reservoir elevation = 418 ft, TW= 180 ft.

Figure 19: Effect of tailwater on plunge of outlet jet from the upper tier gate.

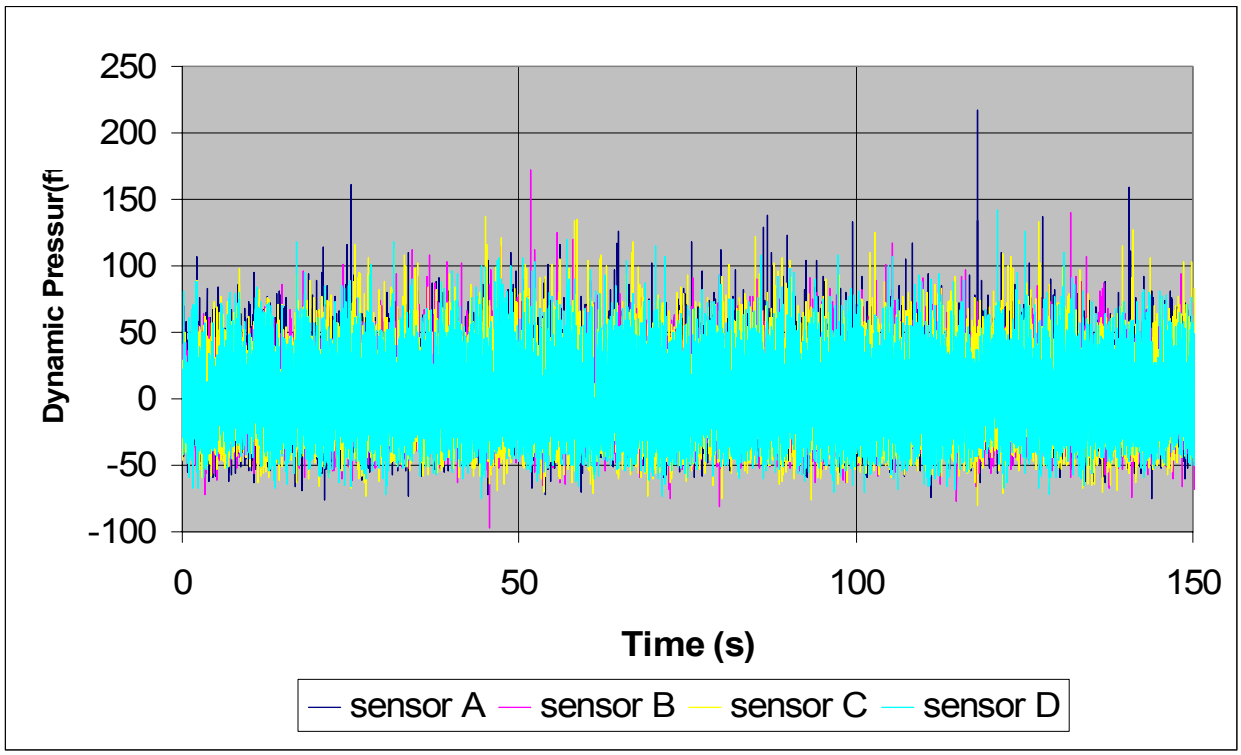

a) No Tailwater

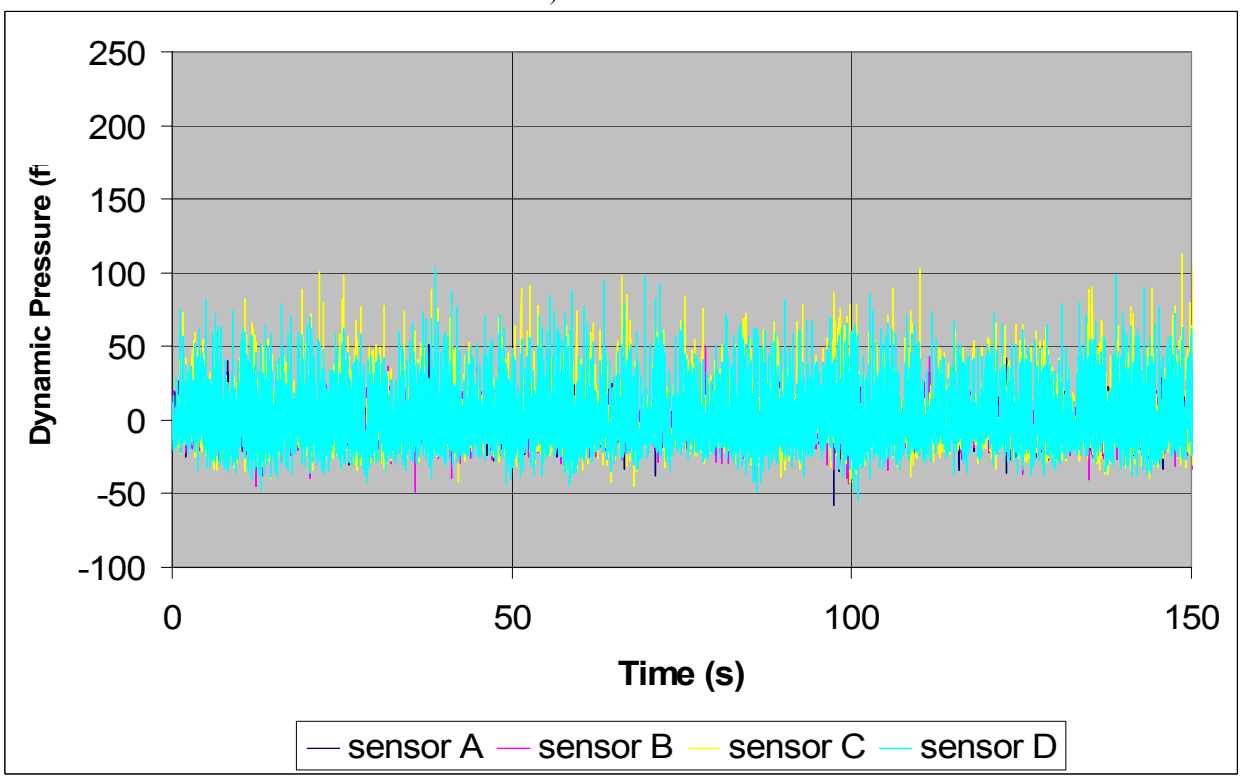

b) Tailwater at 160 ft.

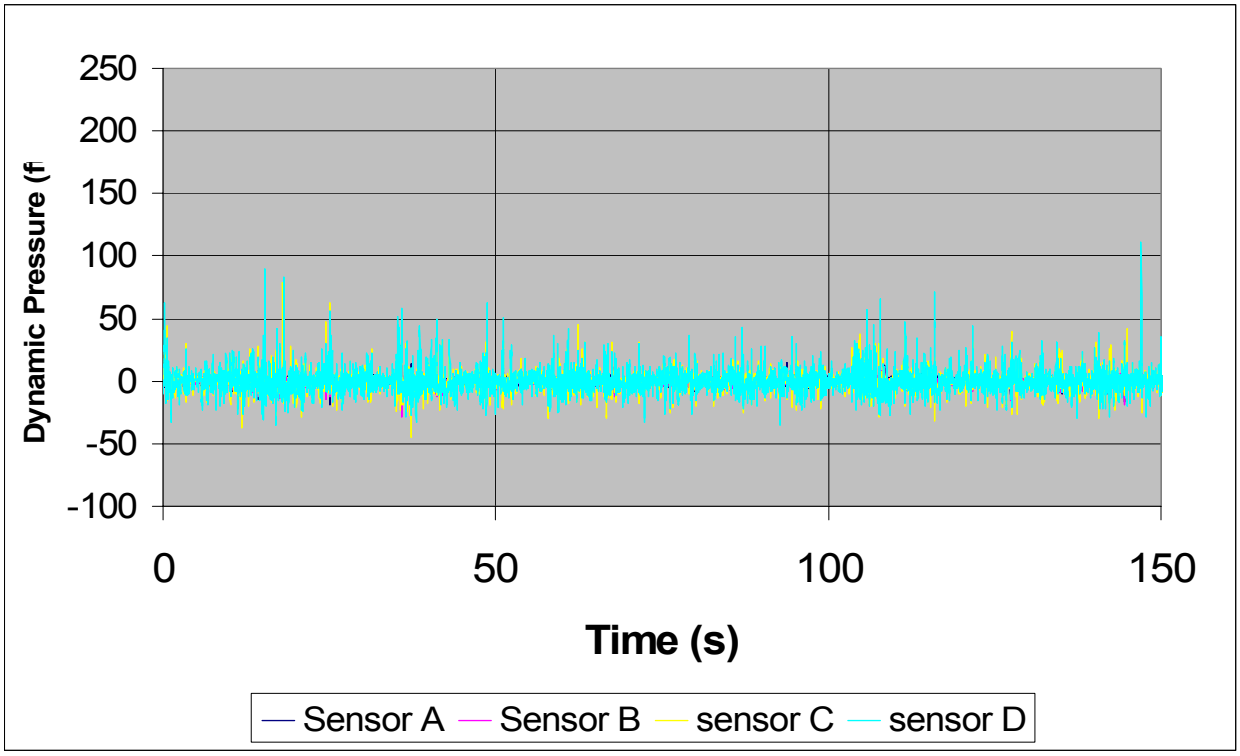

c) Tailwater at 180 ft.

Figure 20: Effect of tailwater on dynamic pressure fluctuations for upper outlet, fully open, reservoir 418 ft. Piezometric pressure must be added to give total pressure.

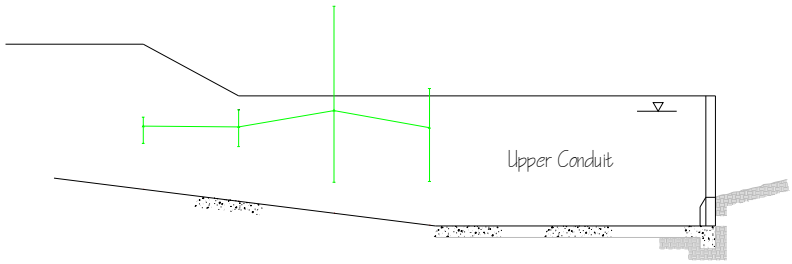

Figure 21: a) Upper conduit only, res. 400 ft, gate full open, tailwater reference is triangular marker, top of wall is elevation 183 ft.

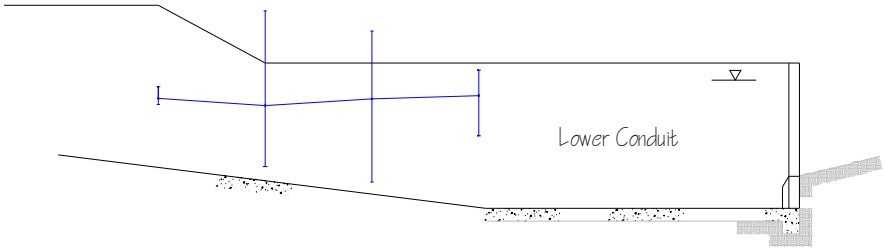

b) Lower conduit only, Res. 400 ft, full open gate.

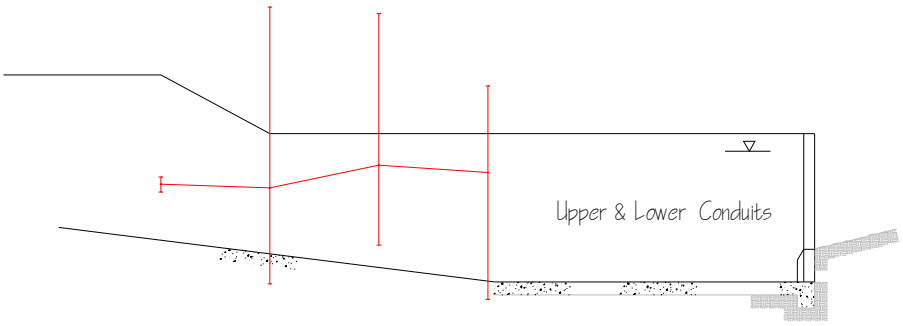

Figure 21: c) Upper and lower gates full open, Res. 400 ft.

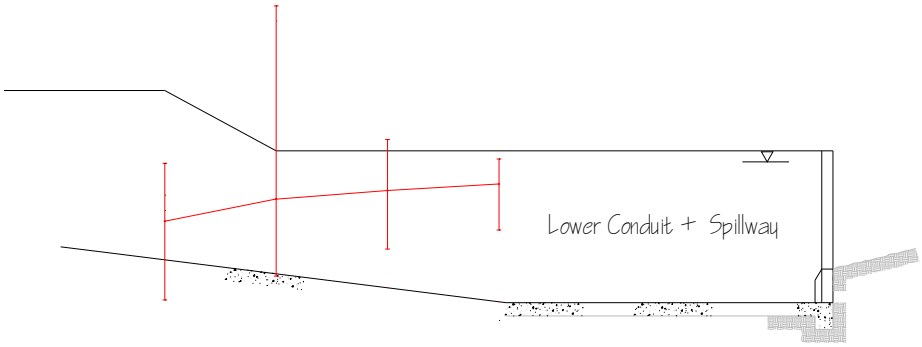

d) Lower gate full open, with Spillway flow, Res. 438.2 ft

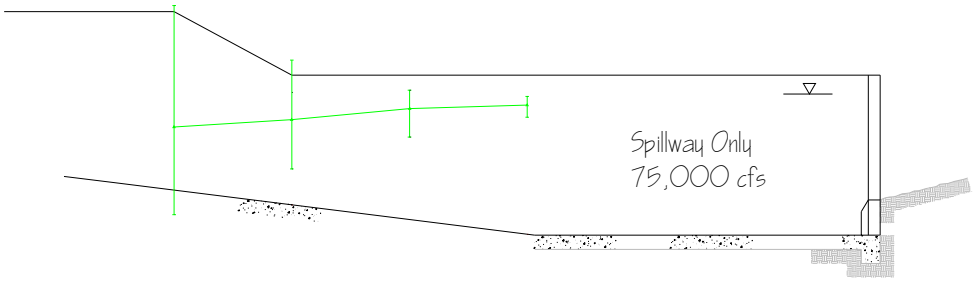

Figure 21: e) Spillway only, discharge 75,000 ft^3/s, free flow, Res. 441 ft.

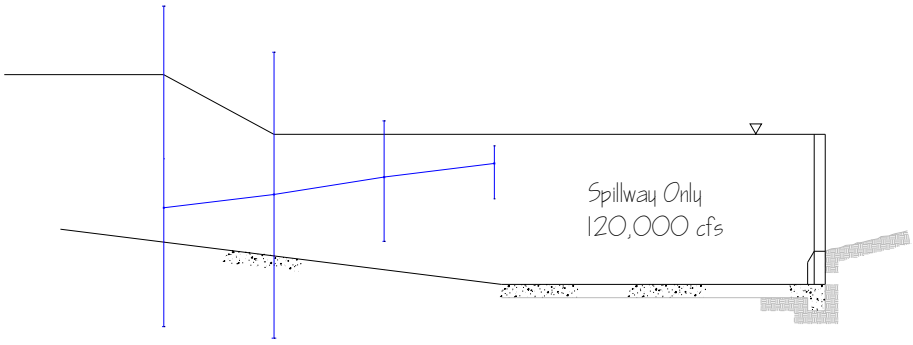

f) Spillway only, discharge 120,000 ft^3/s, gate control, Res. 466 ft.

Figure 21: Pressures through the stilling basin centerline at the lateral joint lines. Mean piezometric pressure is connected by lines, vertical bars represent maximum to minimum extremes in dynamic pressure for that

location over about a 5 minute prototype run. Tailwater is noted by triangular water surface marker near end of basin, top of wall is El. 183 ft.

3.6 Air Vents.

Once a design was chosen for the ramp configuration, the capacity and flow conditions in the air vents was tested. Both the lower and upper tier air vent pipes, as well as half of the intake manifold and junctions with the other vent pipes, were modeled. The objectives of the air demand tests were to determine the hydraulic performance of the air vents and manifold system. Velocity and pressure information will be obtained in the air vents and conduit downstream of the gate.

Velocity profiles in the air vents were collected for a variety of test conditions and then the average velocity was applied over the vent area to yield a discharge. The velocity measurements were taken with a hot-film type velocity probe manufactured by Omega, appendix B. This type of probe is commonly used to determine air flows in duct works. The probe is essentially unidirectional; however you can not differentiate between positive and negative velocities. The probe outputs a voltage that is proportional to velocity. A programmable multimeter was used to collect 100 data samples at each profile location, the meter could then provide the average value to be used in the discharge determination. The air vent discharge curves for the upper and lower tier outlets are shown on figure 22 a and b. The air demand can also be put in terms of the dimensionless parameter β. Beta is defined as the air discharge divided by the water discharge, figure 23 a & b.

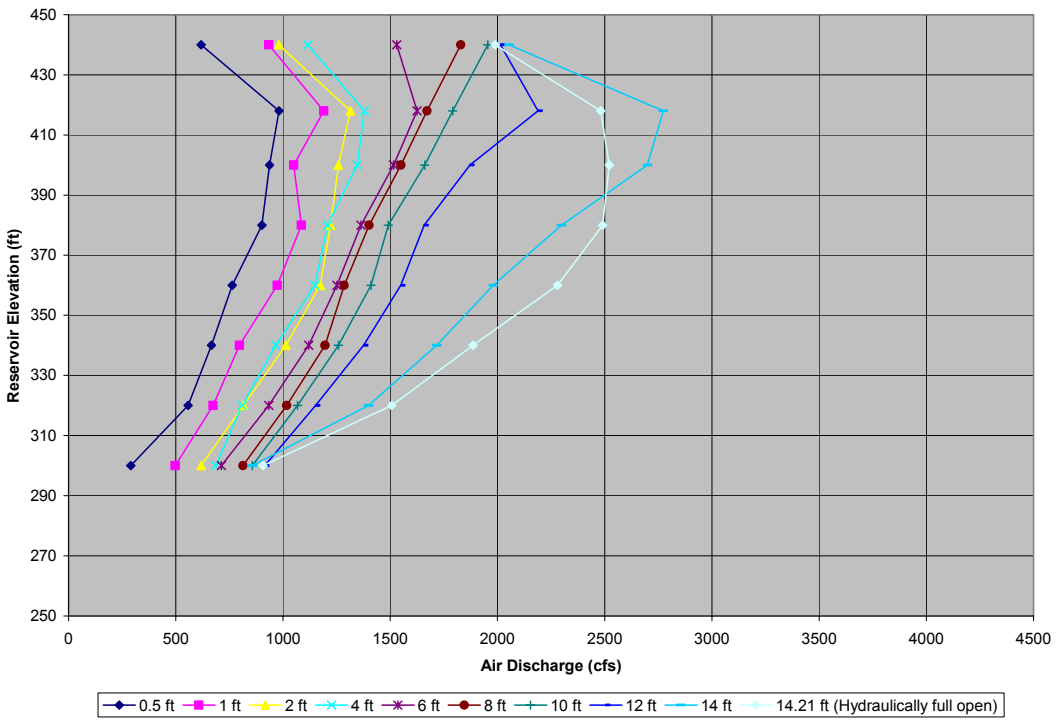

a) Upper tier outlet gate, air vent discharge.

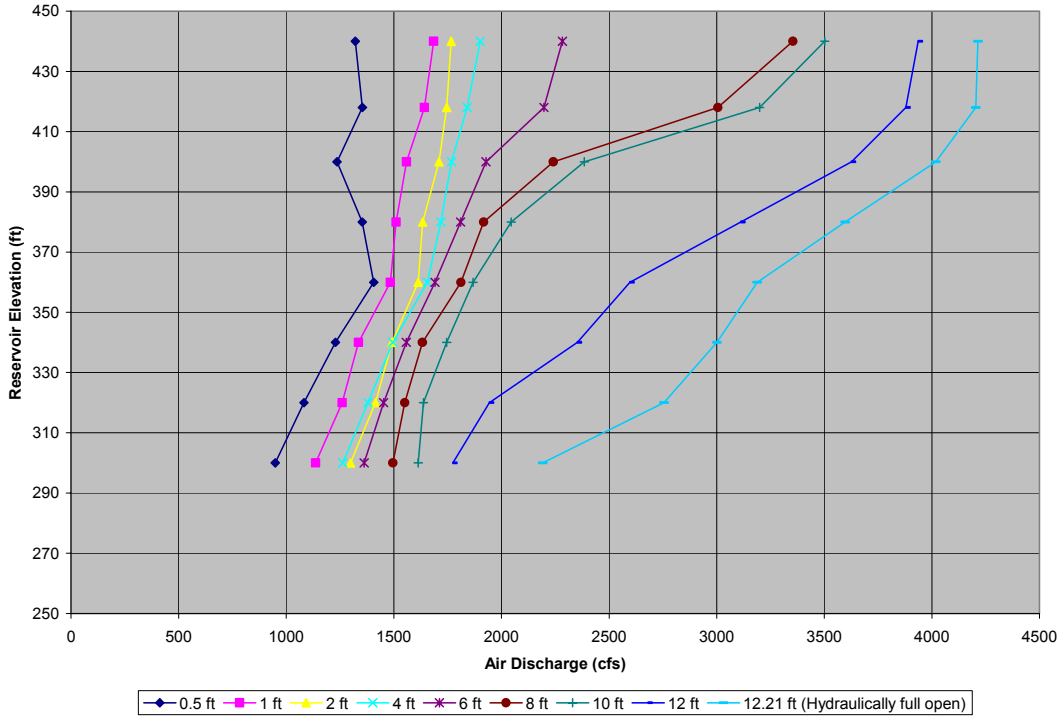

b) Lower tier outlet gate, air vent discharge.

Figure 22: Air vent discharges, upper and lower tiers, outlet only flow.

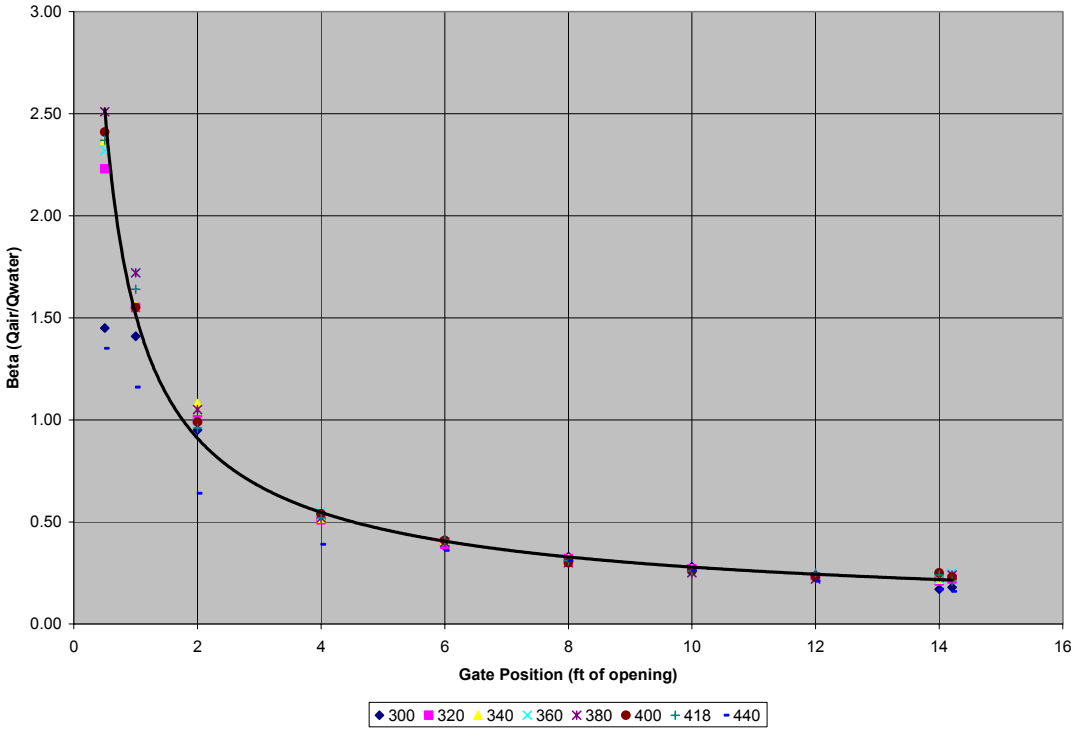

a) Upper tier outlet

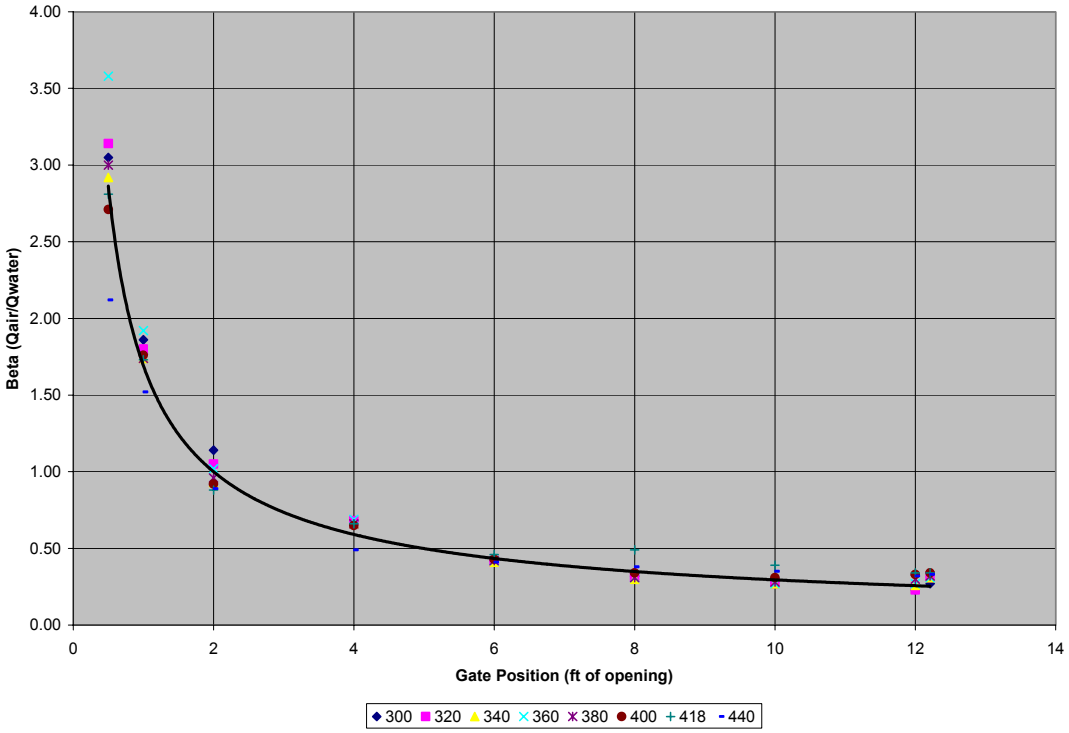

b) Lower tier outlet

Figure 23: Dimensionless air demand data for the upper and lower outlets.

The eyebrow deflector is an important appurtenant feature that directly affects the air discharge entering the outlet conduits. The initial design features eyebrows over each outlet opening with a ramp height of about 3 ft. Data were collected to compare outlet only air demand to that with combined spillway and outlet flows. Initially, we set a 5 ft radial gate opening with a reservoir elevation of 440 ft. We collected air vent discharge and conduit invert pressures and compared these to outlet only flows for a similar reservoir condition, figure 24 a and b. An effective way to view this effect is shown in the ratio of air demand for a combined spillway and outlet flow to one of outlets only, figure 25.

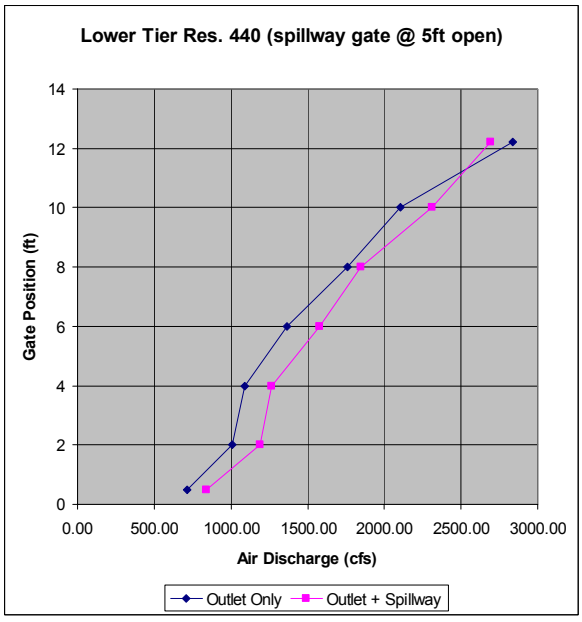

a) lower tier

b) upper tier

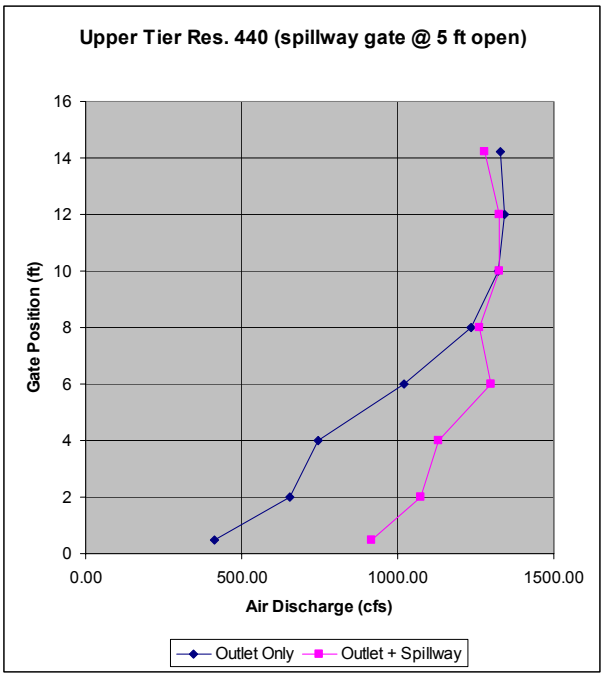

Figure 24: Air vent demand for the condition of combined spillway and outlet flows versus outlet only flows. Radial gates on spillway at 5 ft open, reservoir elevation 440 ft.

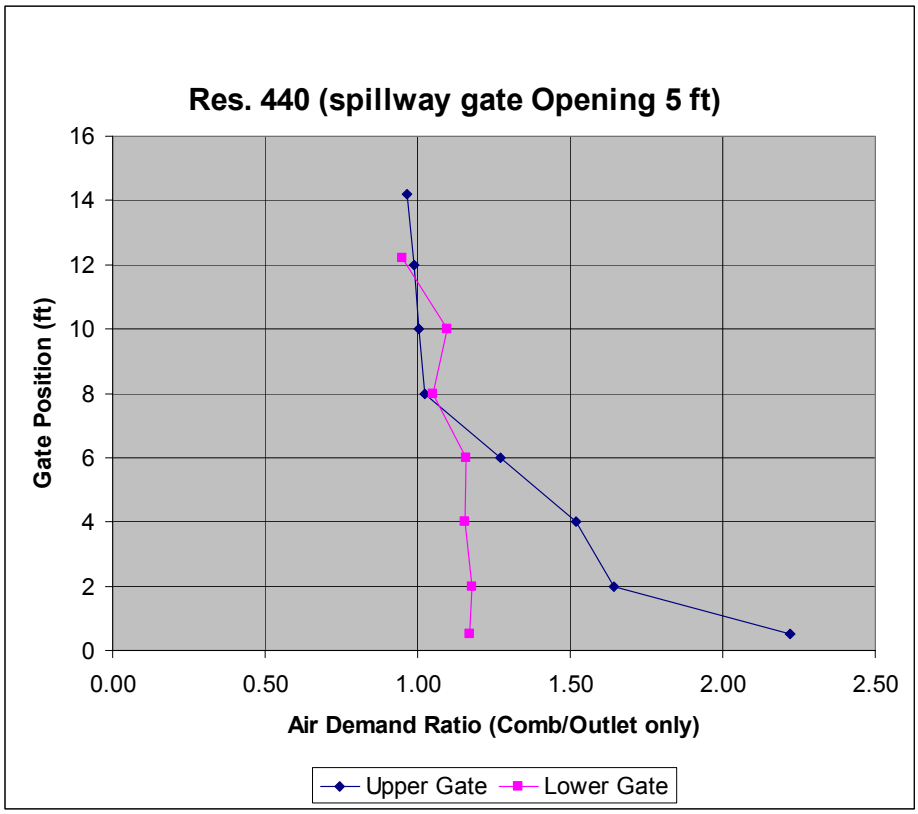

Figure 25: Air demand ratio for the combined spillway and outlet versus outlet only flows.

It is evident from observations during these tests that the flow jumps from the upper eyebrow, completely over the lower outlet eyebrow, impacting directly on the upper jet surface from the lower outlet. In order for the lower eyebrow to be more effective, the height of the upper eyebrow needs to be reduced. Conduit pressures do not change for either case, indicating that sufficient air is reaching the conduit, either through the vent, or a combination of the vent and from the downstream end of the conduit. The lower tier shows almost no increase in air flow during combined operation, in comparison to the upper gate which shows a substantial increase at the lower gate openings. This data supports the premise that the lower eyebrow is not functioning correctly or at least in the same manner as the upper eyebrow.

Due to the apparent lack of function of the lower eyebrow, a smaller eyebrow was also tested in the model. The height of the eyebrow was reduced to 18 inches. Observations indicated that the jet trajectory from the upper eyebrow did reattach to the spillway surface prior to passing over the lower eyebrow, unlike the 3-ft-high original design. In addition, pressures within the conduit and on the face of the spillway near the outlet openings were not adversely affected by this decrease in eyebrow height, remaining positive, figure 26. A comparison of air demands for both the upper and lower gates with the 18-inch-high eyebrows and the 3-ft-high eyebrows is shown on figure 27. The upper outlet showed almost no effect due to the change in size while the lower outlet had a reduction in air discharge in the vent at gate openings above about 8 ft.

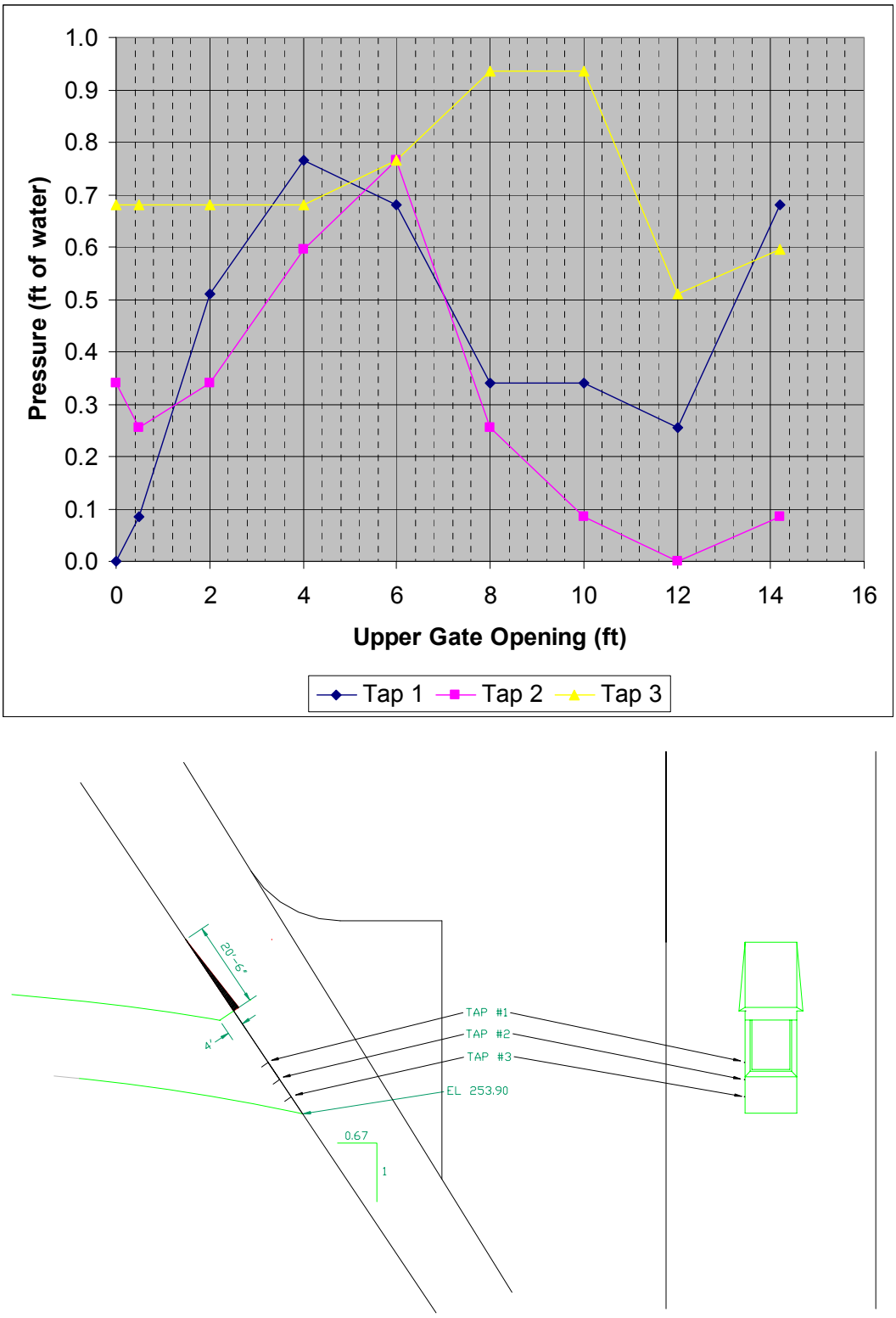

Figure 26: Mean prototype pressure on the spillway face, directly adjacent to the upper conduit exit. Pressures shown are means, fluctuations were minimal.

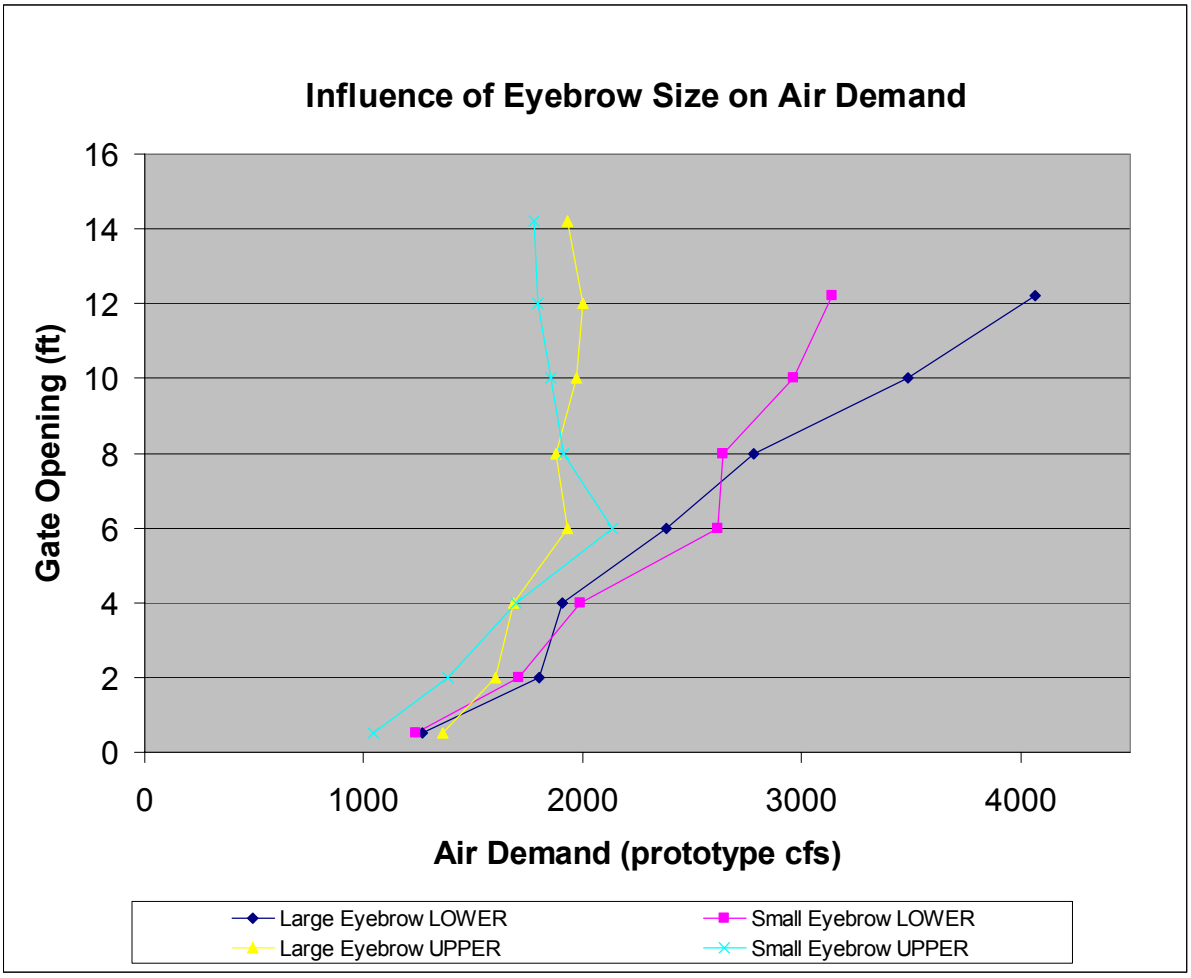

Figure 27: Comparison between the two eyebrow sizes tested: small is 18 inches and large is 36 inches high. This data is for outlet + spillway discharge, outlet only values of air demand are not affected by the eyebrow size.

Additional testing of the air vents included moving the manifold to simulate air vents going to different conduits, figure 28. No measurable differences in air demand were noted at any of the combinations. Loss factors were essentially identical to the accuracy that was possible to measure in the model.

We also varied the loss factor for the vent by inserting different diameter orifice plates in the 5.5-ft-diameter pipe leading down to the outlet conduits. This affected both the amount of air that comes into the conduit and as a result, the pressures in the conduit. Two inserts were used, a 4 ft orifice and a 3 ft orifice. These resulted in a loss coefficient K of 3.58 and 19.74 respectively. The loss coefficient was calculated based on Idelchik (1994),

$$K = \left(\frac{A_{up}}{A_{orifice}}\right)^2 \left[0.707\left(1-\frac{A_{orifice}}{A_{up}}\right)^{0.375} + \left(1-\frac{A_{orifice}}{A_{down}}\right)\right]^2 \qquad (9)$$

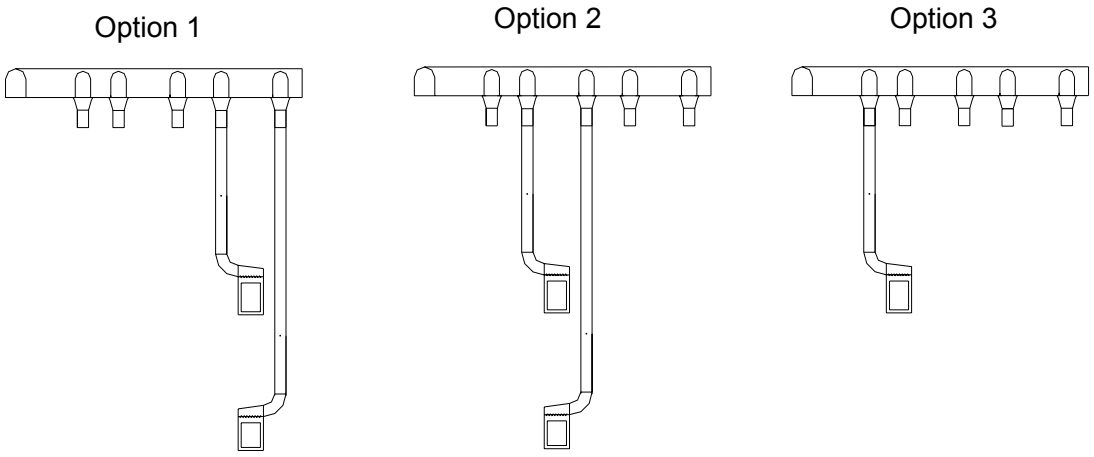

Figure 28: Three air vent arrangements tested, Option 1 simulates vents going to Gates 2 & 7, Option 2 simulates vents going to Gates 1 & 6, and Option 3 simulates a vent going to Gate 5.

The insertion of an orifice plate into the air vent just before the elbow leading to the plenum was an effective way to modify the headloss for the vent system and observe the effect on air flow rates as well as pressures in the conduit downstream from the gate. The effect was not quite as severe as was noted in a previous study of the 5- by 9-ft gates presently installed at Folsom, Frizell (1998). This difference is largely associated with the downstream conduit geometry. In the present Folsom outlets, the downstream conduit is not oversized and actually has a constriction at the end of the conduit near the exit onto the spillway face. These factors along with limiting the air capacity of the vent resulted in lowering of the pressures within the conduit down to a scaled vapor pressure. With the currently proposed design, the downstream conduit is slightly more than 1.6 times larger in area than the gate. This area expansion results in conduit pressures that do not decrease substantially even though there is a reduction in air flow rates through the vent, figure 29 a-d. Data were collected for outlet only flows at a reservoir elevation of 440 ft.

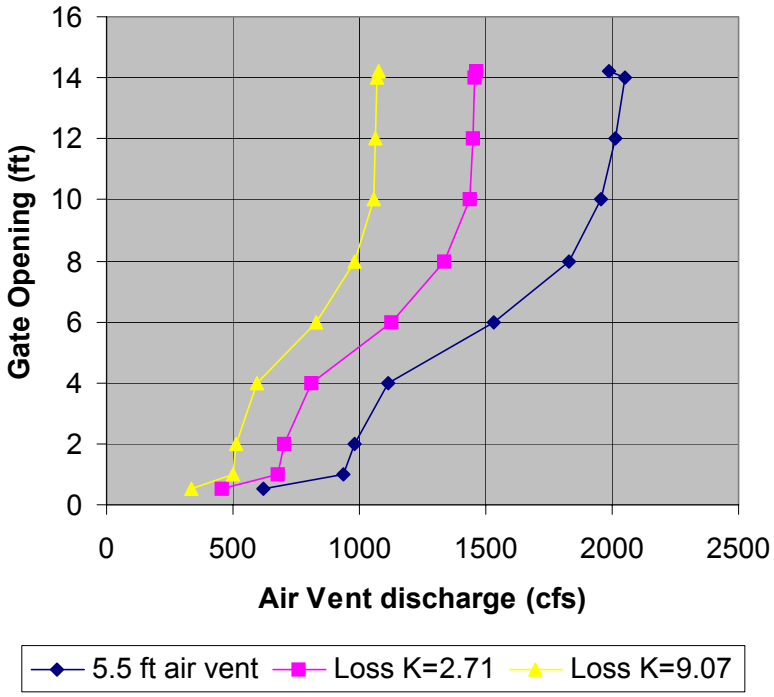

a) Upper gate, Reservoir elevation 440 ft, air vent discharges for different loss factors.

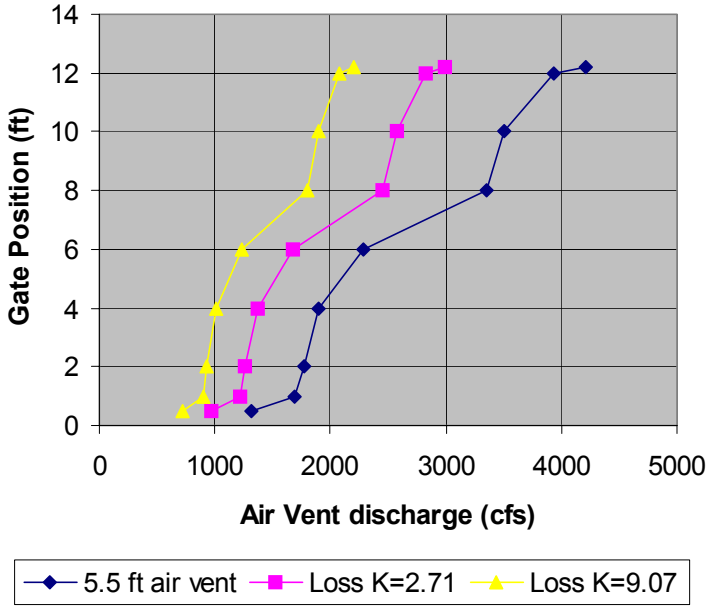

b) Lower gate, Reservoir elevation 440 ft, air vent discharges for different loss factors.

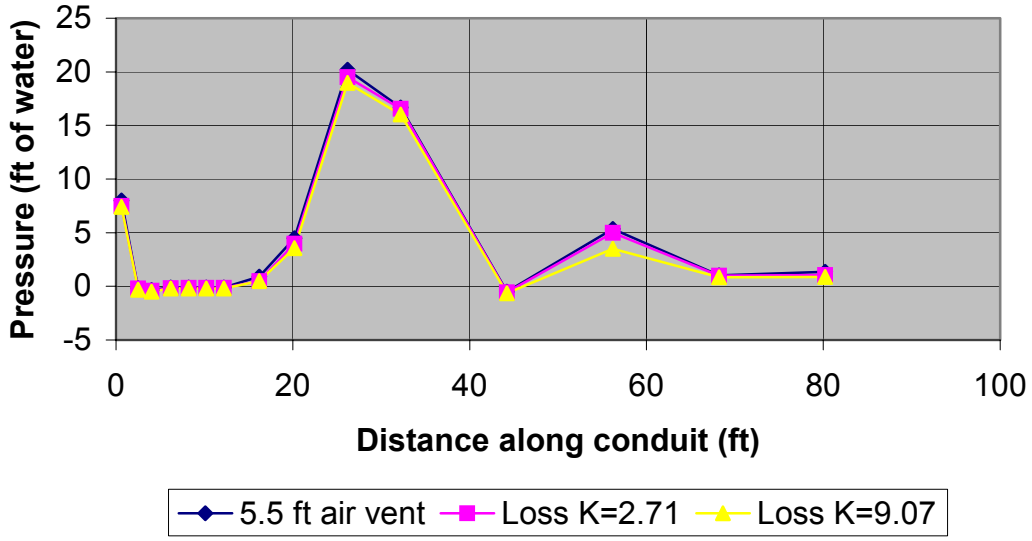

c) Pressures along downstream conduit centerline, Upper conduit, reservoir elevation 440 ft.

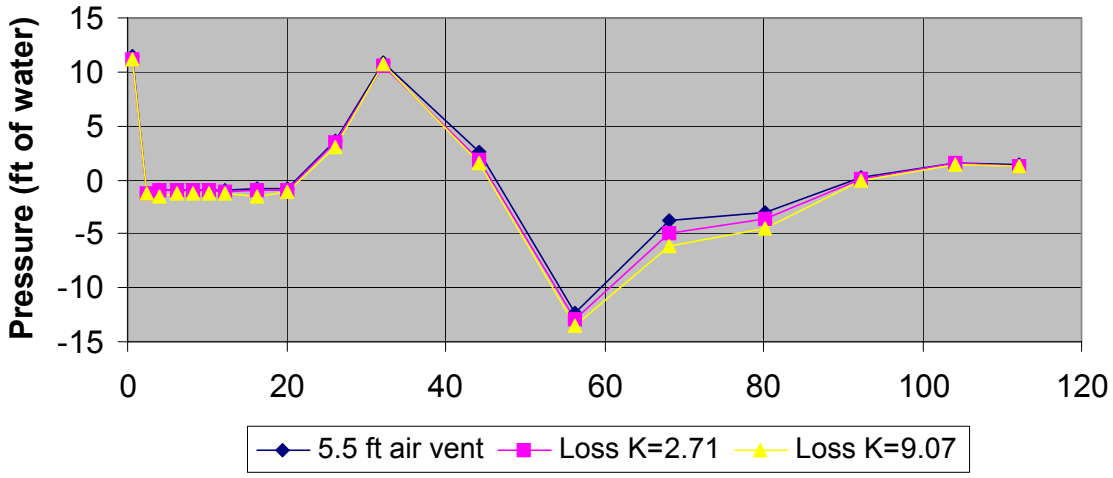

d) Pressures along downstream conduit centerline, lower conduit, and reservoir elevation 440 ft.

Figure 29: Air flow rates and pressures along each conduit as a result of changing the air vent loss coefficient.

3.7 Gate Ratings.

The gate ratings for the upper and lower tier gates were completed according to the scope of work. In addition to recording water discharge for each condition, air demand and pressures in the invert of the conduits were recorded. Water flow data for the lower and upper tier gates are shown on figure 30 a & b. Putting the data in terms of coefficient of discharge, results in figure 31 a & b.

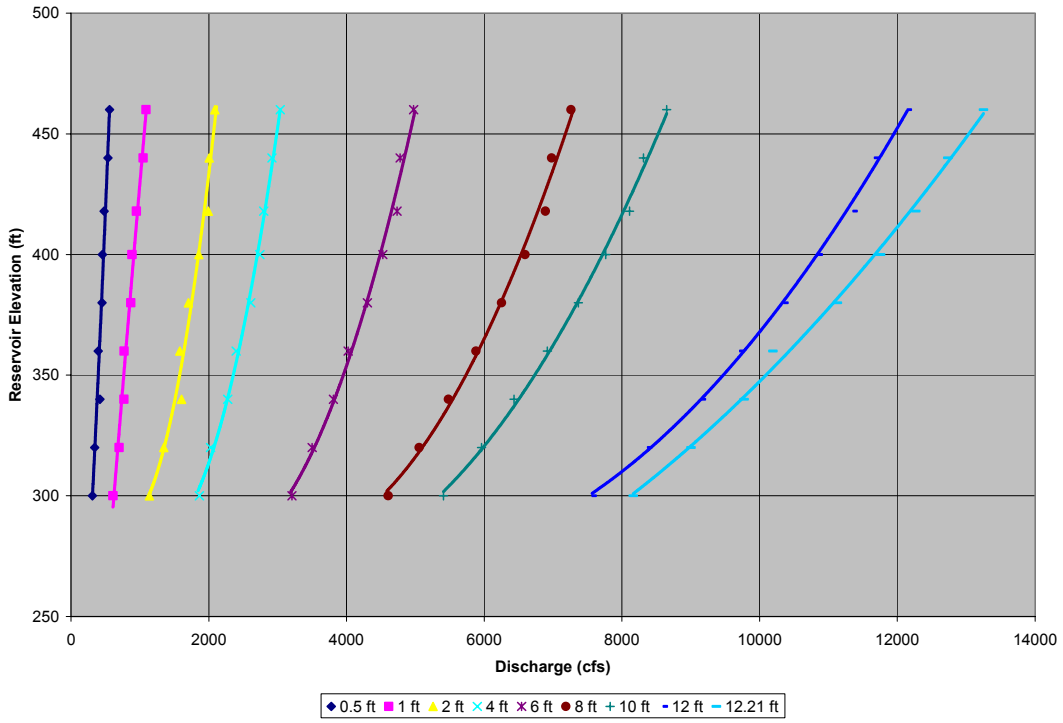

a) Lower tier water discharge.

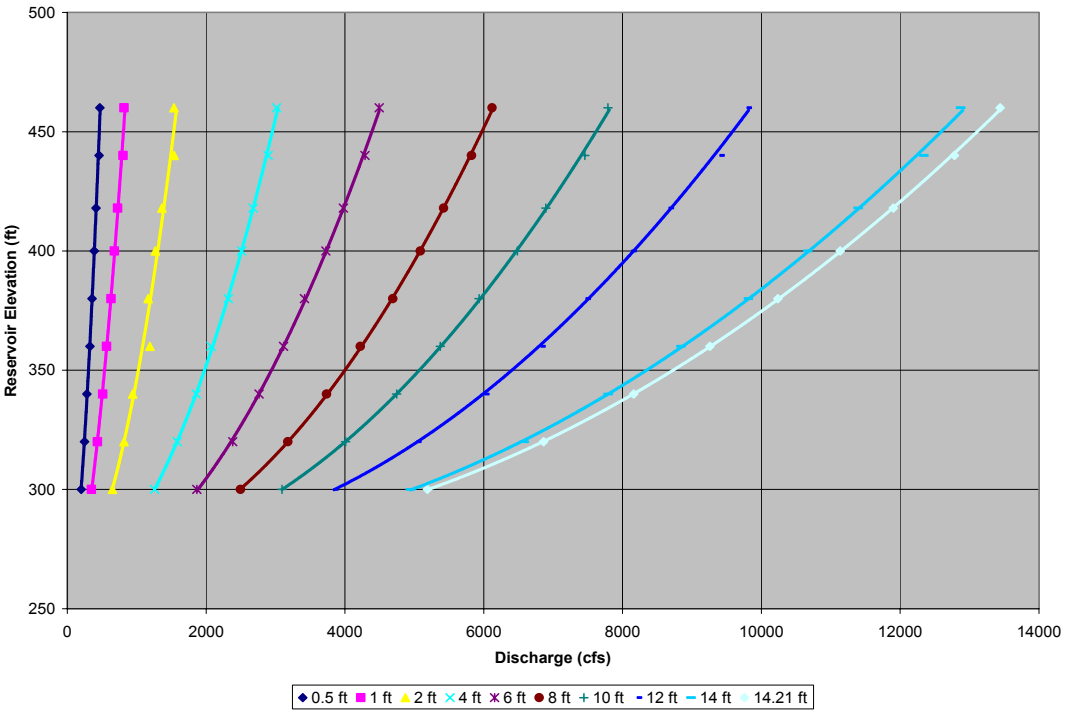

b) Upper tier water discharge

Figure 30: Upper and Lower tier water discharges for reservoir elevations from 300 ft to 460 ft.

The coefficients of discharge are defined as:

$$C_d = \frac{Q}{A\sqrt{2g\Delta H}} \quad \text{and} \quad C_d' = \frac{Q}{A'\sqrt{2g\Delta H}} \tag{10}$$

where A=area of conduit upstream from the gate and A' is the open area of the gate, ΔH includes *all losses* from the intake, conduit, guard gate, and regulating gate.

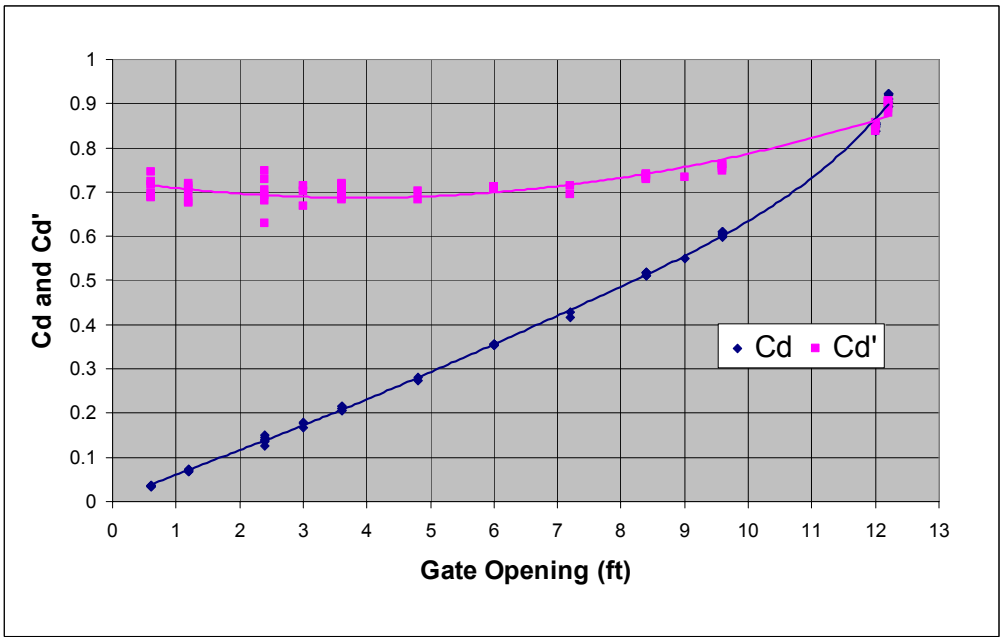

a) C_d and C_d' for the lower tier outlet gate.

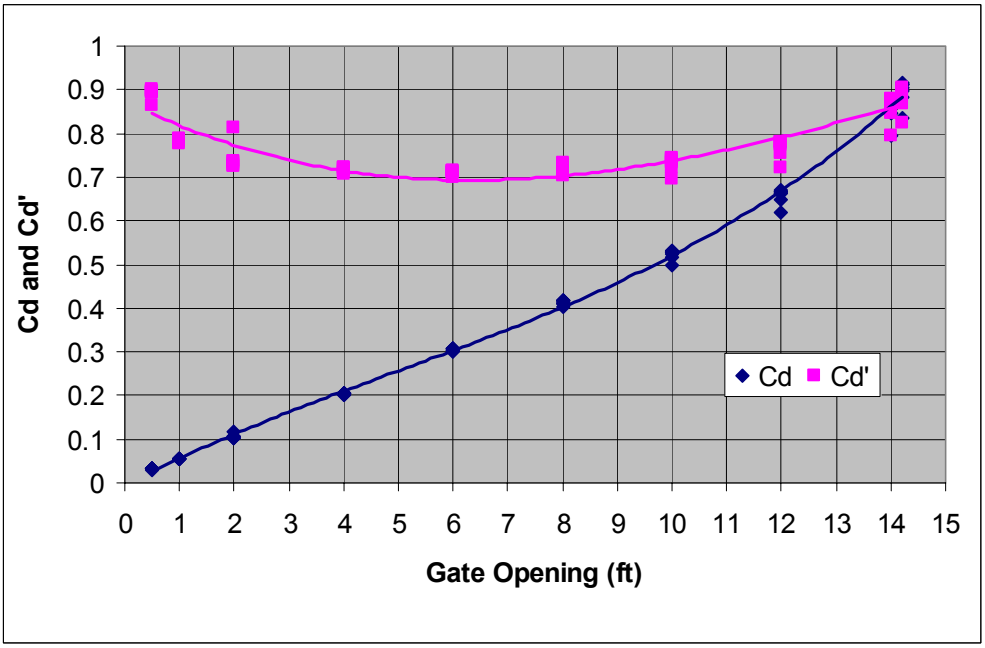

b) C_d and C_d' for the upper tier outlet gate.

Figure 31: C_d and C_d' for the lower and upper tier outlet gates.

Pressure profiles along the centerline of the conduits downstream from the regulating gates for the recommended configuration are shown in figures 32 a-i and 33 a-i.

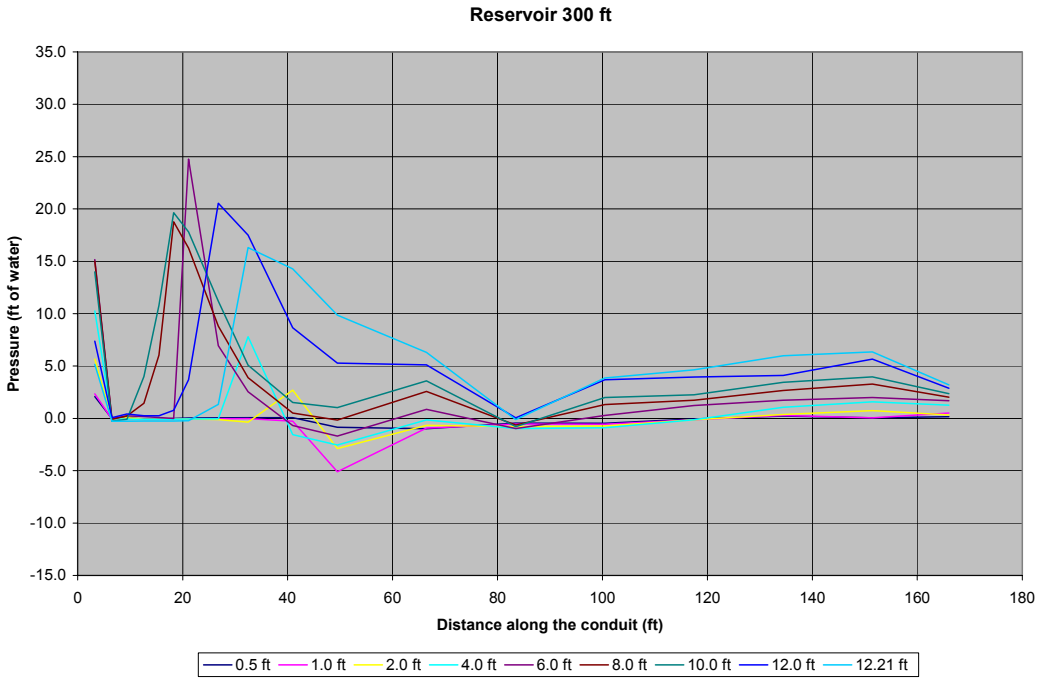

Figure 32a: Lower Tier conduit pressures at a Reservoir Elevation of 300 ft.

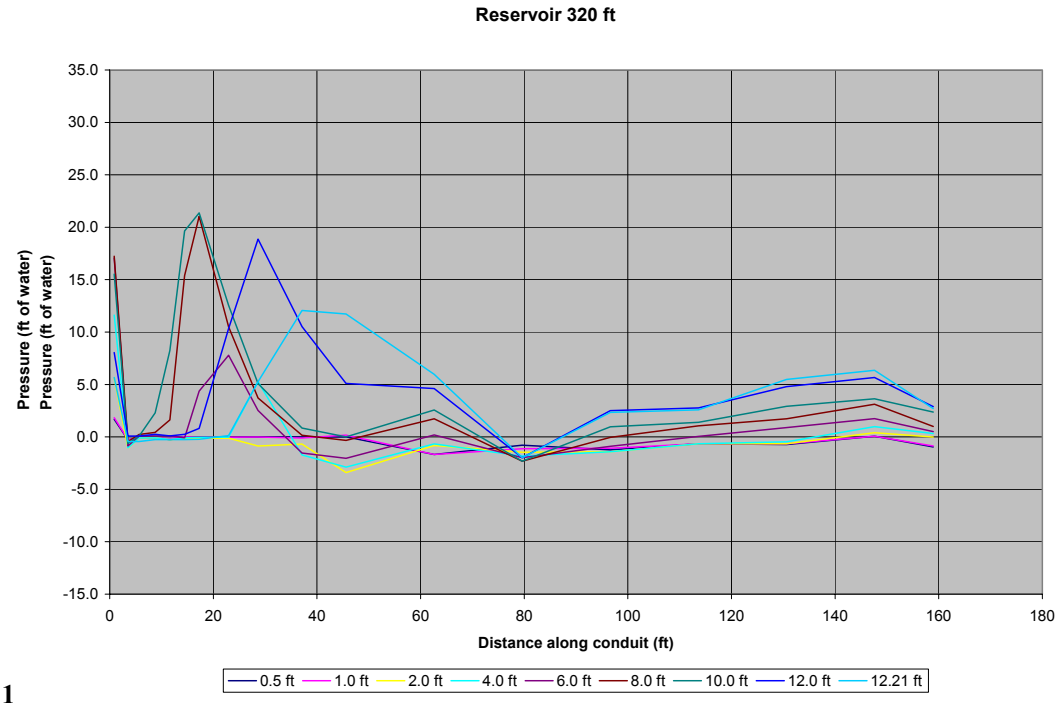

1

Figure 32b: Lower tier conduit pressures at a Reservoir elevation of 320 ft.

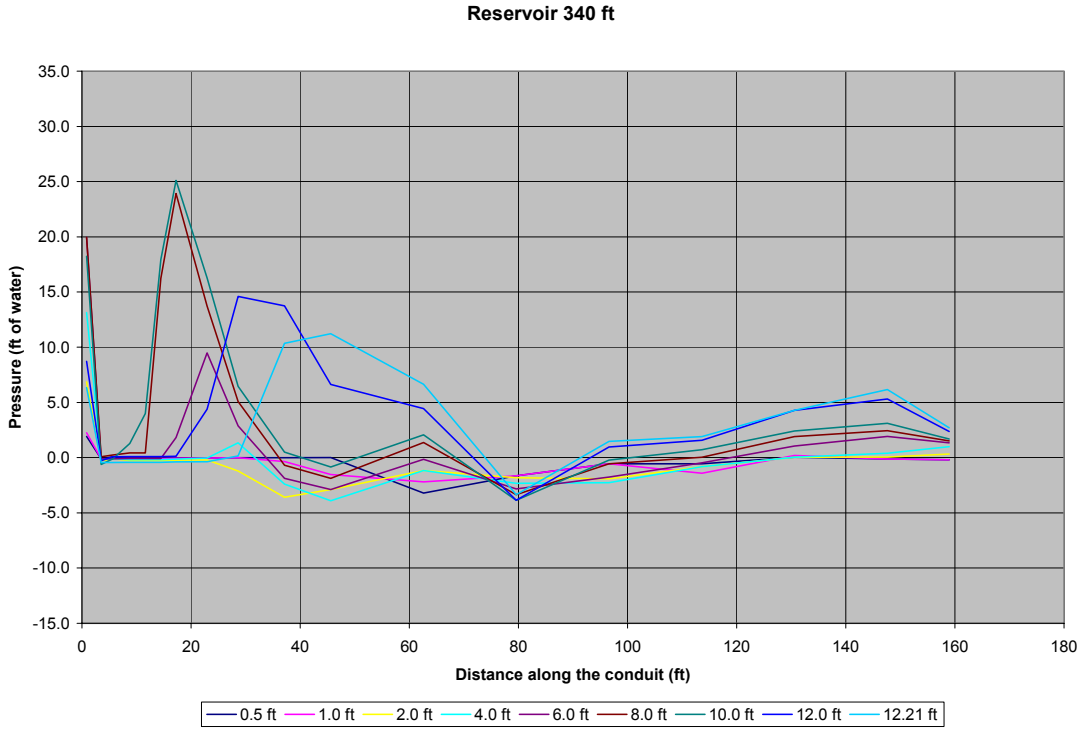

Figure 32c: Lower tier conduit pressures at a Reservoir Elevation of 340 ft.

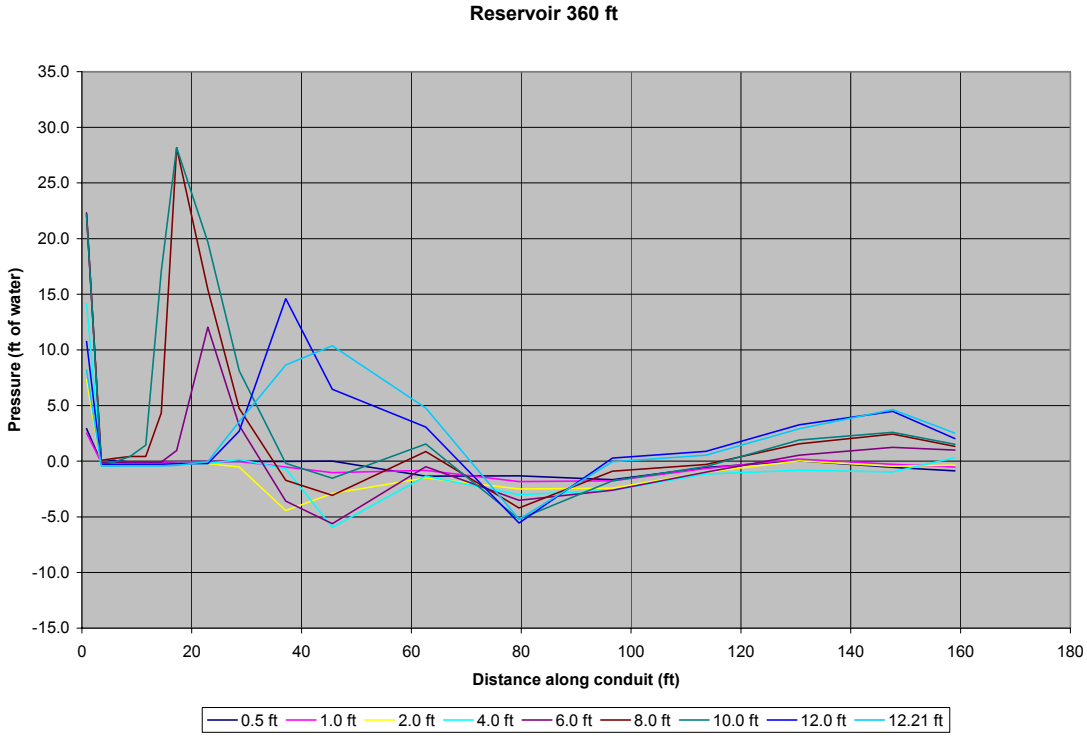

Figure 32d: Lower tier conduit pressures at a Reservoir elevation of 360 ft.

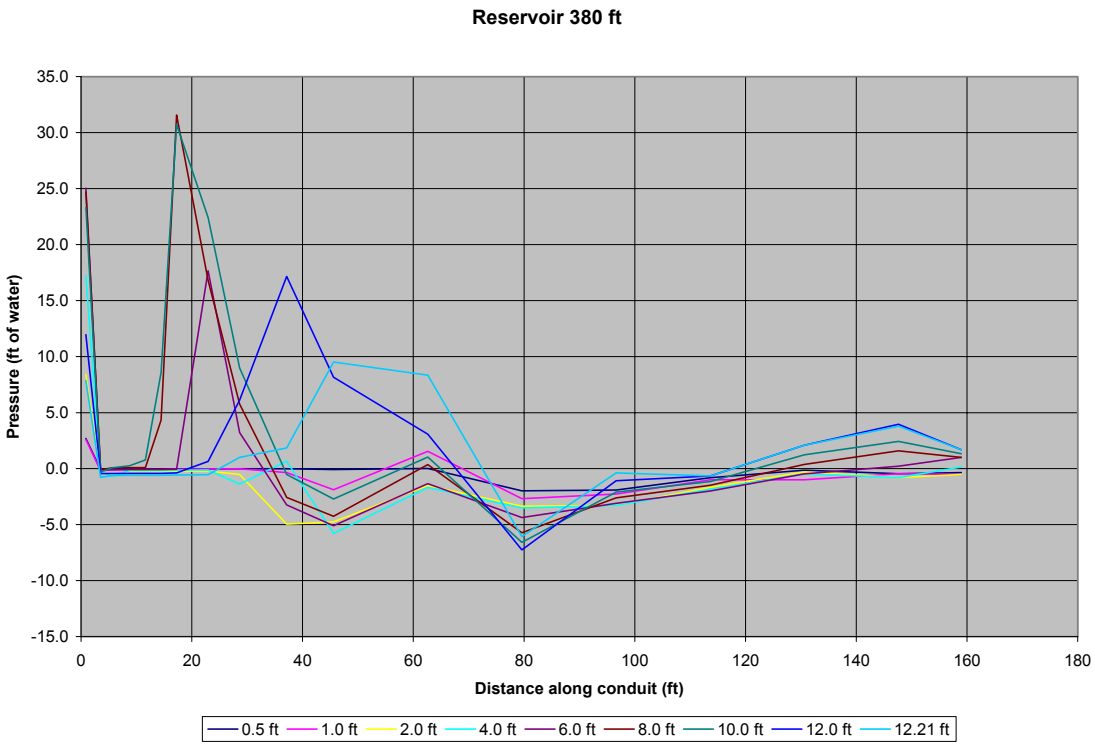

Figure 32e: Lower conduit pressures at a Reservoir elevation of 380 ft.

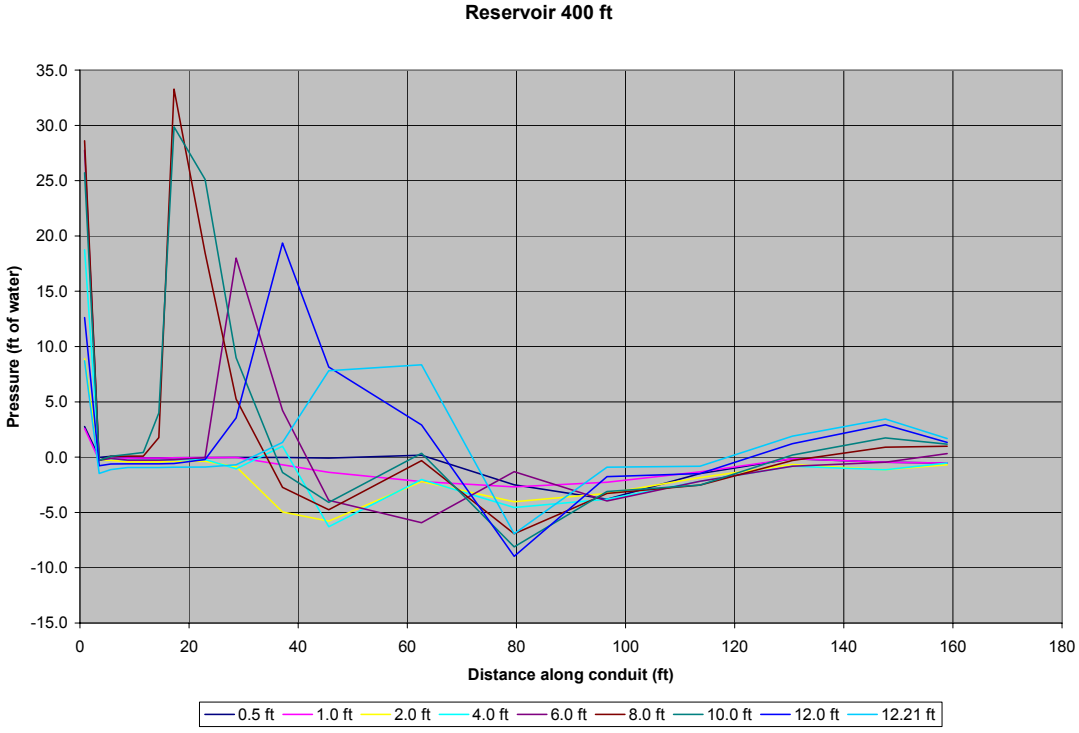

Figure 32f: Lower conduit pressures at a Reservoir elevation of 400 ft.

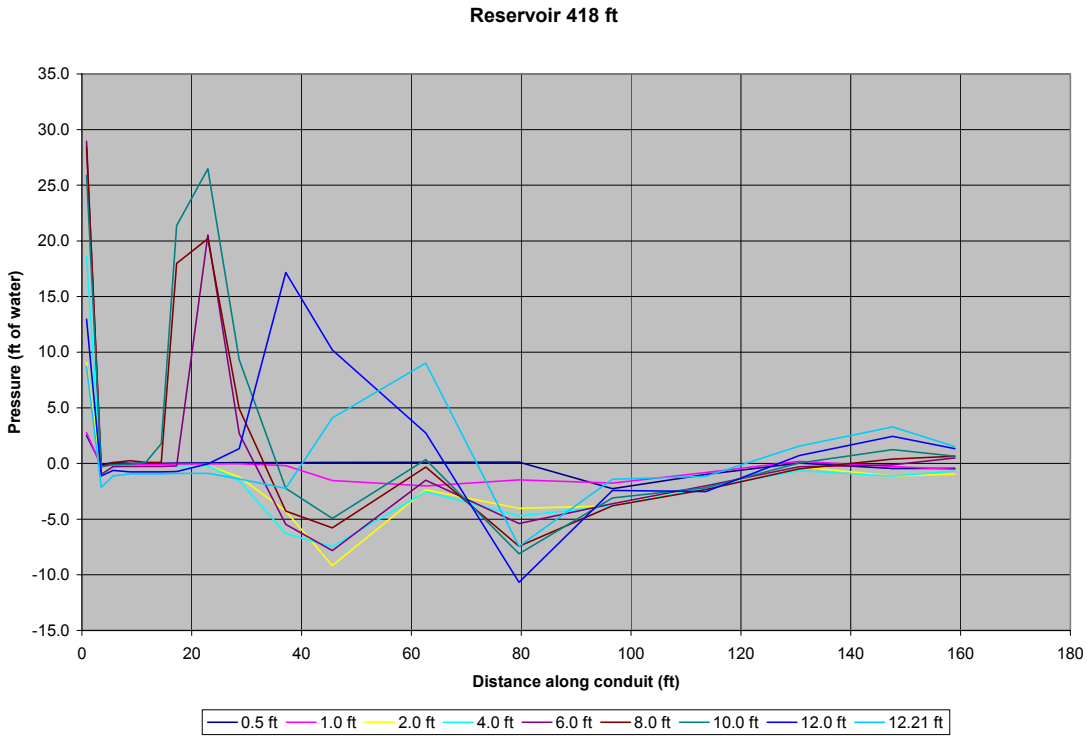

Figure 32g: Lower conduit pressures at a Reservoir elevation of 418 ft (crest of spillway).

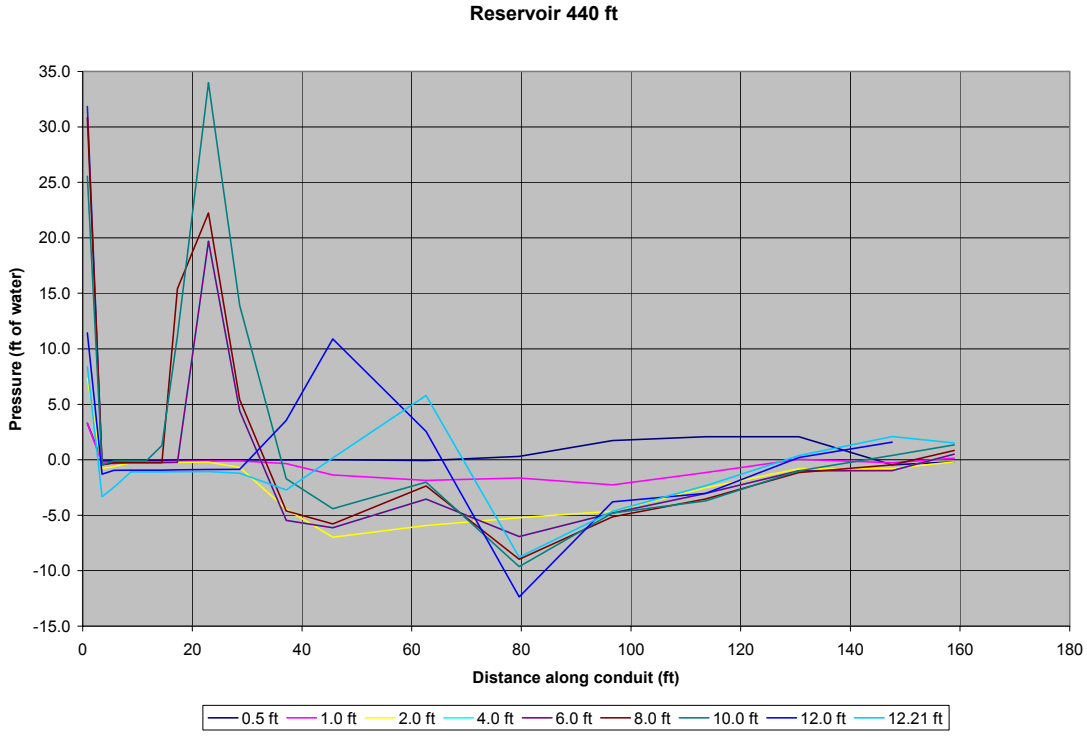

Figure 32h: Lower conduit pressures at a Reservoir elevation of 440 ft.

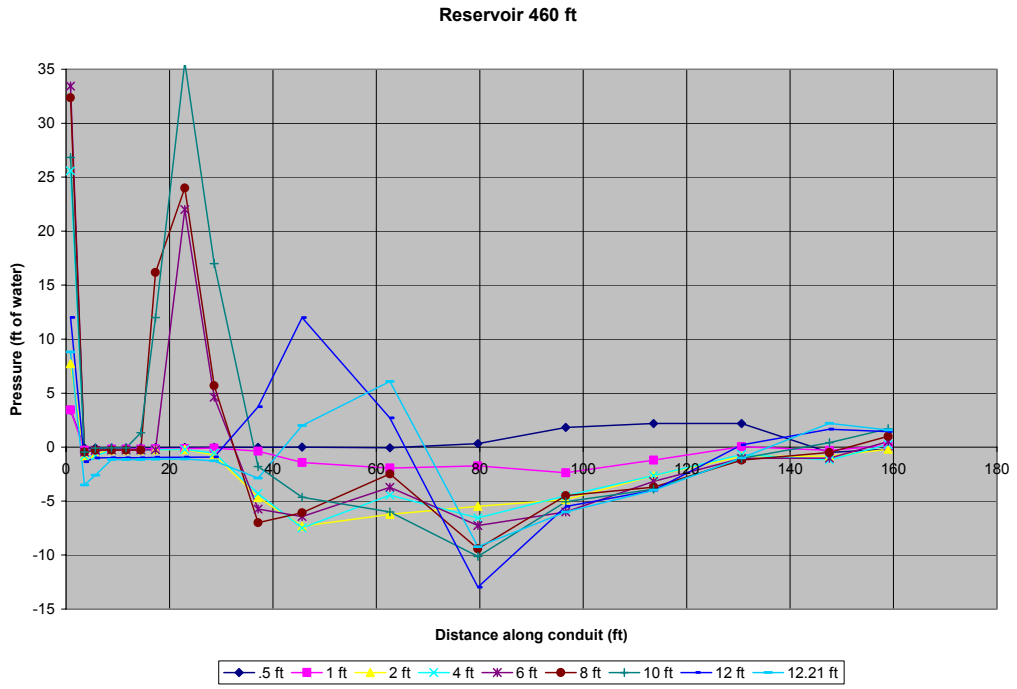

Figure 32i: Lower conduit pressures at reservoir elevation 460 ft.

Figure 32(a-i): Lower conduit pressures at various reservoir elevations.

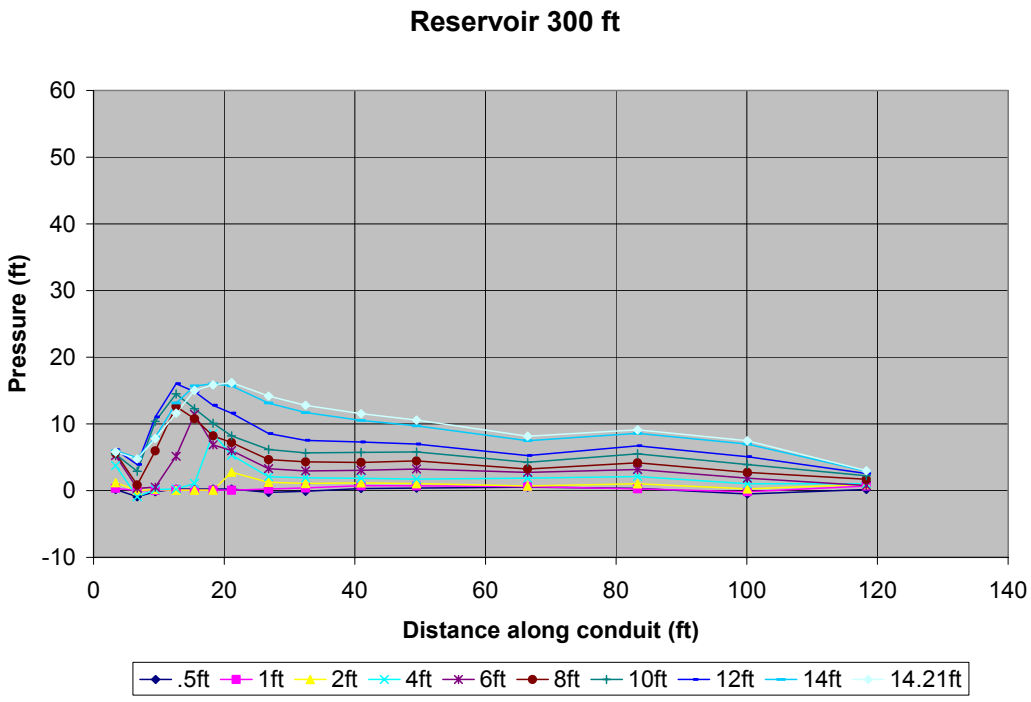

Figure 33a: Upper conduit pressures, reservoir 300 ft.

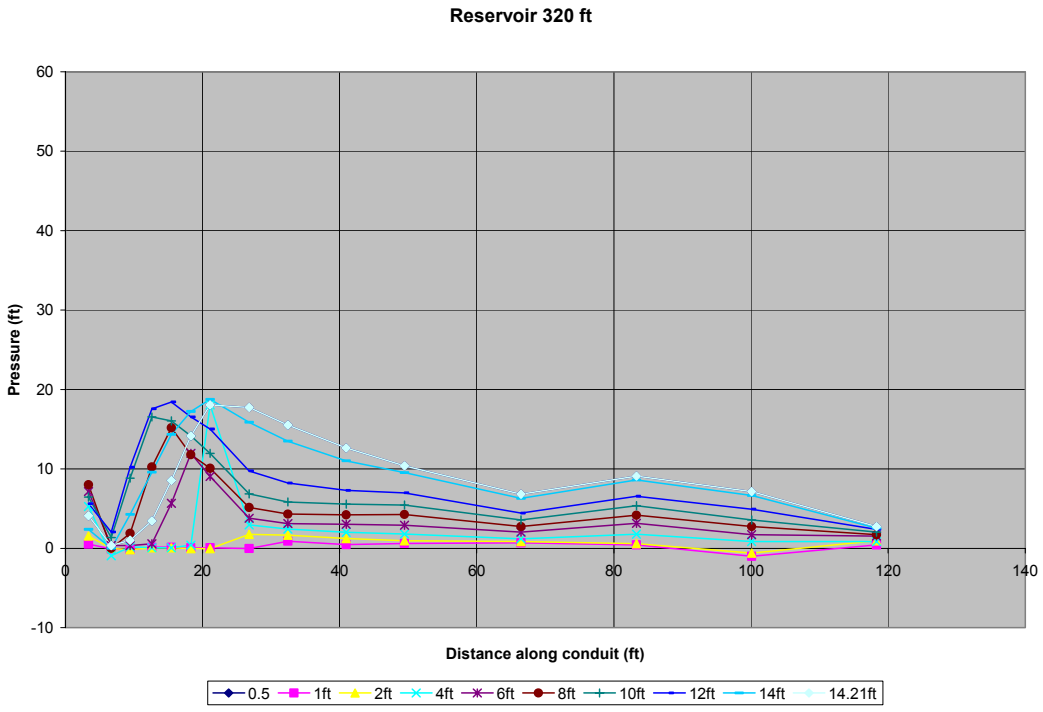

Figure 33b: Upper conduit pressures, reservoir 320 ft

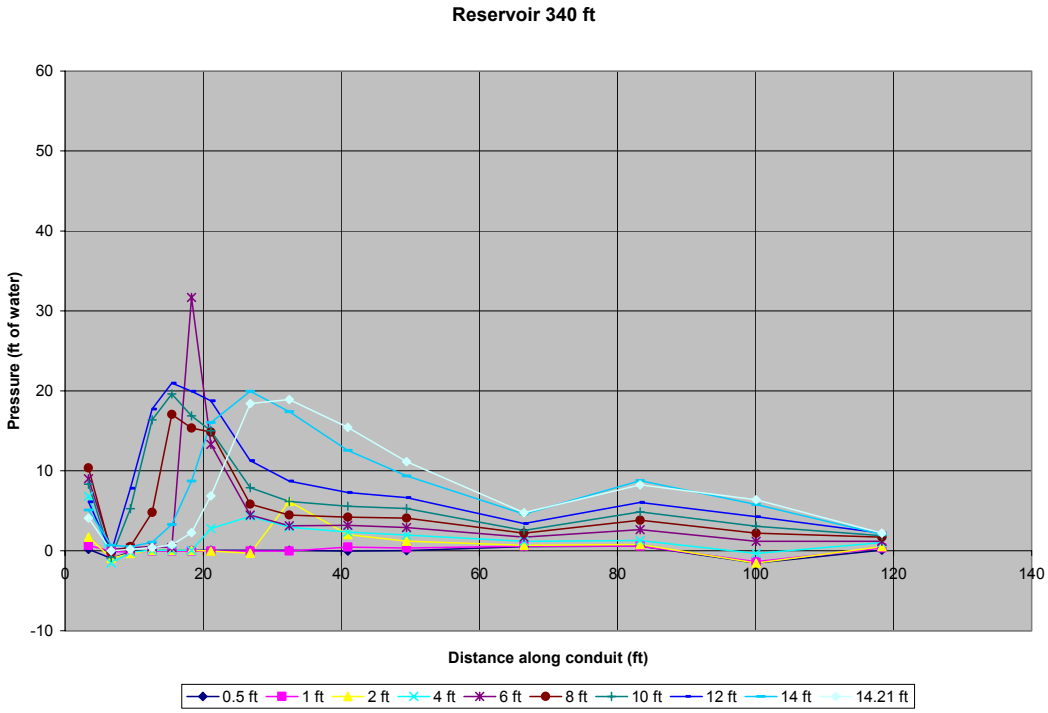

Figure 33c: Upper conduit pressures, reservoir 340 ft.

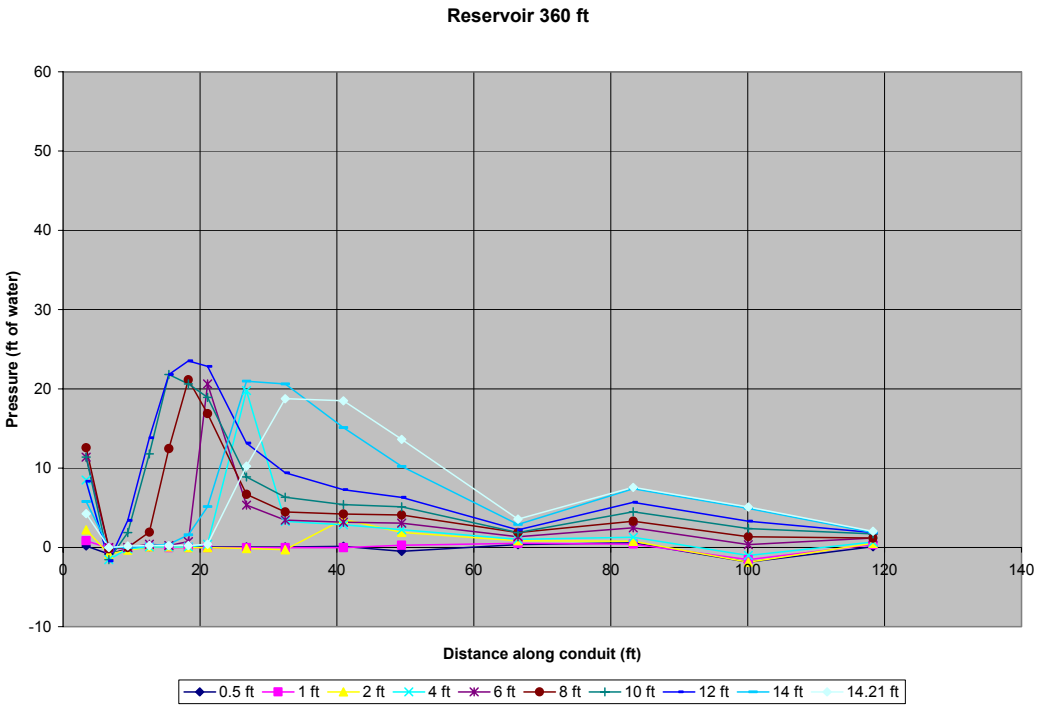

Figure 33d: Upper conduit pressures, reservoir 360 ft.

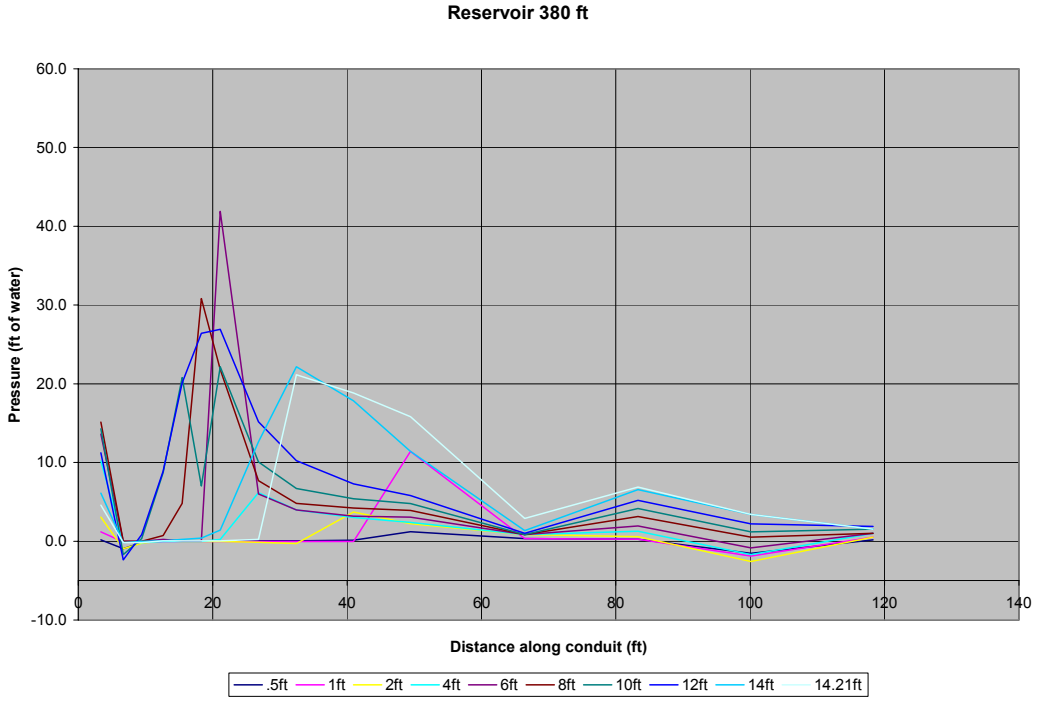

Figure 33e: Upper conduit pressures, reservoir 380 ft.

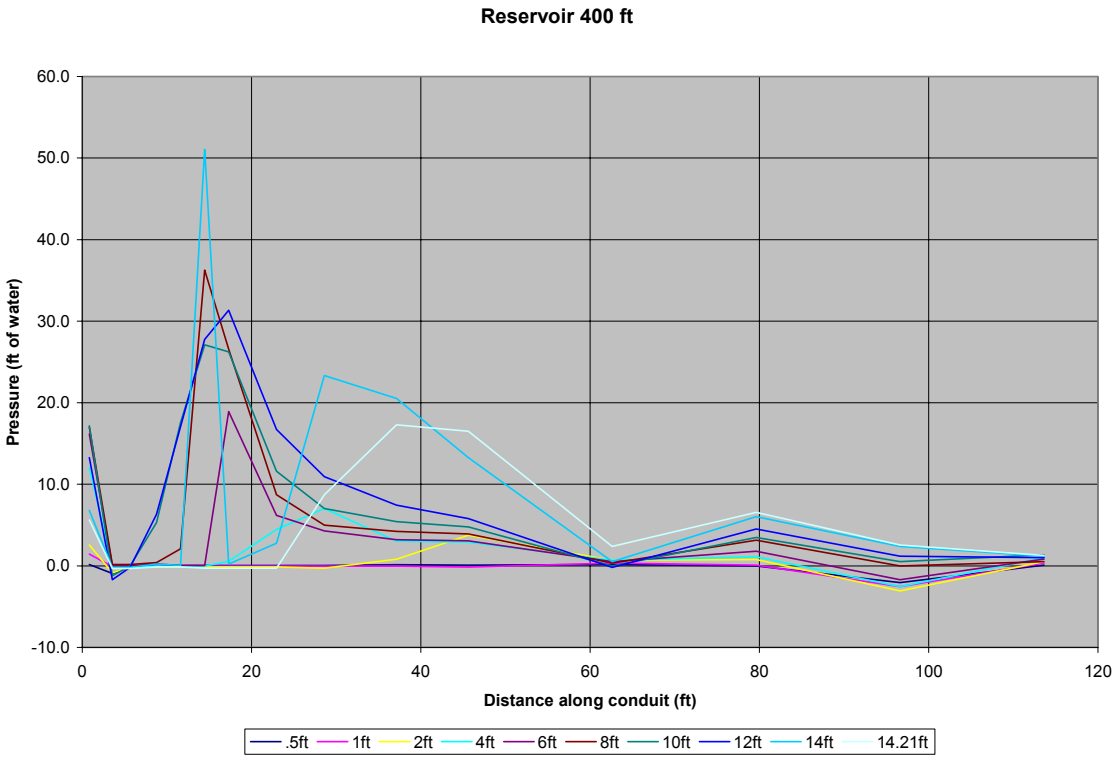

Figure 33f: Upper conduit pressures, reservoir 400 ft.

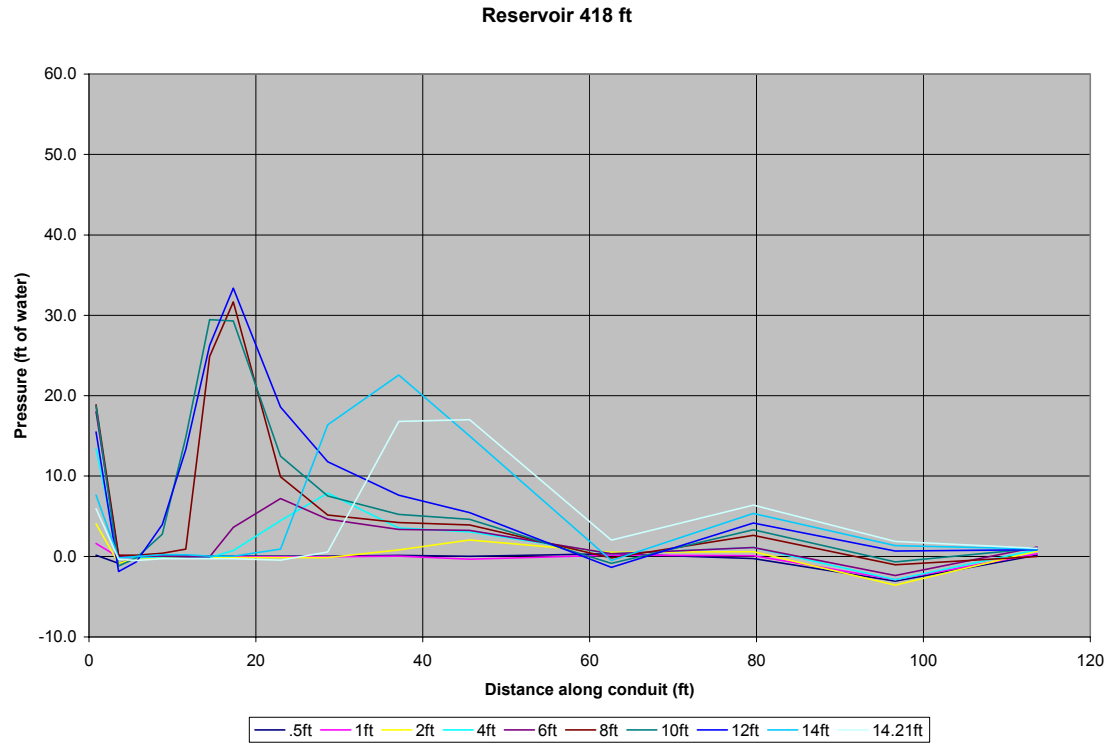

Figure 33g: Upper conduit pressures, reservoir 418 ft.

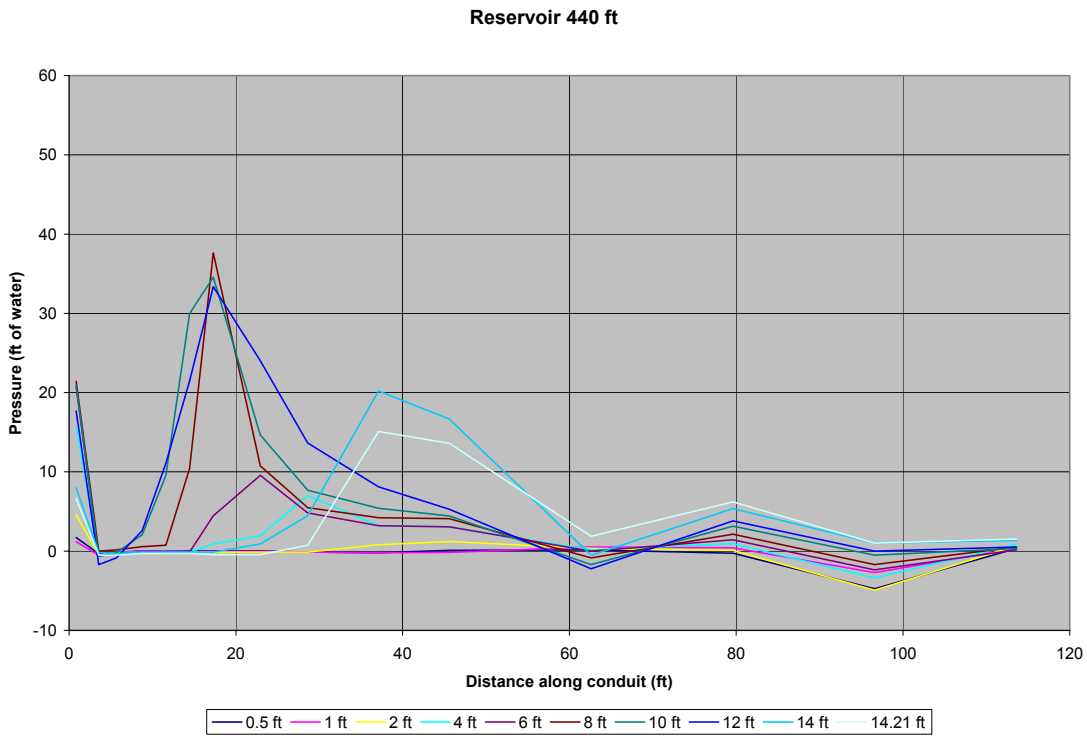

Figure 33h: Upper conduit pressures, reservoir 440 ft.

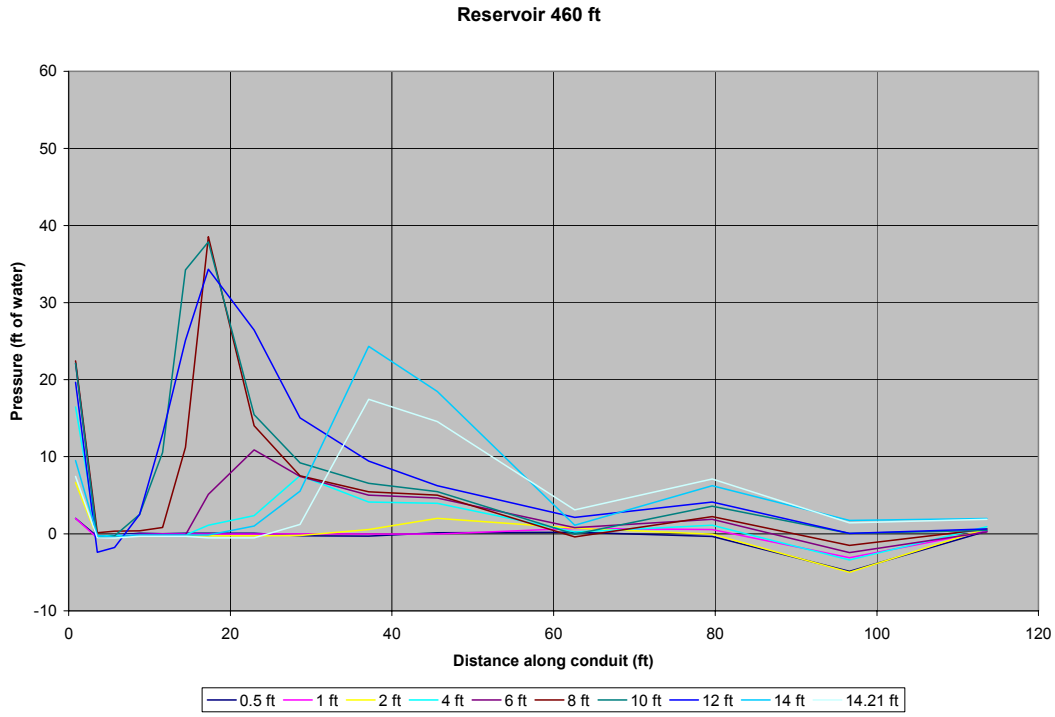

Figure 33i: Upper conduit pressures, reservoir 460 ft.

Figure 33(a-i): Upper conduit pressures for a range of reservoir elevations.

4. Discussion

The 1:17 scale hydraulic model has given a good representation of many features of the proposed outlet works expansion at Folsom Dam. Its design is that of a sectional model so there are definite limitations in its application to some of the three-dimensional flows that result, particularly in the stilling basin. Scale factors were chosen based on initial meetings with the COE and their consultants in order to provide the least amount of scale effects possible in the areas of interest. The combination of existing modeling data and experience with model/prototype conformance as well as physical limitations of the laboratory space and pumping capacity resulted in selecting a scale of 1 to 17.

Model construction also offered many challenges, specifically in the construction of the intake structures. Several attempts to form the intakes from clear acrylic proved unsuccessful with stress cracks occurring as the acrylic cured. The solution was to use clear PVC, a slightly softer and less brittle material, however it doesn't offer the same visibility and definitely required significant exterior bracing and stiffening supports. The workmanship was generally good with some additional work required at the flanged joints to ensure no offsets. Numerous piezometer taps were installed along the crown centerline and one side centerline, and a few additional taps near the upper corners. The pressure coefficient data collected was very consistent and essentially constant for a wide variety of different reservoir heads and gate openings. A couple points warrant a mention concerning the pressure coefficient data: 1) aspect ratio of the intake appears to have a significant impact on the coefficient values, and 2) the sloping dam face is an important factor. The original design was based on the HDC Hydraulic Design Chart 211-1/1. This combined elliptical entrance was based originally on ES802 test data with an aspect ratio h/w=1.765. The new conduit aspect ratios at Folsom are 1.501 for the upper conduit, and 1.286 for the lower conduit. In addition, the face of the dam is sloped on a 1:10 ratio or 5.71-degrees. The lower conduit is approaching square and the pressure drop coefficient along the crown centerline exceed a value of 1 for a good portion of the length of the intake. The side curves matched the HDC data quite well for both upper and lower conduits. Results from the mathematical model (FLOW-3D) verified the model results for a upper straight conduit configuration. With good agreement on the straight conduit, the skewed geometry was also tested in the computer model. The results for the skewed conduit were essentially identical to the straight results. Due to the good agreement between the 1:17 model results and the FLOW-3D results, we believe the skewed predictions to be accurate. The 1:36 model results for the skewed conduits (in progress) have shown no reason to question the computer model results.

Flow conditions in the conduits vary from pressurized flow upstream from the regulating gate to free flow conditions in the downstream section. This design features very high velocities, forcing careful design and maybe more importantly construction of the conduits. Cavitation potential exists for flow conditions such as seen in the Folsom outlet works. The intake curves have been shown to have no cavitation potential based on their shape alone. However, additional studies are being performed to evaluate the size of singular offsets or irregularities that may cause localized cavitation damage. Analysis and model measurements on flows through the gate chambers, including the gate slot areas, have shown no probability for cavitation damage. The free-flow conduits downstream from the gate do have some areas on the

invert where measured model pressures are subatmospheric. Additional piezometer taps were placed around the lowest pressure location to verify the piezometer tap installation. Figures 34 and 35 show that the low pressures were verified, and not resultant of a poor tap installation.

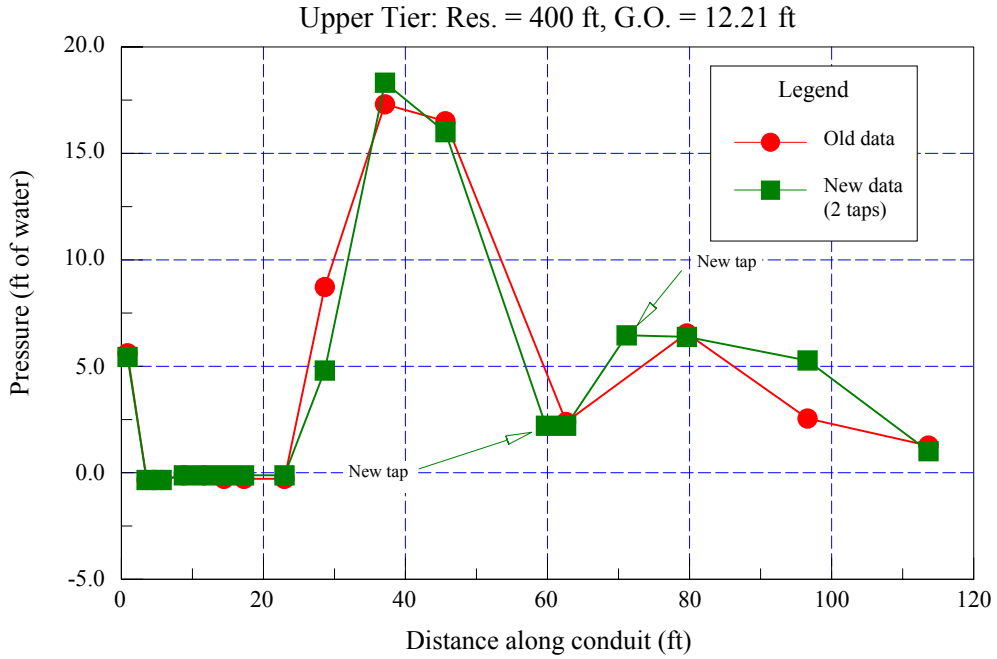

Figure 34: Upper tier, additional 2 piezometer taps along invert at location of lowest pressures.

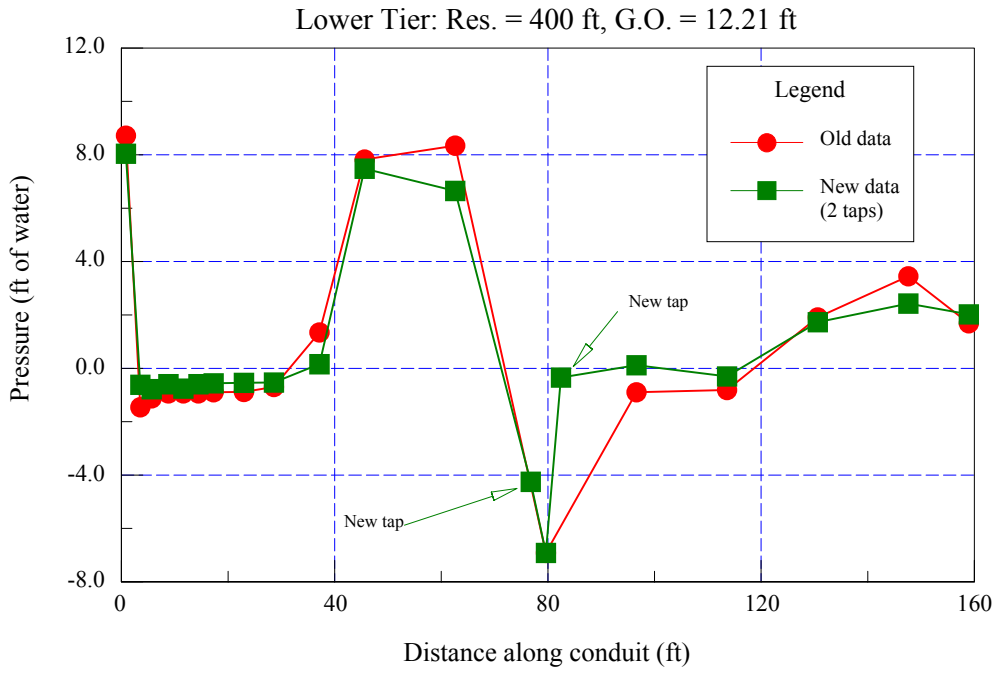

Figure 35: Lower tier, additional 2 piezometer taps along invert at location of lowest pressures.

The aeration that takes place at the beginning of this expanded conduit is adequate to preclude cavitation damage; however Reclamation would still recommend a severe finishing criteria for the concrete surfaces in this area, (0.5 in offset, 1:8 slope). There appears to be no indication of problems with the spillway surfaces near the conduit exits with the reduced-size eyebrow. Reduced air flow into the vents does not result in a proportional reduction in pressures in the conduit, this reflects the oversized conduit's ability to satisfy air demand from the downstream end of the conduit.

Vortex formation was very strong in the preceding study of the 9.33-ft by 16.25-ft gates for full open gate flow. The observations of these vortices in the model lead us to evaluate possible shortcomings in the model design, mostly regarding the size of the headbox and the baffling of flow entering the box. Prior studies have shown that slight asymmetries in the approach flow can be responsible for vortex formation. The vortices observed vented with air downstream from the gate but the vortex core then traveled upstream and on occasion entered the headbox. These vortices did not head toward the free surface, but rather would tend to attach on a sidewall or on the dam face fairly near the intake structure. With the new gate configuration, it was expected that there may still be similar vortex formation as no modifications were done to the headbox, only the size of the intakes.

Vortices were observed in the upper conduit when the gates were full open, but were not observed in the lower conduit under similar conditions. One possible explanation for this is again the aspect ratio of the lower gate is approaching 1.0 or a square shape. Installation of a series of straightening vanes in the headbox surrounding the upper intake eliminated the vortex formation in that intake as well. The approach length of the box (85- to 95-ft) however is still not long enough to simulate the distance out in the reservoir that a normal submergence type vortex would form. The 1 to 36 model is expected to provide additional data concerning vortex formation.

Dynamic pressure fluctuations within the stilling basin were expected to vary considerably from the current design, possibly requiring additional reinforcement or modifications. The stilling basin is a typical hydraulic jump basin for an overflow spillway. There is a considerable depth of tailwater within the basin and the current 5-ft by 9-ft gates have discharged into the basin pool without noticeable damage since the dam's construction. The new outlet design results in larger jets entering the basin that in turn require longer distances to disperse to similar levels of energy as the current arrangement. Large amounts of data were collected to document the dynamic pressures on the stilling basin floor in the vicinity of the jet impact.

There are several ways to analyze and present the data to assist designers in the interpretation of the results. Basic statistics were presented in Table 4 for the most critical design condition identified by the COE. It can be seen that the maximum pressures are many standard deviations (up to 10) away from the mean, yielding a skewed (non-Gaussian) probability distribution. An example of the variation of the probability distributions between actual data and a Gaussian distribution with the same mean and standard deviation are shown in figure 36. These skewed distributions are also typical of pressure fluctuations found in hydraulic jumps (Toso and Bowers, 1987). Further laboratory investigations also yielded that the maximum pressure pulses

were at higher frequencies (>300 Hz), so it seems unlikely that there will be high spatial correlations of these maximum pressures.

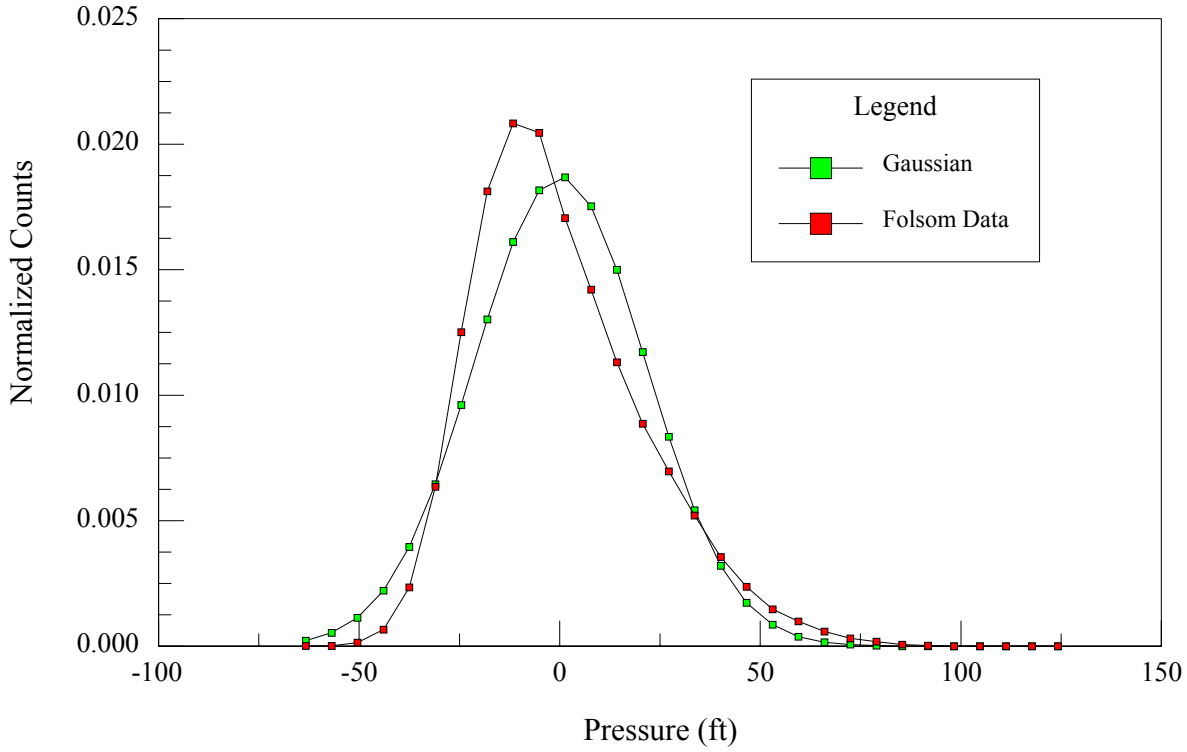

Figure 36: Data distribution compared to a Gaussian distribution with identical mean and standard deviation, upper conduit, 100% gate, TW = 160 ft, piezometric head +62 ft.

Frequency analysis of the pressure fluctuations show that there are no significant periodic frequencies, see figure 37.

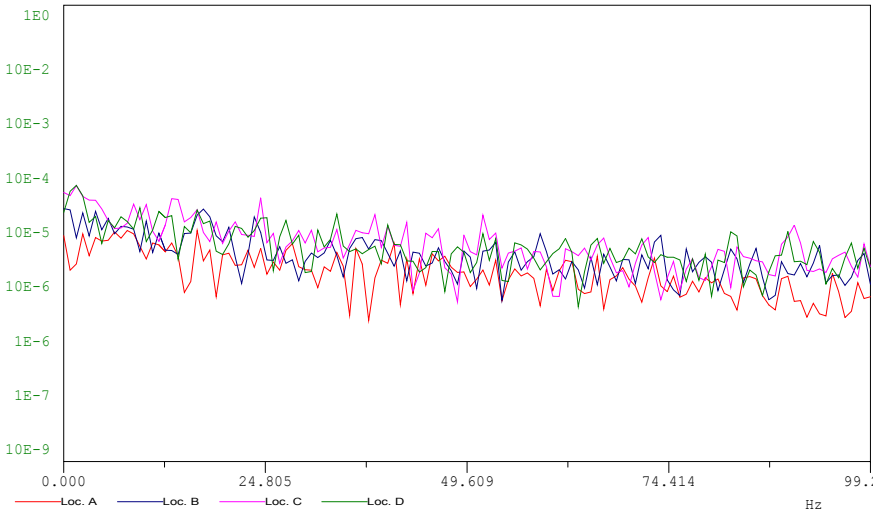

Figure 37: Power spectra for dynamic pressure signals for upper conduit at full open, reservoir 418 ft, TW = 160 ft.

The analysis can be taken a step further to look at correlation or coherence between pairs of

transducer outputs to check for spatial correlation. The coherence is closely related to the cross spectrum and is given by equation 11:

$$\hat{\gamma}_{xy}^2(f) = \frac{\left|\hat{S}_{xy}(f)\right|^2}{\hat{S}_x(f)\,\hat{S}_y(f)} \tag{11}$$

where $\hat{S}_{xy}(f)$ is the cross spectral density, and $\hat{S}_x(f)$ and $\hat{S}_y(f)$ are the power spectra of the two transducer outputs of choice. The coherence is a real-valued quantity and is bounded between 0 and 1. The coherence is the frequency domain counterpart of the square of the correlation coefficient in basic time series statistics. An ideal, no noise, linear system will give $\gamma_{xy}^2 = 1$. This results in a theoretical coherence of unity at all frequencies for a linear system (Input=Output*Constant + Constant). When the coherence is less than unity, the system contains nonlinear elements, or a major source of noise. The main goal of these analyses is to look at possible coherence between transducer outputs for all flow cases and all combinations of transducers. One would expect high values of coherence as a function of frequency if two signals are similar in composition. This means if a flow field has a peaked response at 25 Hz, and this response was correlated over the distance of separation between two transducers, that the coherence between the two signals at that frequency would approach 1. In a physical sense, the pressure pulse at that specific frequency is affecting an area covered by the two transducers. If you have transducers at several different spacings, you can effectively look at the areal extent of the pressure fluctuations of interest. The value of the coherence is also degraded by noise in the system. Flow-induced phenomena are typically not mono-frequency unless a structural resonant frequency has been excited, or some type of periodic excitation such as a von Karman vortex street is formed. Observations of the power spectra of individual transducer outputs (figure 36) did not yield strong periodic components, but tended toward more broadband general noise. The coherence results presented show that the highest values of coherence are for the smallest transducer spacing, 4.25 ft in the prototype. These values tended to approach a maximum of about 0.75 and for most cases were limited to fairly small bands of frequency. Coherence at frequencies above 100 Hz was almost always below a value of 0.5. Values of coherence near 1 are not present at any frequency for any flow condition or transducer spacing. This would yield the result that the maximum pressure pulses are not well correlated, even over the shortest distances (4.25 ft) in the model. Previous investigations have shown that the peak values of dynamic pressures are generated by high frequency events (usually greater than 300 Hz). Figures 38-49 show coherence over a frequency range of 250 Hz, for a variety of test conditions and transducer spacing. No coherence >0.8 was present for any test condition.

Correlation gives a similar result in the time domain, however a single value of correlation for an entire time series has the effect of time averaging and so low values of correlation are to be expected in any type of a non-linear system. Figures 50-52 and Tables 5-7, show correlation results for the critical condition.

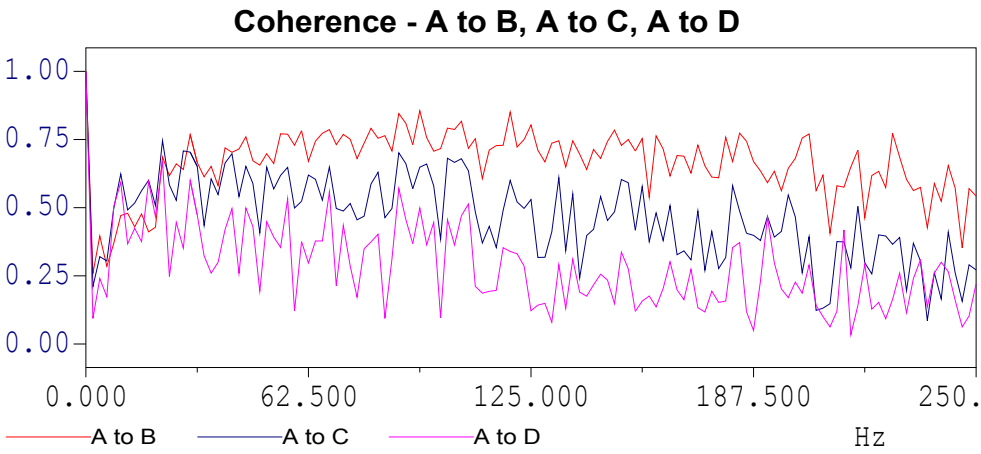

a) Lower outlet 100%, res. 418 ft, no tailwater

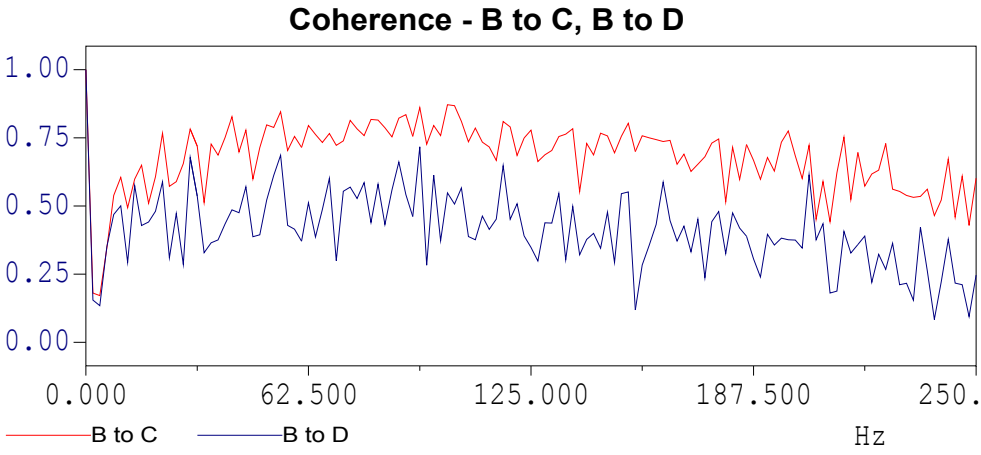

b) Lower outlet 100%, res. 418 ft, no tailwater

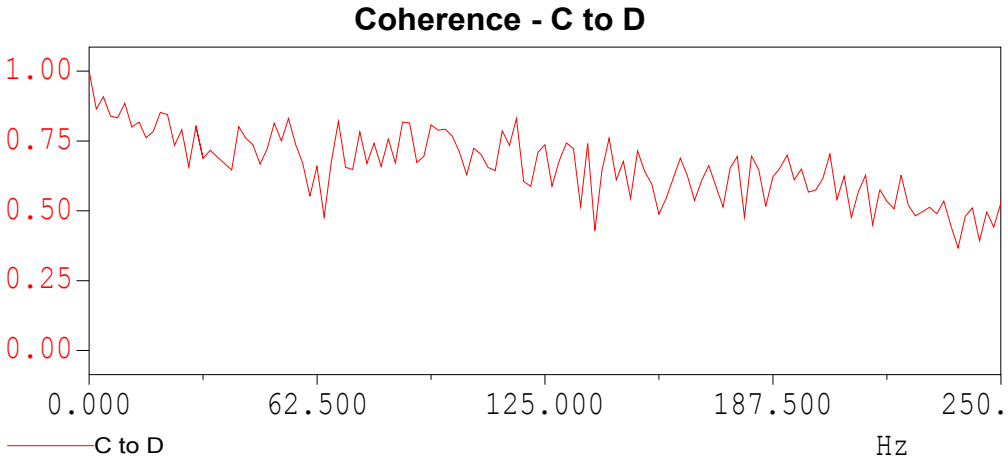

c) Lower outlet 100%, res. 418 ft, no tailwater

Figure 38: Lower outlet 100%, res. 418 ft, no tailwater.

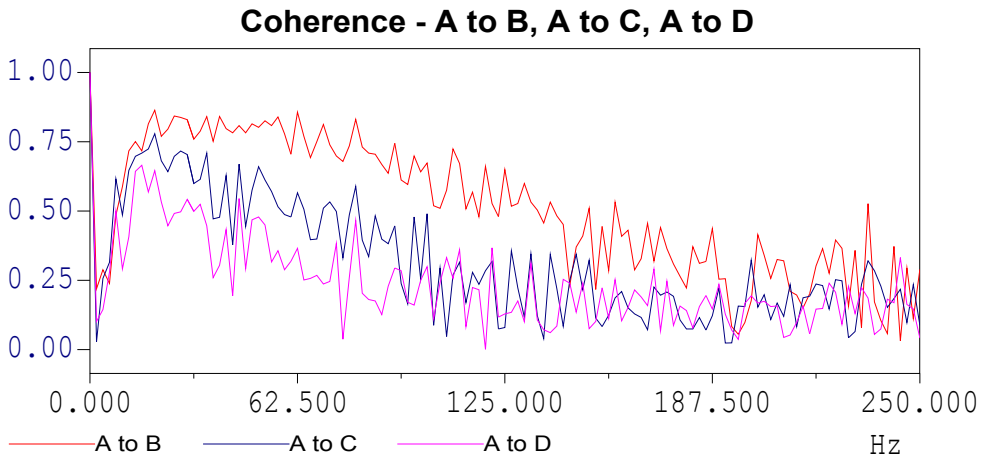

a) Lower outlet 100%, res. 418 ft, tailwater 160 ft.

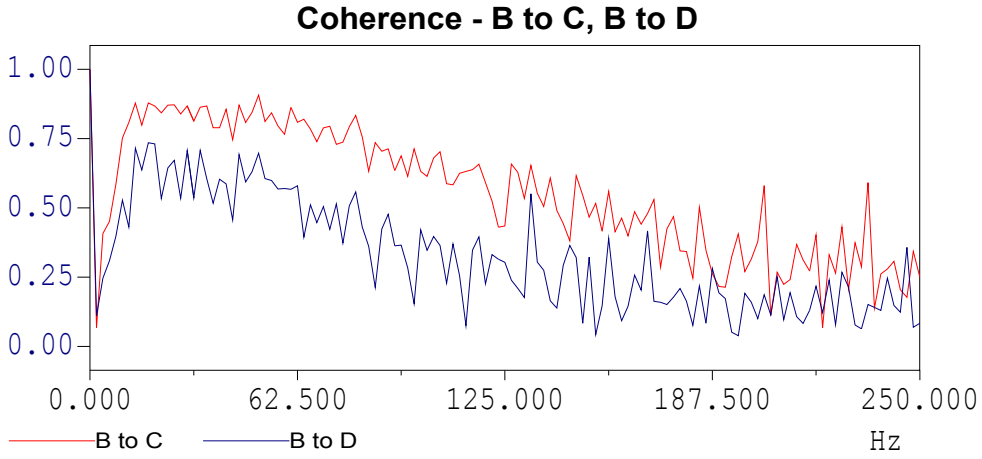

b) Lower outlet 100%, res. 418 ft, tailwater 160 ft.

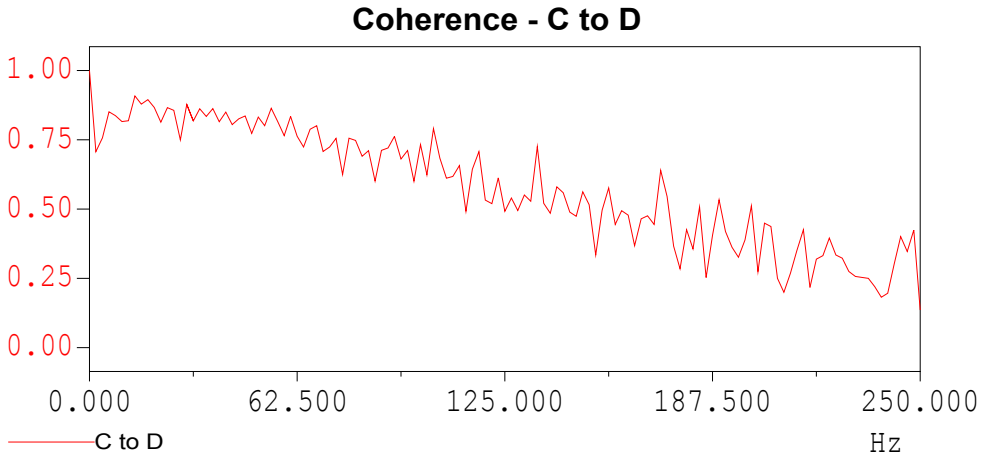

c) Lower outlet 100%, res. 418 ft, tailwater 160 ft.

Figure 39: Lower outlet 100%, res. 418 ft, tailwater 160 ft.

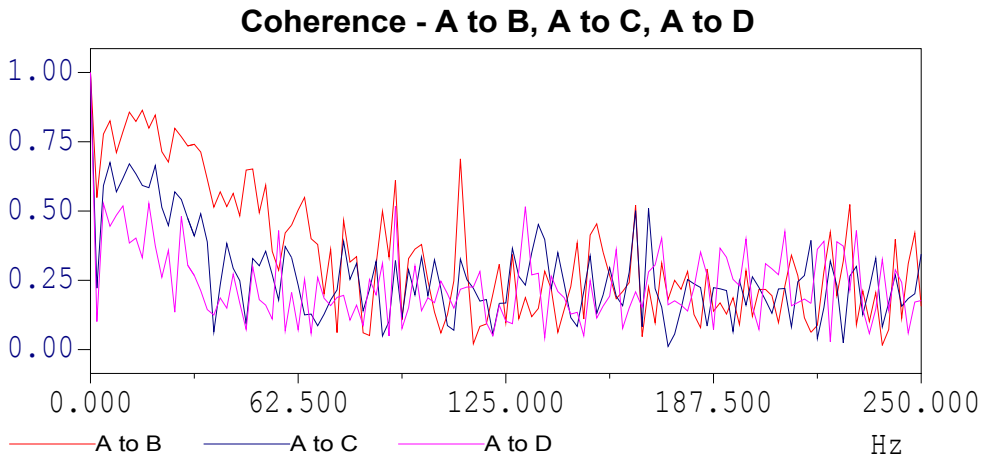

a) Lower outlet 100%, res. 418 ft, tailwater 180 ft.

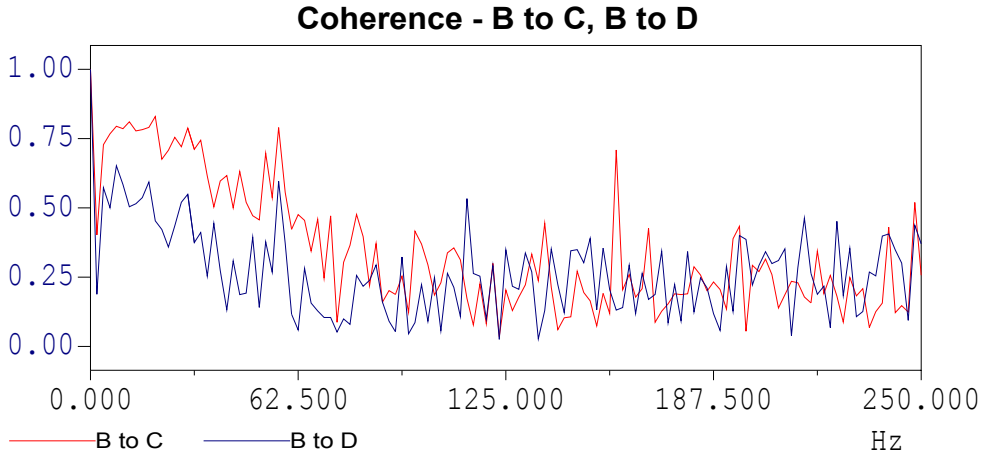

b) Lower outlet 100%, res. 418 ft, tailwater 180 ft.

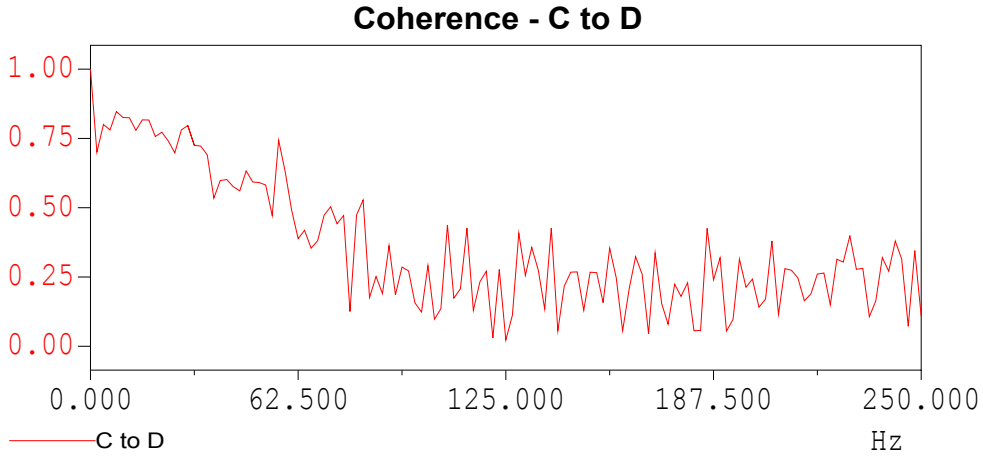

c) Lower outlet 100%, res. 418 ft, tailwater 180 ft.

Figure 40: Lower outlet 100%, res. 418 ft, tailwater 180 ft.

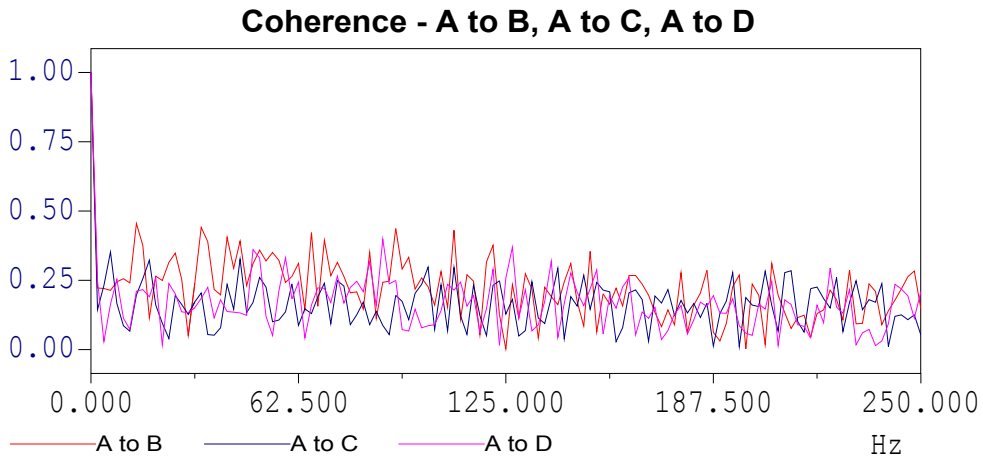

a) Upper outlet 100%, res. 418 ft, no tailwater.

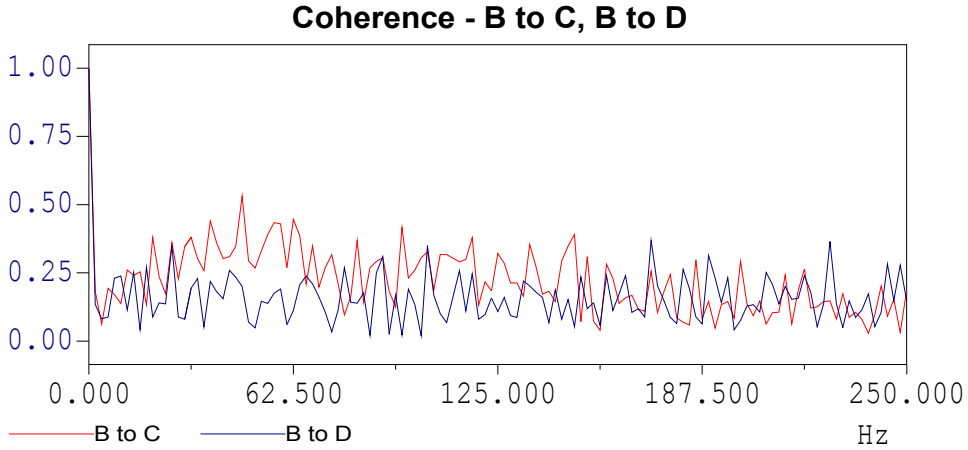

b) Upper outlet 100%, res. 418 ft, no tailwater.

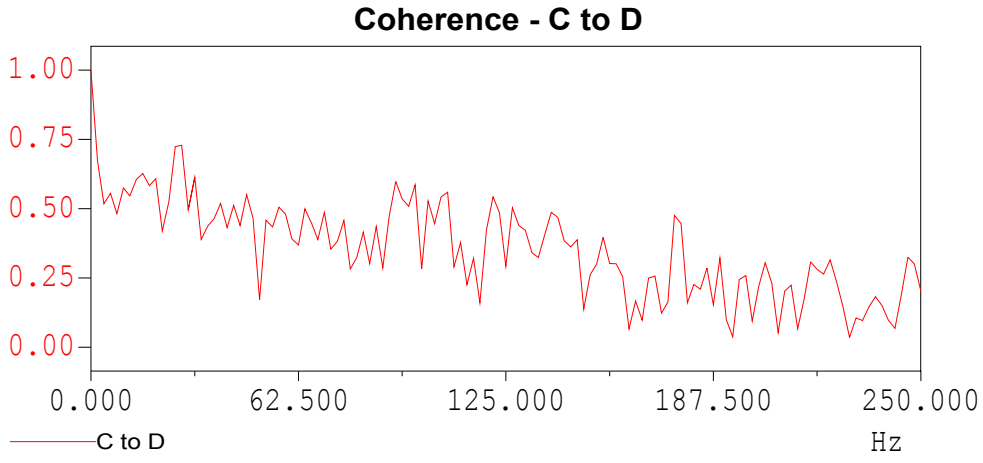

c) Upper outlet 100%, res. 418 ft, no tailwater, coherence location C to D.

Figure 41: Upper outlet 100%, res. 418 ft, no tailwater.

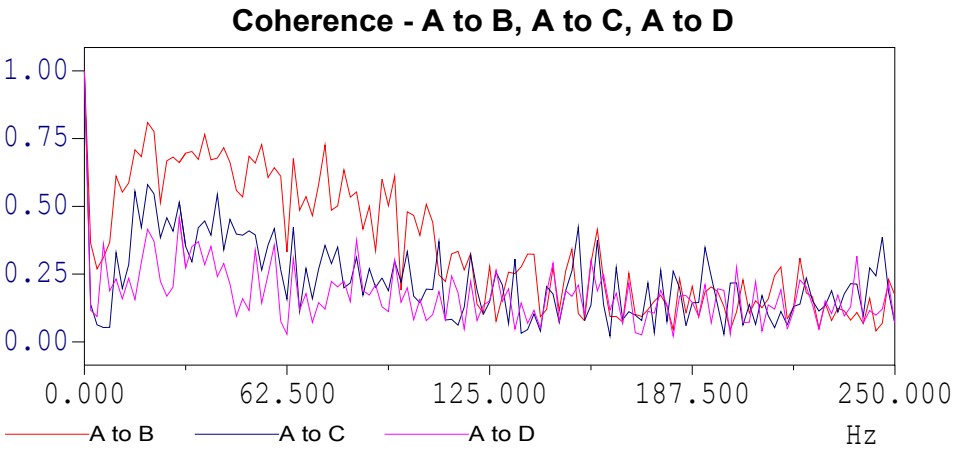

a) Upper conduit 100%, res. 418 ft, tailwater 160 ft.

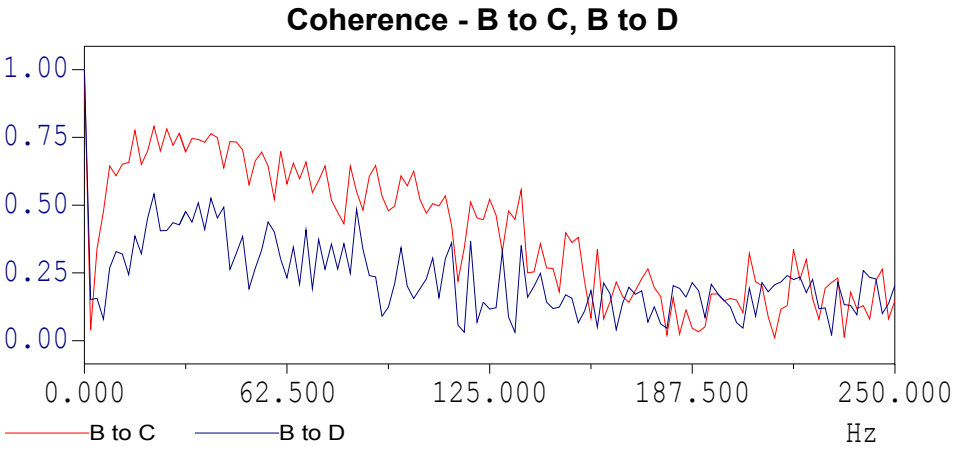

b) Upper conduit 100%, res. 418 ft, tailwater 160 ft.

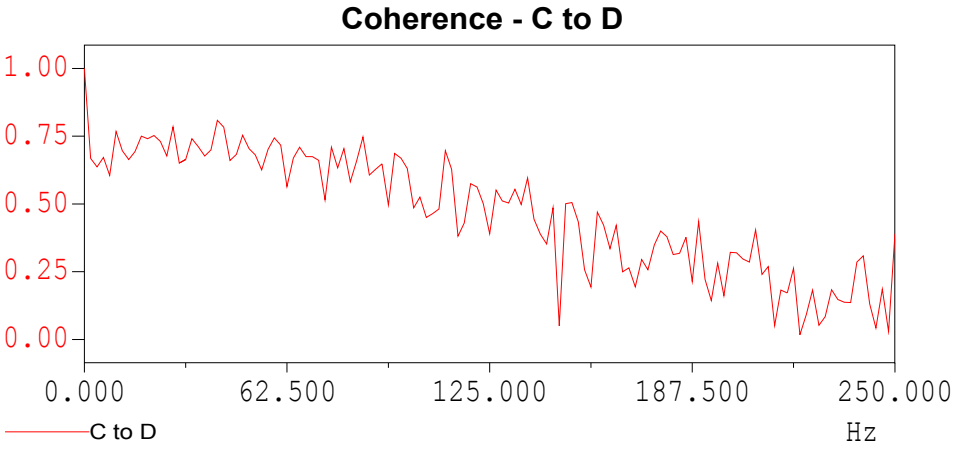

c) Upper conduit 100%, res. 418 ft, tailwater 160 ft**.**

Figure 42: Upper conduit 100%, res. 418 ft, tailwater 160 ft, coherence between transducers.

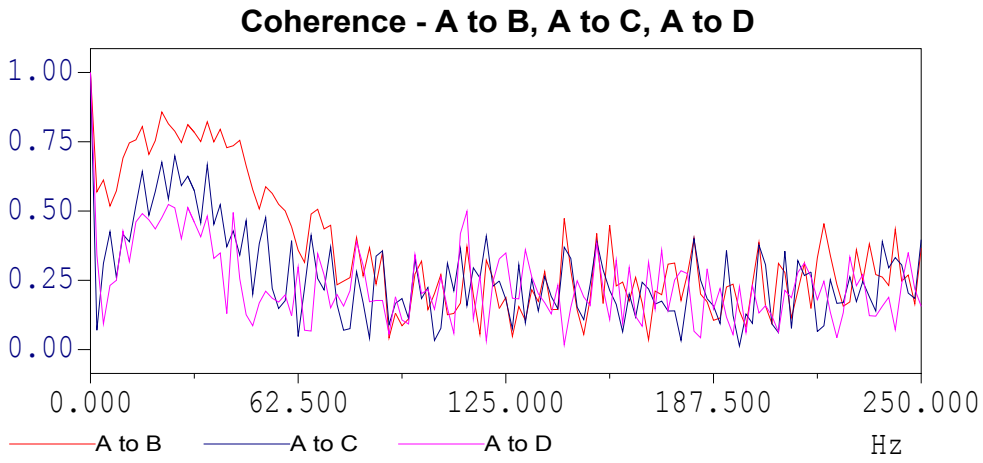

a) Upper conduit 100%, res. 418 ft, tailwater 180 ft**.**

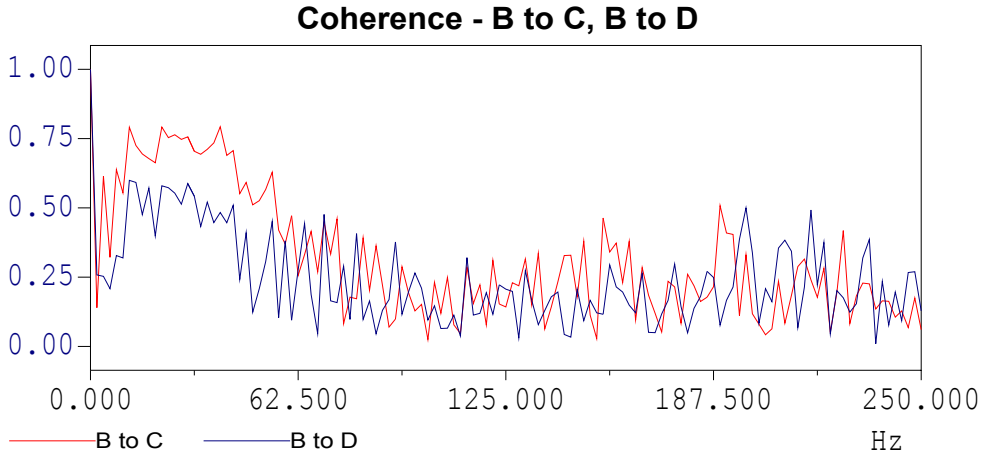

b) Upper conduit 100%, res. 418 ft, tailwater 180 ft.

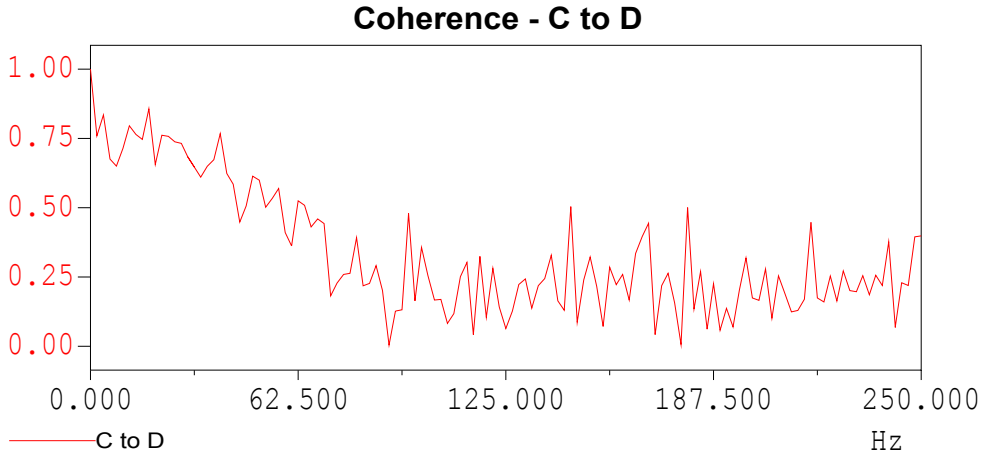

c) Upper conduit 100%, res. 418 ft, tailwater 180 ft.

Figure 43: Upper conduit 100%, res. 418 ft, tailwater 180 ft, coherence between transducers.

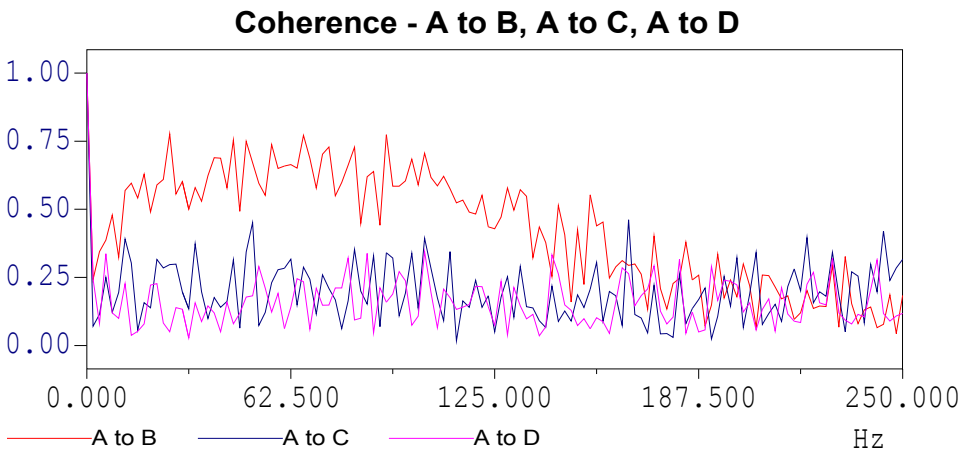

a) Upper and lower conduits 100%, res. 418 ft, no tailwater.

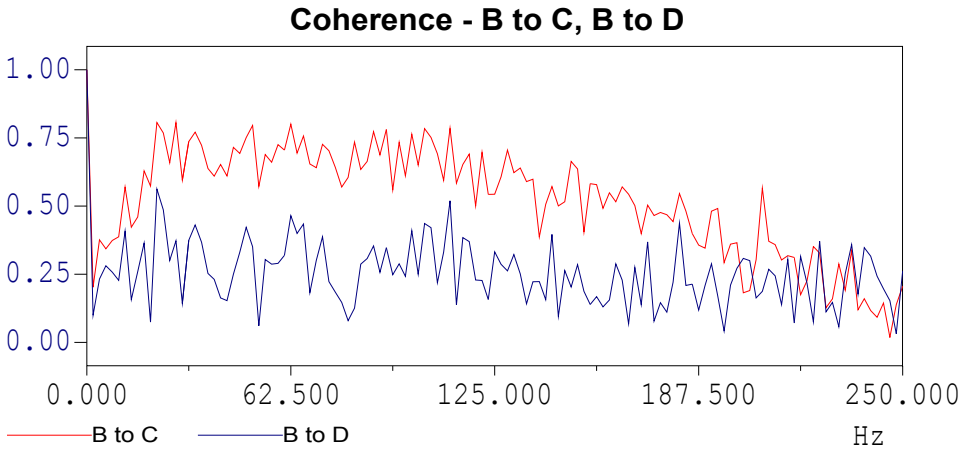

b) Upper and lower conduits 100%, res. 418 ft, no tailwater.

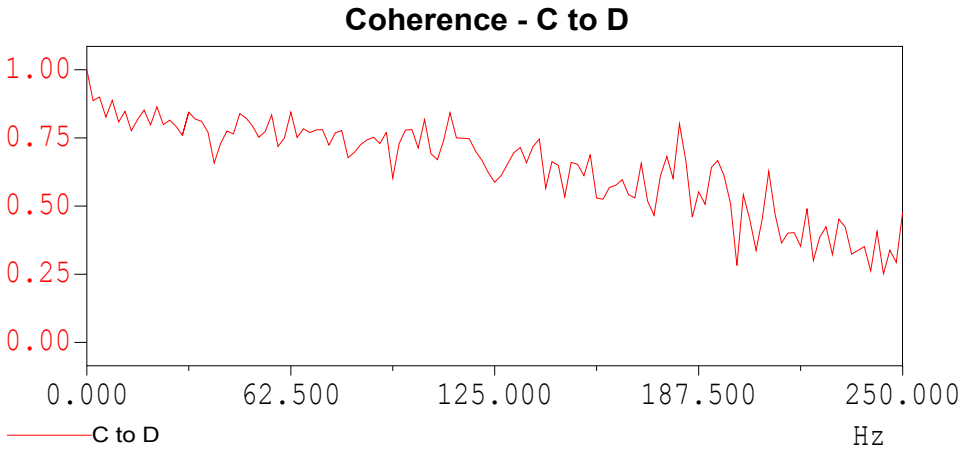

c) Coherence between sensors, location C and D.

Figure 44: Upper and Lower conduits operating, 100 % gate, res. 418 ft, no tailwater.

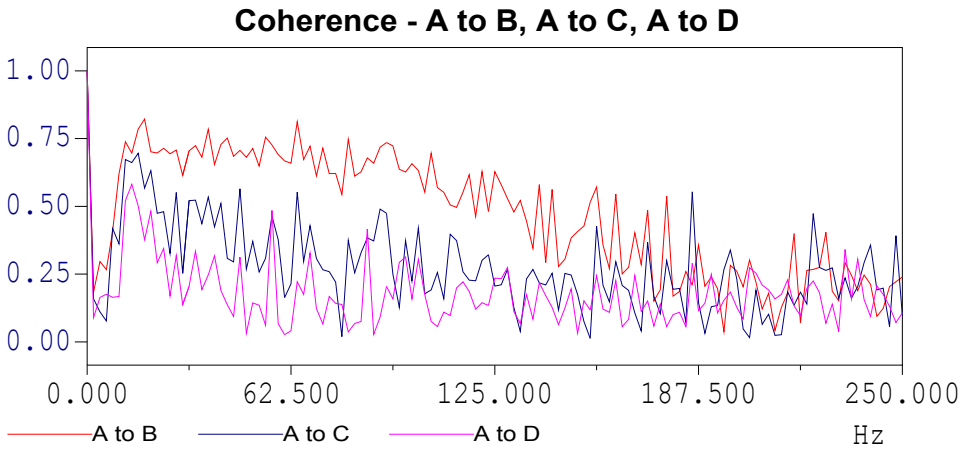

a) Upper and lower conduits 100%, res. 418 ft, tailwater 160 ft

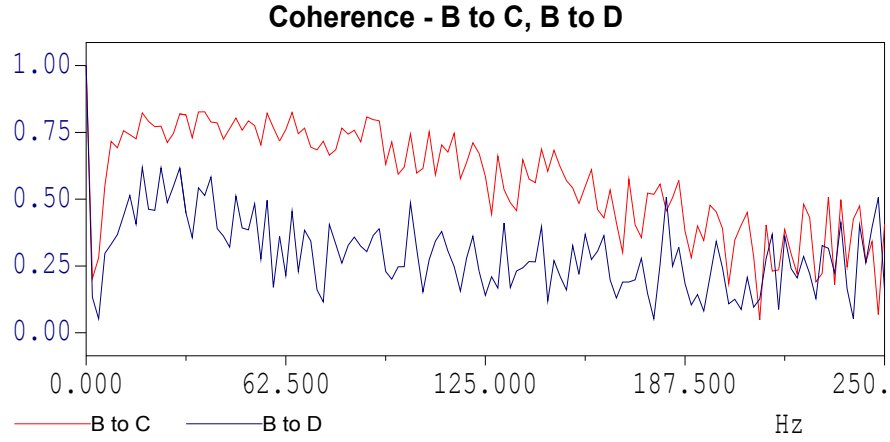

b) Upper and lower conduits 100%, res. 418 ft, tailwater 160 ft.

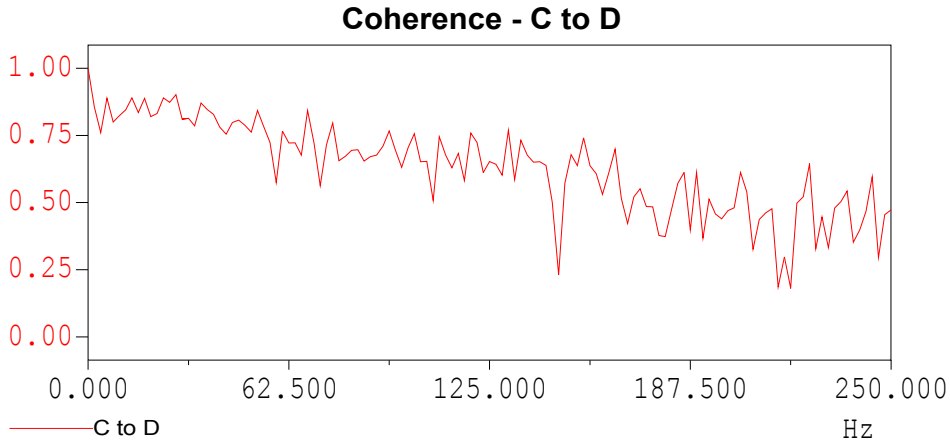

c) Upper and lower conduits, 100%, res. 418 ft, tailwater 160 ft.

Figure 45: Upper and Lower conduits operating, 100% gate, res. 418 ft, tailwater 160 ft.

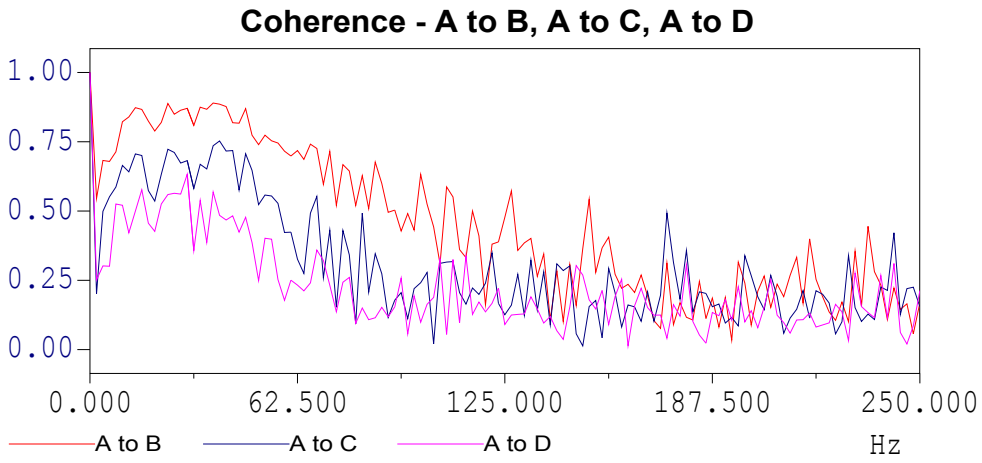

a) Upper and lower conduits 100%, res. 418 ft, tailwater 180 ft**.**

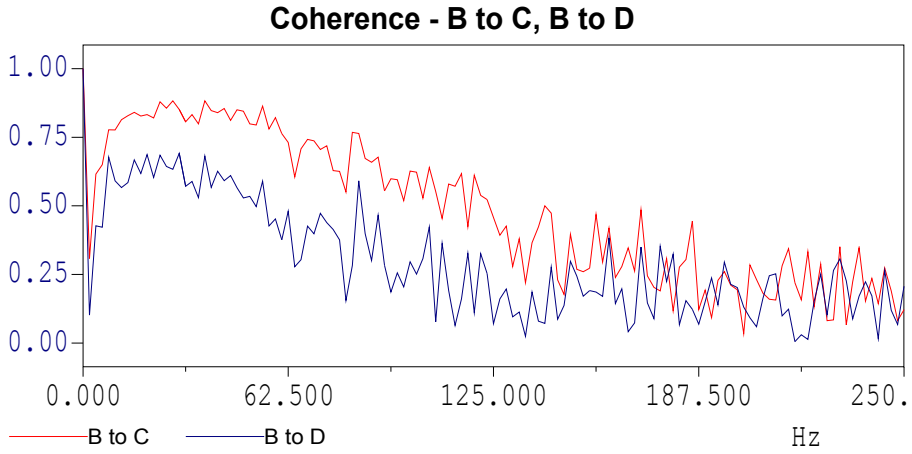

b) Upper and lower conduits 100%, res. 418 ft, tailwater 180 ft.

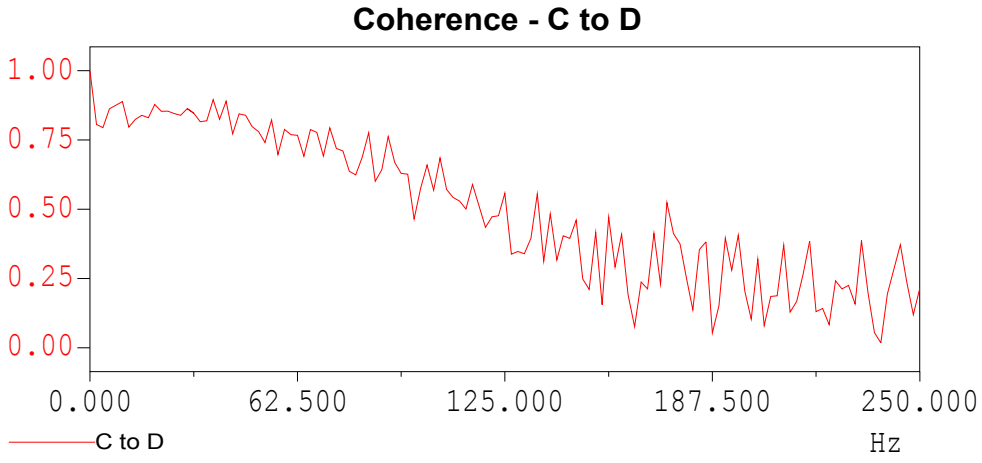

c) Upper and lower conduits 100%, res. 418 ft, tailwater 180 ft.

Figure 46: Upper and Lower conduits operating, gate 100%, res. 418 ft, tailwater 180 ft, coherence.

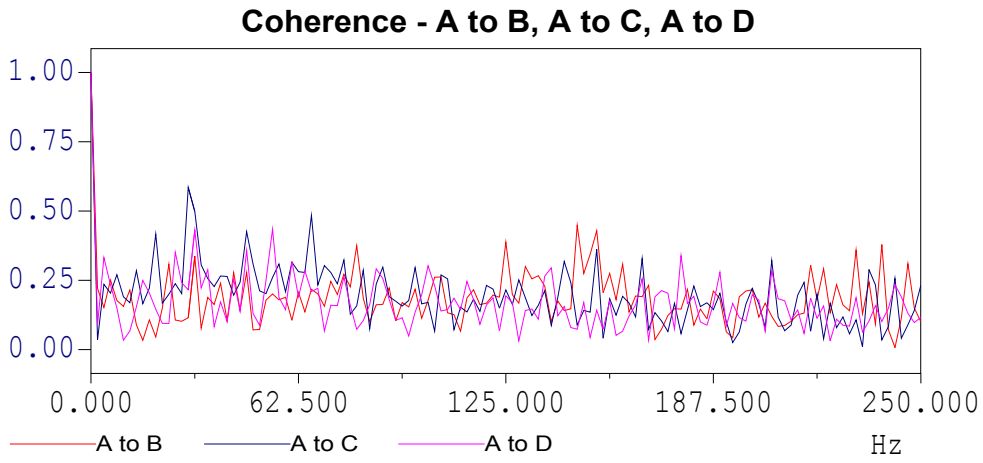

a) Spillway flow only, no tailwater.

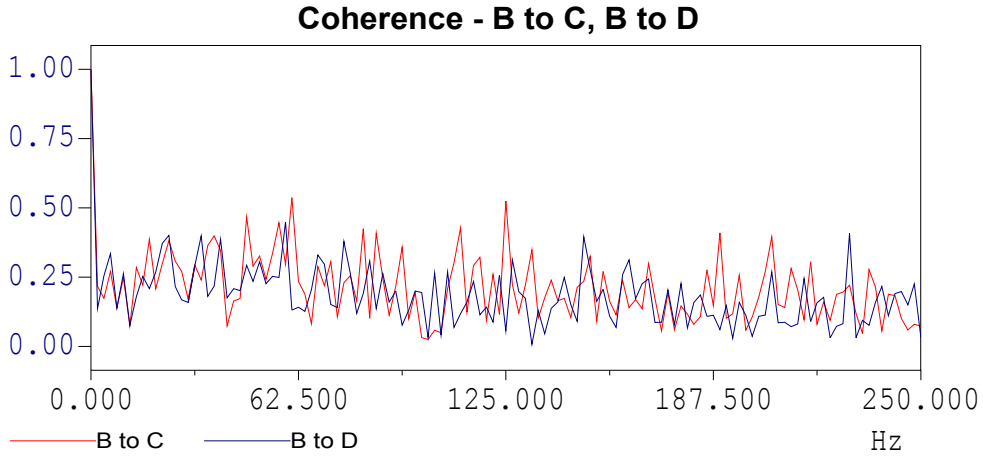

b) Spillway flow only, no tailwater.

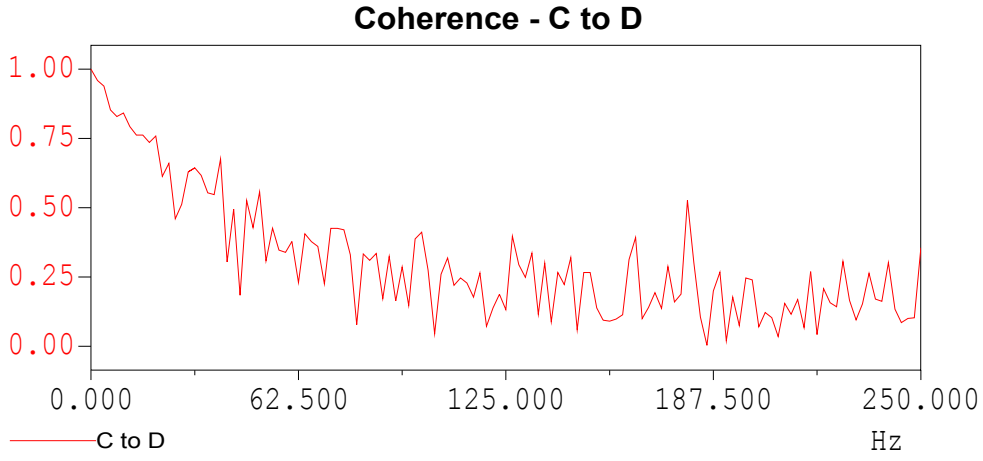

c) Spillway flows only, no tailwater.

Figure 47: Spillway flow only, no tailwater, coherence.

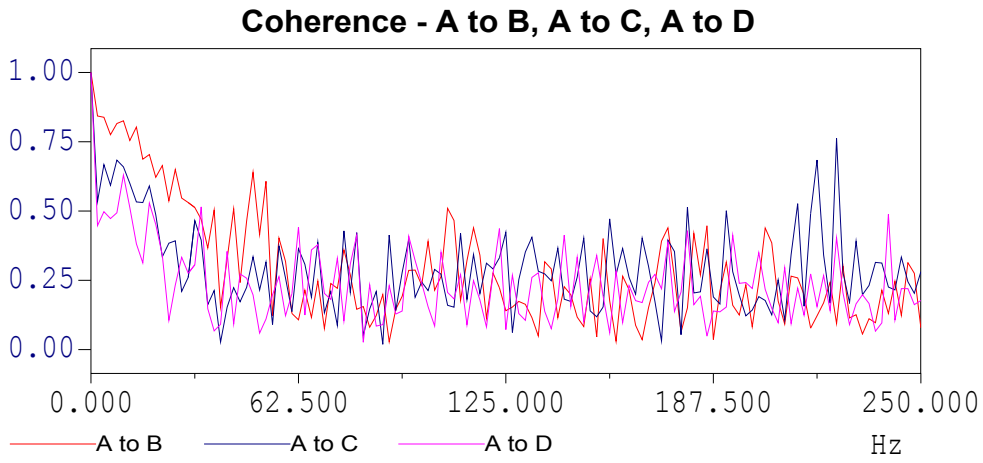

a) Spillway flow only, tailwater 160 ft.

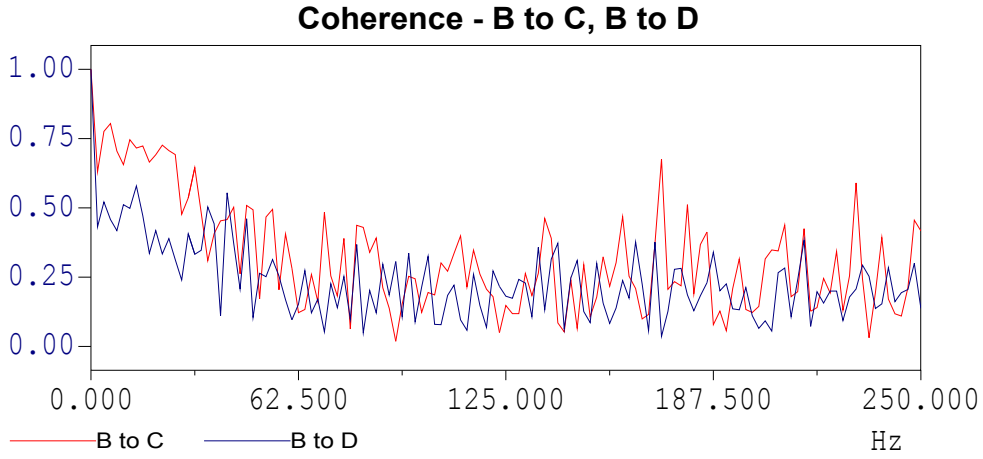

b) Spillway flow only, tailwater 160 ft.

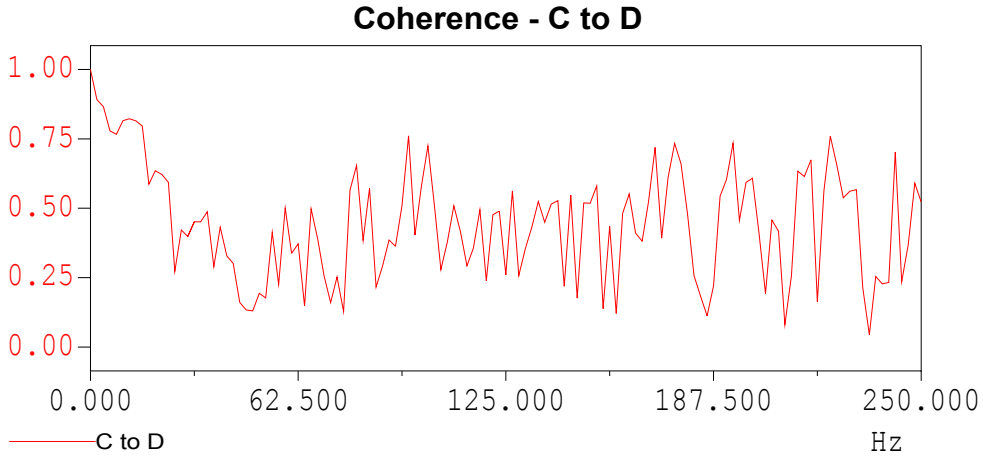

c) Spillway flow only, tailwater 160 ft.

Figure 48: Spillway flow only, tailwater 160 ft, coherence.

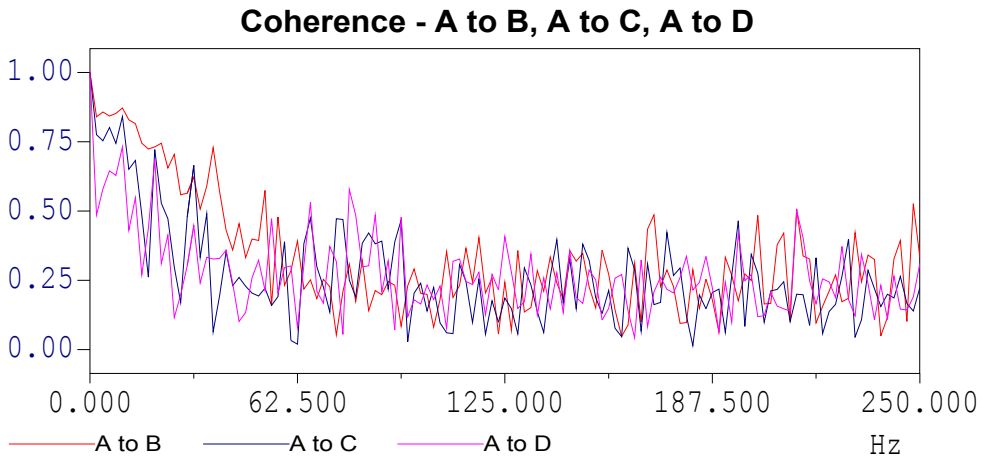

a) Spillway flow only, tailwater 180 ft.

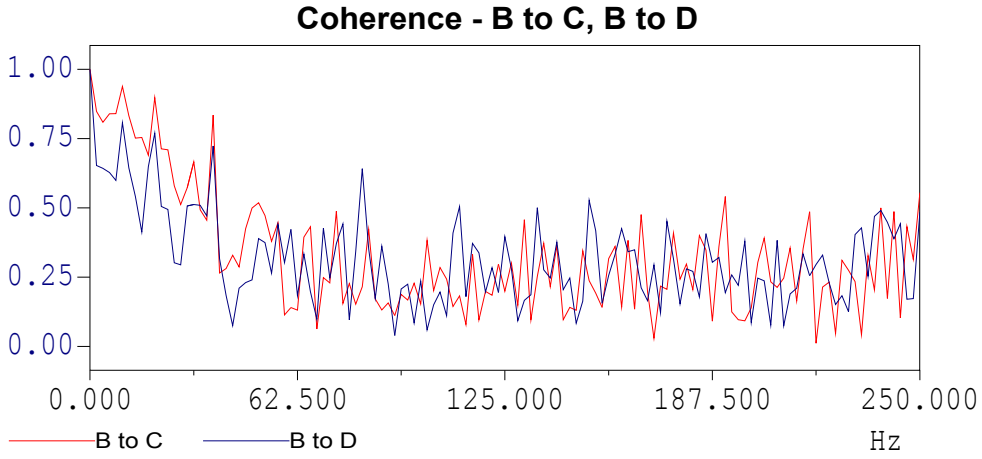

b) Spillway flow only, tailwater 180 ft.

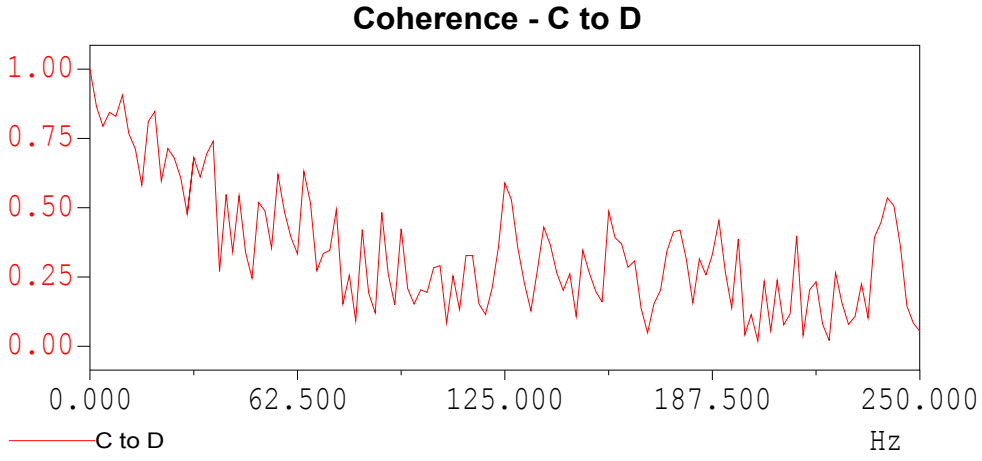

c) Spillway flow only, tailwater 180 ft.

Figure 49: Basin dynamic pressure coherence, spillway flow only, tailwater 180 ft.

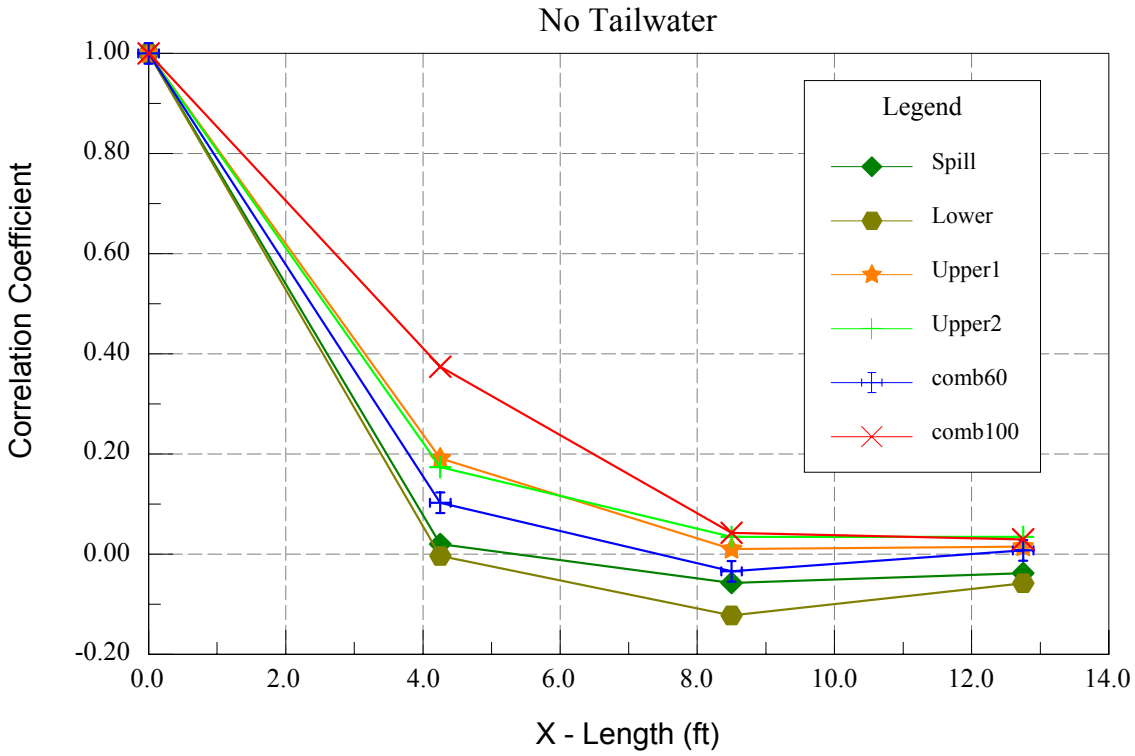

Figure 50: Spatial correlation plot for developing correlation lengths in Table 5. All discharges were approximately equal except for the combined outlets at 100%. Reservoir was at 418 for all outlet works flows.

Table 5: Correlation lengths for no tailwater condition resulting from integration of curves in Figure 44

Location	Correlation Length (ft)
Spillway only	2.34
Lower outlet (100%)	2.75
Upper outlet (100%) run 1	2.67
Upper outlet (100%) run 2	2.73
Combined outlets (60%)	2.33
Combined outlets (100%)	3.70

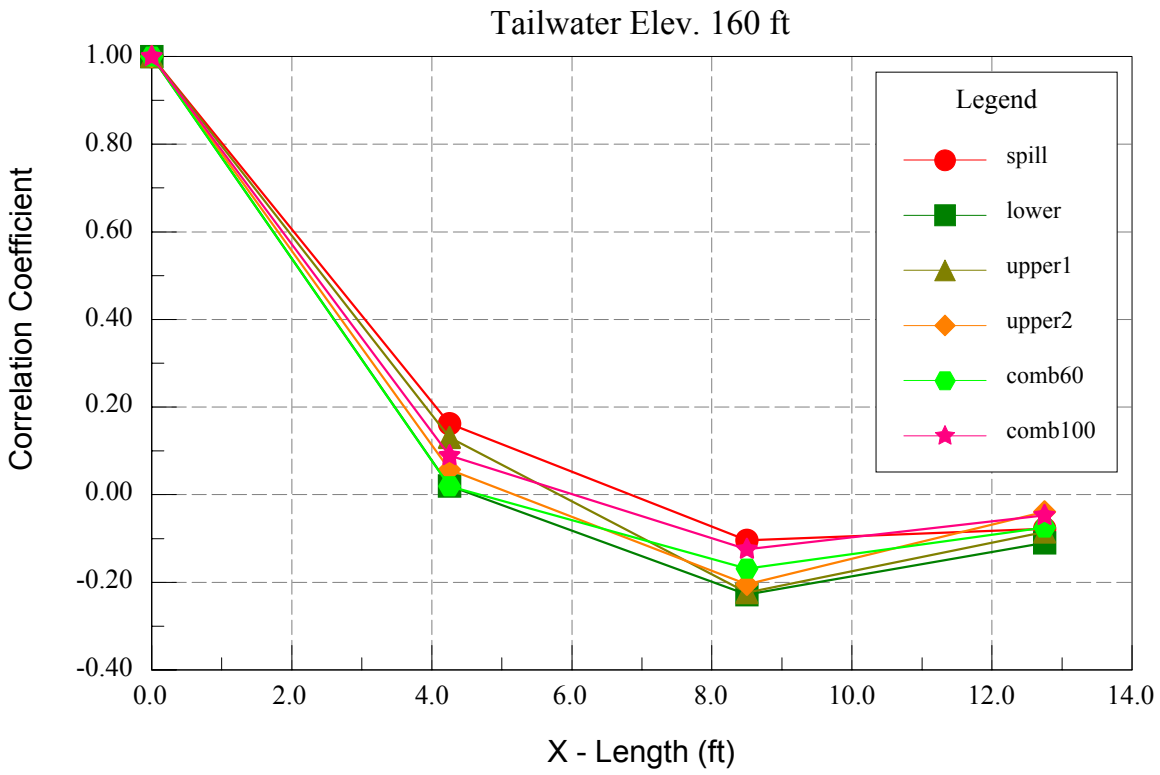

Figure 51: Spatial correlation plot for developing correlation lengths in Table 6. All discharges were approximately equal except for the combined outlets at 100%. Reservoir 418 ft for all outlet flows. Tailwater elevation 160 ft.

Table 6: Correlation lengths for tailwater elevation 160 ft resulting from integration of curves in Figure 45.

Location	Correlation Length (ft)
Spillway only	2.99
Lower outlet (100%)	3.42
Upper outlet (100%) run 1	3.52
Upper outlet (100%) run 2	2.99
Combined outlets (60%)	3.03
Combined outlets (100%)	2.82

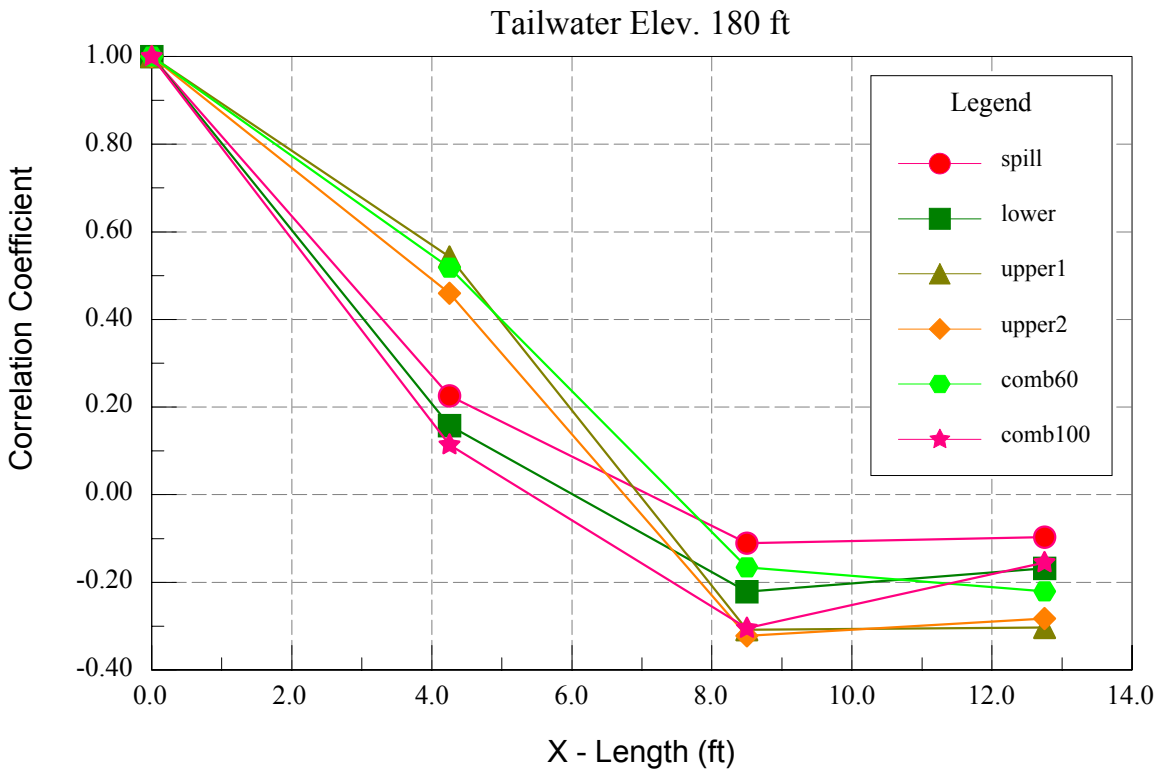

Figure 52: Spatial correlation plot for developing correlation lengths in Table 7. All discharges were approximately equal except for the combined outlets at 100 %. Reservoir elevation 418 ft for all outlet flow cases. Tailwater 180 ft.

Table 7: Correlation lengths for tailwater elev. 180 ft resulting from integration of curves in Figure 46.

Location	Correlation Length (ft)
Spillway only	3.34
Lower outlet (100%)	3.73
Upper outlet (100%) run 1	6.01
Upper outlet (100%) run 2	5.64
Combined outlets (60%)	5.23
Combined outlets (100%)	4.04

The general trend is for the correlation lengths to increase with an increase in tailwater depth, however the correlation lengths are still small and in most cases less than the smallest spacing between transducers (4.25 ft). This would lead the designers to apply the pressure load as a point load with hydrostatic pressure everywhere else when doing their slab design. The small correlation lengths make the frequency of the pressure pulses unimportant as the areal extent of the force is small. In addition the extreme pressure values appear to be higher frequency occurrences, meaning they occur infrequently and only for very short time periods. Correlation lengths were calculated by integrating an absolute valued correlation plot, as the negative correlations have essentially the same meaning, just phase difference.

The slab dimensions within the stilling basin floor are mostly 50 ft by 50 ft, with a couple of rows of 21 ft by 50 ft. The data presented above make it seem unlikely that a correlated pressure event will act on an entire slab or even half of the slab at a single point in time. Additional studies looked at a single line of transducers placed on transverse joint lines at 50 ft spacings down the stilling basin beginning at Sta. 12+51. A correlation analysis yields correlation lengths of about 25 ft, figure 52 and Table 8. However looking at figure 53, and noting that the smallest spacing between two transducers is 50 ft, the correlation lengths calculated by this method are almost certainly skewed too high when determined by this method.

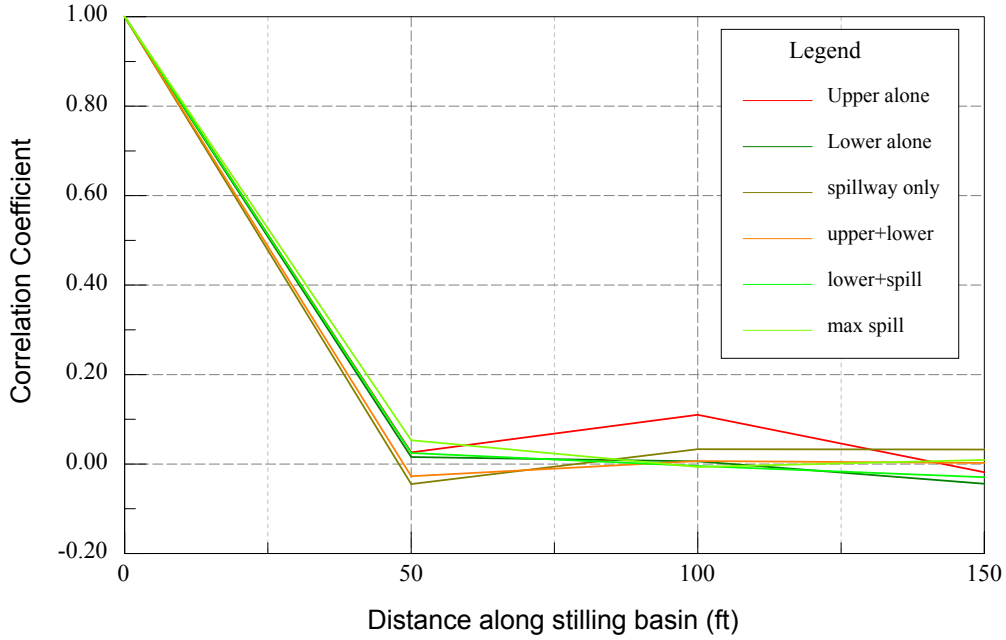

Figure 53: Spatial correlation plot for developing correlation lengths in Table 8. Note, minimum transducer spacing is 50 ft, so integrated correlation lengths are skewed high. Tailwater elevation 175 ft.

Table 8: Correlation lengths for tailwater elev. 180 ft resulting from integration of curves in Figure 47.

Location	Correlation Length (ft)
Spillway 75000 ft^3/s, res. 441	25.0
Lower outlet (100%) res. 400	24.8
Upper outlet (100%) res. 400	27.0
Combined outlets (100%) res. 400	25.8
Lower outlet + spillway, res. 438	25.0
Spillway 120000 ft^3/s, res. 466	25.8

If we look at the coherence functions in the frequency domain, we see quite a different picture. The upper gate at full open with a reservoir elevation of 400 ft and a tailwater elevation of 165 ft yields some reasonably high correlations between the transducer at Sta. 12+51, and Sta. 13+01, a distance of 50 ft, figure 54 a-c.

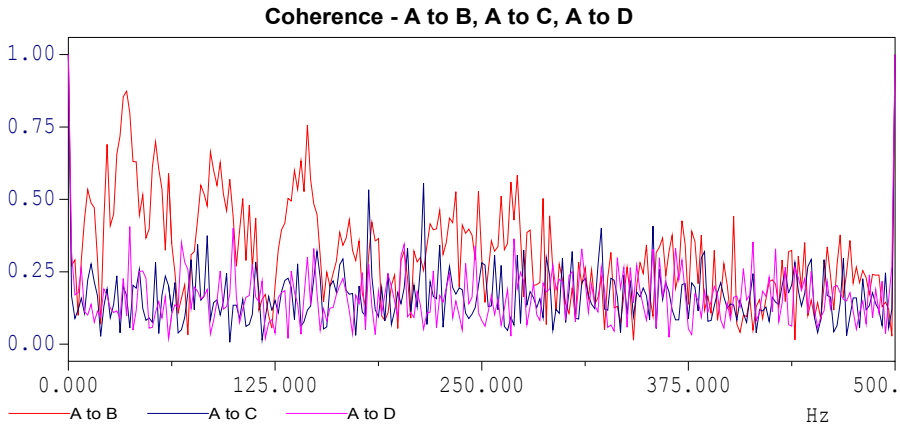

a) Upper outlet, full open, res. 400 ft, TW. 165 ft, note high correlation at about 35 Hz.

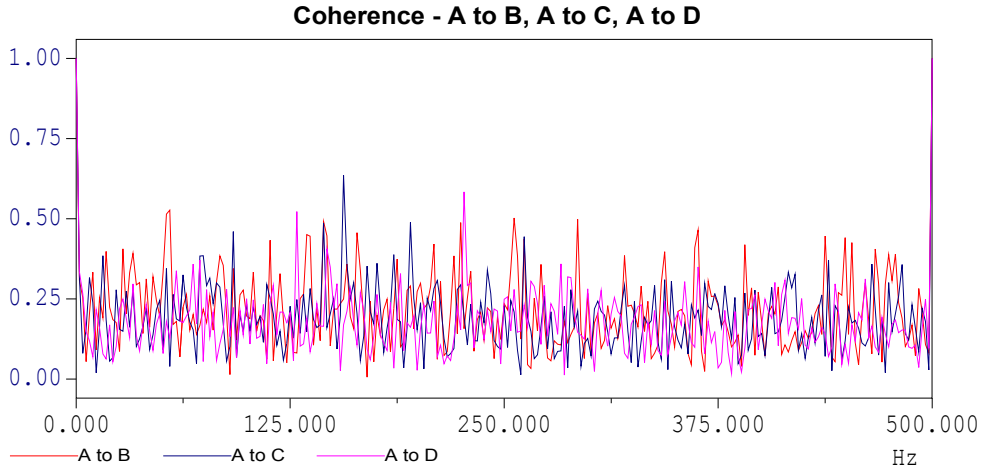

b) Lower outlet full open, res. 400 ft, TW. 165 ft,

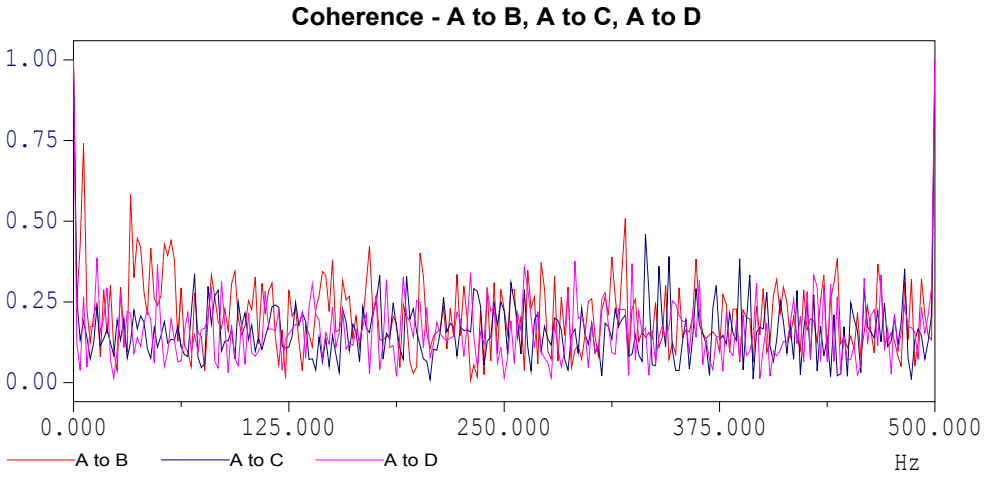

c) Upper and lower outlets full open, res. 400 ft, TW. 165 ft.

Figure 54: Coherence for various outlet flow combinations, 100% gate, res. 400 ft, tailwater 165 ft.

We did further investigations, looking at the upper outlet operating at full open with various reservoir head conditions and reasonably constant tailwater (175 ft). Reservoir heads were varied in ~25 ft increments from 350 ft to 418 ft (crest elevation), figure 55 a-d.

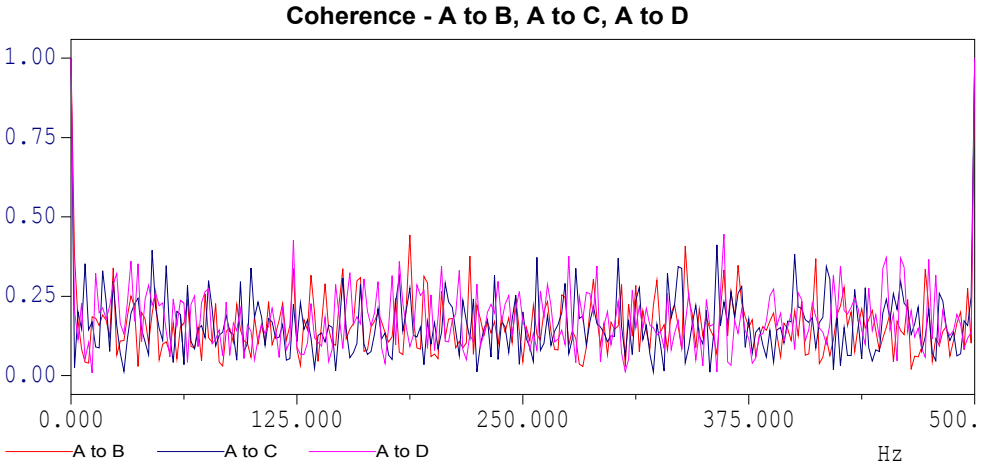

a) Upper conduit operating, full open, res. 350 ft, TW. 165 ft.

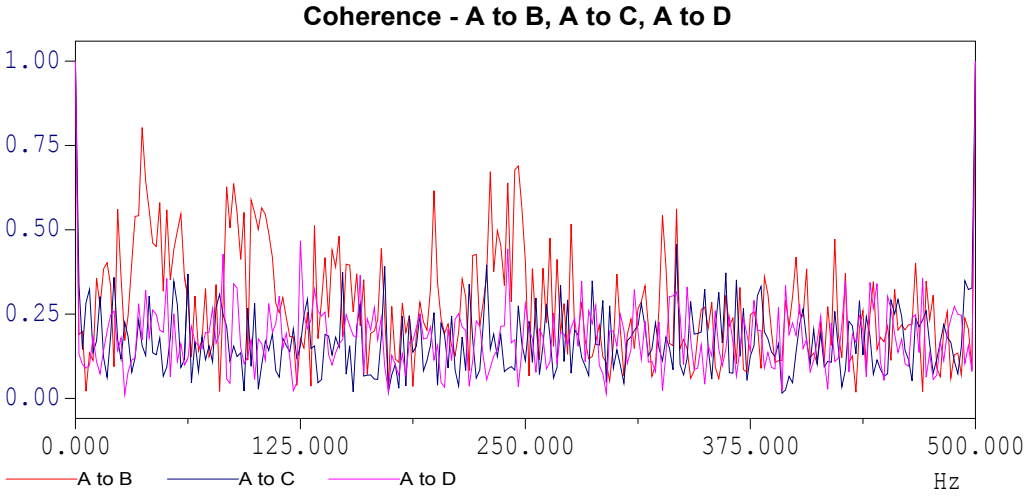

b) Upper conduit operating, full open, res. 375 ft, TW. 165 ft.

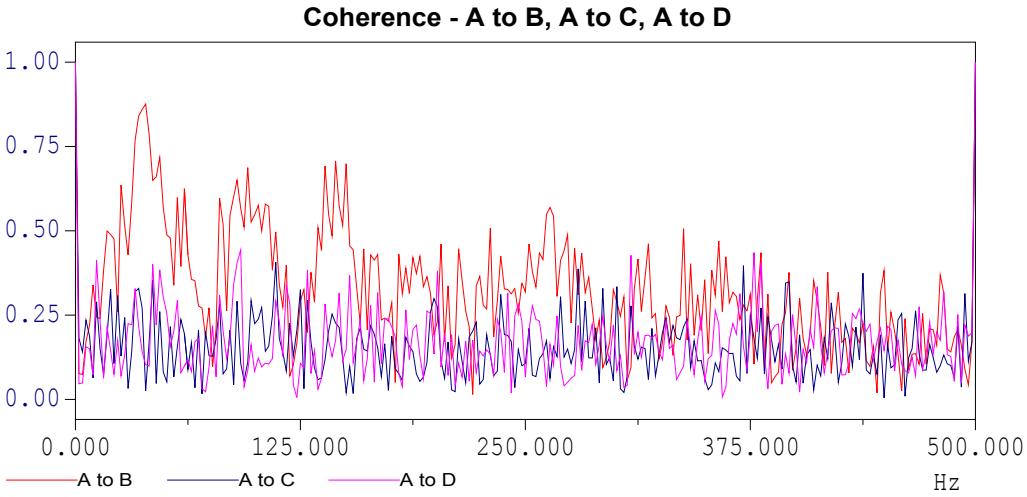

c) Upper conduit operating, full open, res. 400 ft, TW. 165 ft.

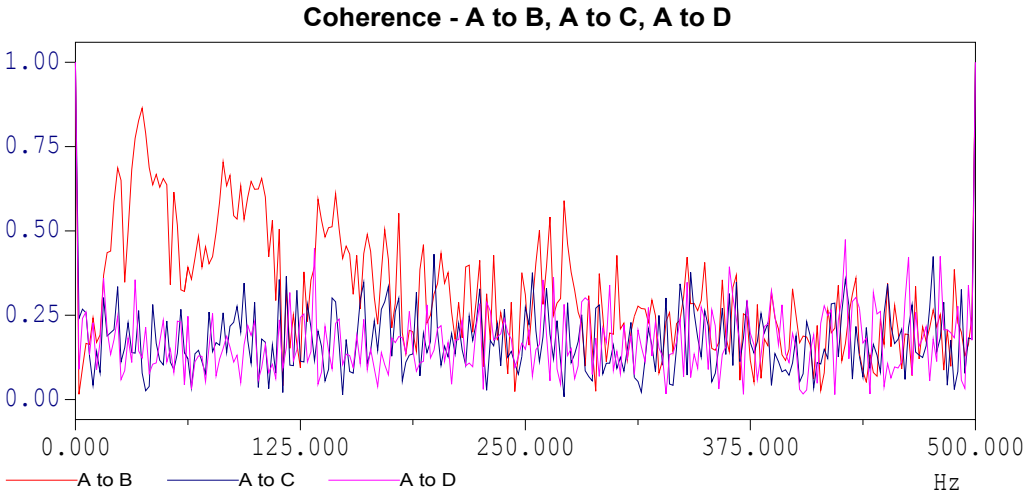

d) Upper conduit operating, full open, res. 418 ft (crest), TW. 165 ft.

Figure 55: Coherence plots for upper conduit operating 100%, at various reservoir elevations and tailwater 165 ft.

These plots show the correlation at 35 Hz increases as the jet impact moves downstream in the basin with increasing reservoir water surface. A coherence value greater that 0.8 is considered reasonably high, meaning that the pressure signals across the first slab instrumented are well correlated at this frequency, but appear to be in phase with each other. Figure 56 shows the mean piezometric pressure along with maximum/minimum envelopes as a function of reservoir elevation for upper outlets only at full open with a tailwater setting of 165 ft.

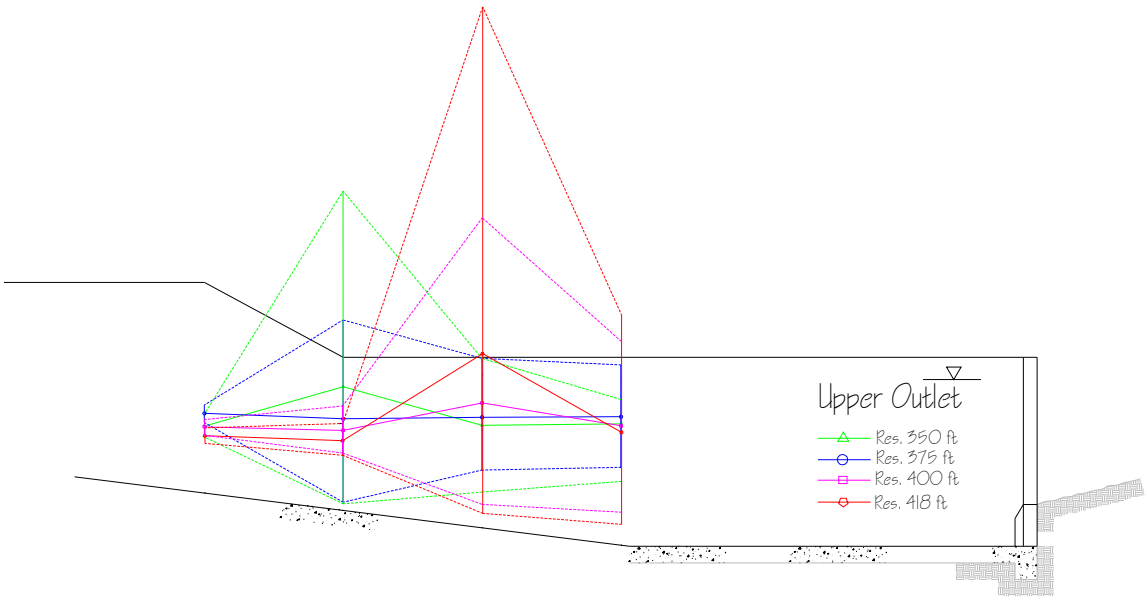

Figure 56: Upper conduit only at various reservoir elevations for a tailwater setting of 165 ft. Solid line with symbol is the mean piezometric pressure, dotted lines represent maximum to minimum envelope for a 5 min prototype run.

Depending on the current structural design of the stilling basin concrete, it may be advisable to further investigate the consequences of failure of the waterstops between the construction joints. Failure of these waterstops could allow amplified pressure pulses (Bollaert and Schleiss 2002) to reach the underside of the slab and act to uplift the structural slabs. While normal operations will almost always provide a minimum tailwater elevation of greater than 180 ft, operation at lower heads may expose the basin floor to more coherent water jets at lower submergences (sloped portion of the basin floor). Computer modeling may be the most efficient method to investigate these possibilities and evaluate the risk potential.

5. References

Ball, J.W. (1959). Hydraulic Characteristics of Gate Slots. *Journal of the Hydraulics Division,* Proceedings of the American Society of Civil Engineers, pp. 81-114, Volume 85 No. HY10, October, 1959.

Bollaert, E. and Schleiss, A. (2001). A new approach for better assessment of rock scouring due to high velocity jets at dam spillways, *Proceedings of the 5th ICOLD European Symposium*, Geiranger, Norway.

Falvey, H. (1990). Cavitation in Chutes and Spillways. *Bureau of Reclamation, Engineering Monograph 42,* United States Department of the Interior, Bureau of Reclamation, Denver, CO.

Frizell, K. W. (1998). Aeration Enhancements at the Folsom Dam Outlet Works: Reducing Cavitation Damage Potential, Internal Memorandum PAP-786, Water Resources Research Laboratory, United States Department of the Interior, Bureau of Reclamation, Denver, CO.

Idelchik, I.E. (1994). *Handbook of Hydraulic Resistance*, 3rd Edition, CRC Press, Boca Raton, FL.

Pinto, N.L. de S. (1982). Model Prototype Conformity in Aerated Spillway Flow. *International Conerence on Hydraulic Modeling of Civil Engineering Structures, BHRA Fluid Engineering, pp. 273-284*, Coventry, England

Speerli J. (1999). Strömungsprozesse in Grundablassstollen. *Doctoral Dissertation, VAW Mitteilung 163*, ETH Zürich (in German).

Toso, J. and Bowers, E.C. (1988). Extreme pressures in hydraulic jump stilling basin, *Journal of Hydraulic Engineering*, American Society of Civil Engineers, Vol.114 (8).

Wood, I. (1991) editor. Air Entrainment in Free-Surface Flows. *International Association for Hydraulic Research, Hydraulic Structures Design Manual 4,* A.A. Balkema/ Rotterdam/ Brookfield.

APPENDIX A

1:17 Hydraulic Model Study of the 9.33- by 16.25-ft high pressure slide gates: Data Summary

Introduction

Beginning in June of 2000, the Bureau of Reclamation's Water Resources Research Laboratory began testing a 1:17 scale sectional model of the outlet works modification at Folsom Dam. The design was prepared by the Sacramento District of the Corps of Engineers and featured replacing the current eight 5-ft by 9-ft slide gates with eight 9.33-ft by 16.25-ft slide gates. These new gates were designed to pass a flow of 115,000 ft^3/s at a reservoir elevation of 418 ft. There were several features of this design that were studied in a large sectional model. The gates themselves are some of the largest high-pressure slide gates currently known to exist in the physical or planning stage. The flow amounts are considerably increased, requiring a significant increase in the air venting system. The high heads will result in flow velocities above 100 ft/s in the conduits leading to the gates, there are several areas that cavitation potential may exist, including the intake curves, the gate area, and the conduits downstream from the gates. The stilling basin action needed to be verified for this slightly different inflow arrangement. The design goal was also to allow full operation of the outlets when the spillway is operating. These combined flows have proved damaging in the past, requiring a physical modification (eyebrows) and a restriction on operations.

As the testing progressed, data were presented to the Corps of Engineers and their consultants and also to Reclamation's Consultants Review Board. At the May 2001 meeting of the CRB with the 1:17 model study nearing about 75-percent complete, the Consultants Review Board (CRB), consisting of Messrs. Norm Bishop and Ron Kubit, raised significant issues about the hydraulic and mechanical designs associated with the Folsom Outlet Works Modifications. In the months following this meeting, additional meetings were held to address the CRB's concerns and eventually this resulted in the Corp's of Engineers issuing a Gate Sizing Memorandum in which they recommended changing the design to include 2 new conduits on the upper level, resulting in 6 outlets of 9.33-ft by 14-ft, and 4 lower level outlets that were 9.33-ft by 12-ft in size. This modification resulted in similar design discharges but with smaller gates and hopefully improved hydraulic conditions.

This summary will present major results from the testing of the original sectional model in order to provide documentation on the performance of the large 9.33-ft by 16.25-ft gates.

The Model

A 1:17 scale Froude-based sectional model of the Folsom Outlet Works Modification was constructed in Reclamation's Denver Laboratory. The model featured an upper and lower conduit, a portion of the overflow spillway and corresponding section of the stilling basin, figures A1 and A2. Traditional materials were used to construct the model including; marine-grade plywood, clear acrylic, high-density polyurethane foam, aluminum, and sheetmetal. The headbox featured a perforated plate baffle to calm the incoming flow and direct it towards the gate intakes. Water was introduced to the model through two 12-inch gate valves, connected to the lab system's supply pipe network. Flowrates were measured using the laboratory system of calibrated venturi meters. Multiple pumps are required to attain the maximum flows needed for

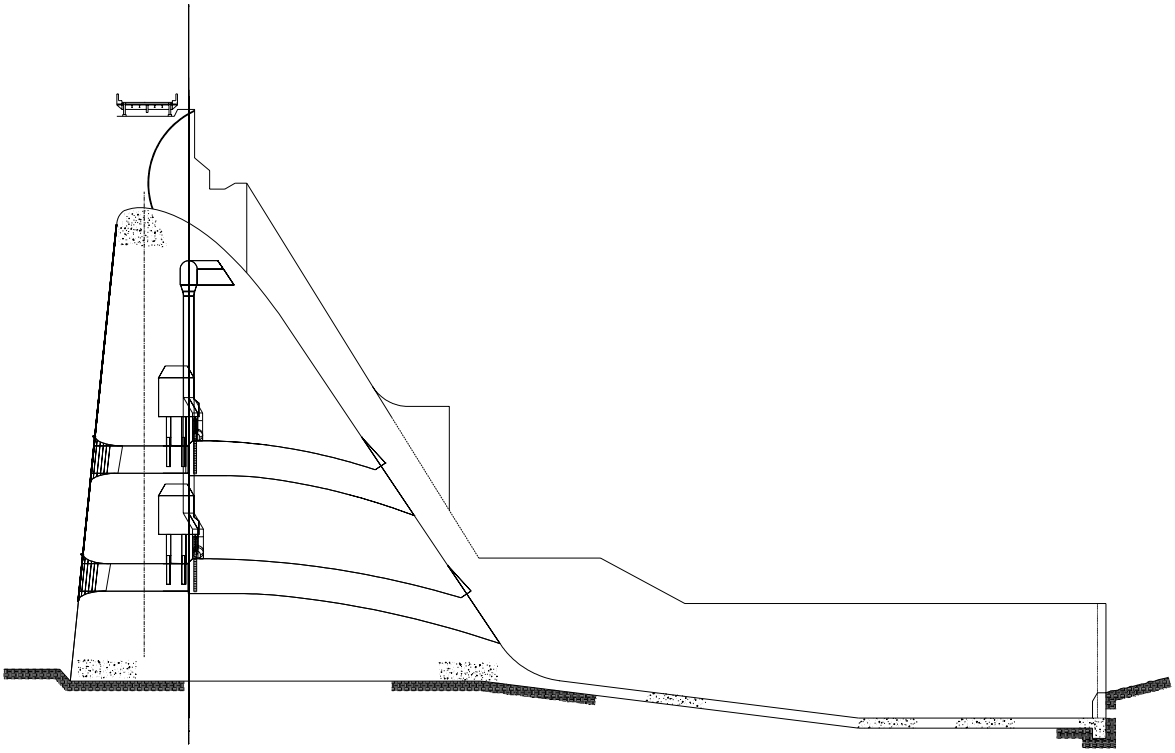

Figure A1: Section through the dam that was modeled.

Figure A2: Photograph of the completed model

the modeling. Pressures were measured using standard piezometer taps and either electronic pressure transducers or water column manometers. Air flow rates were measured using a calibrated air velocity meter using constant temperature anemometry. Gate position was measured using string-type displacement transducers, read with a portable voltmeter.

Testing and Results

Testing began with measurements of the pressure drop coefficient on the elliptical intakes to the conduits. The intakes were a simple 1:3 ellipse, leading to the conduit which had a aspect ratio of H/W = 1.74. The data were collected using a scanivalve and transducer. This allowed for the reading of multiple piezometer taps with a single transducer. There were several problems with the piezometer taps, especially in their stability over time. Small diameter copper tubing was used for the taps, and just inserted flush with the high density polyurethane foam that made up the intake. Eventually, the taps were stabilized using Bondo® body filler. This filler was added to the inner surface of the intakes and sanded smooth to yield a good piezometer installation.

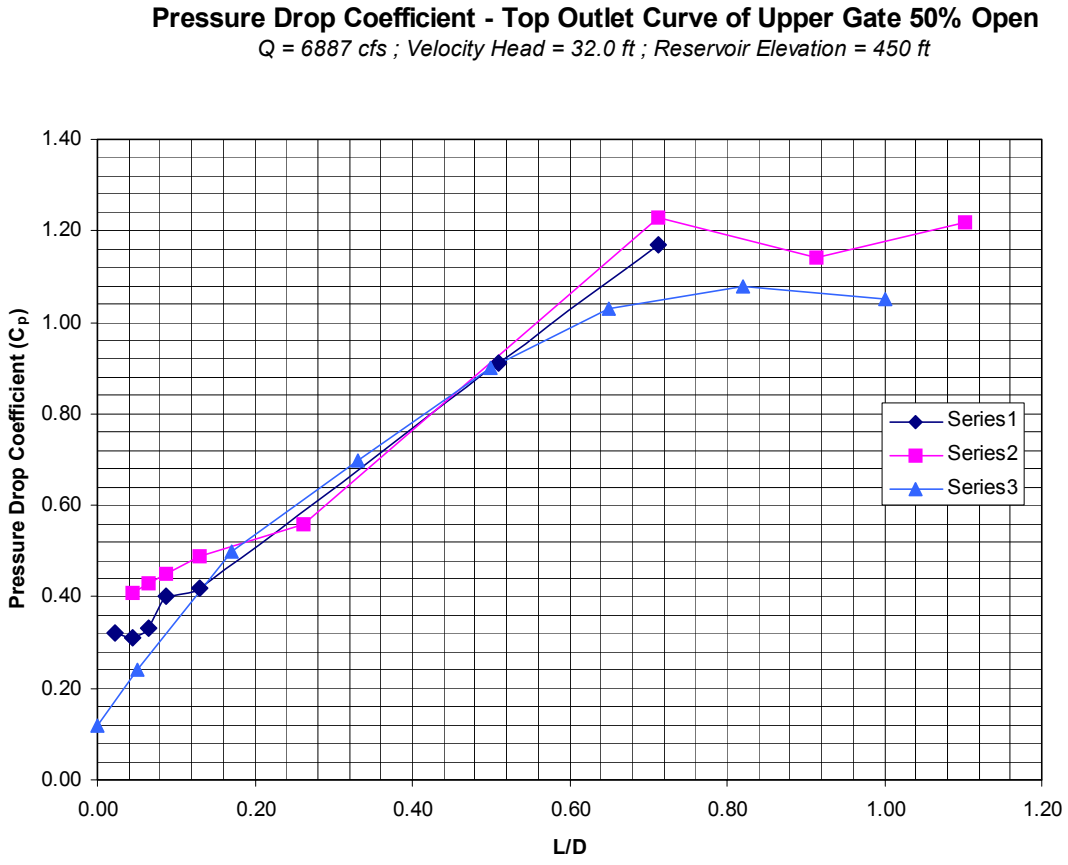

Figure A3: Upper conduit, top centerline piezometers, pressure drop coefficient.

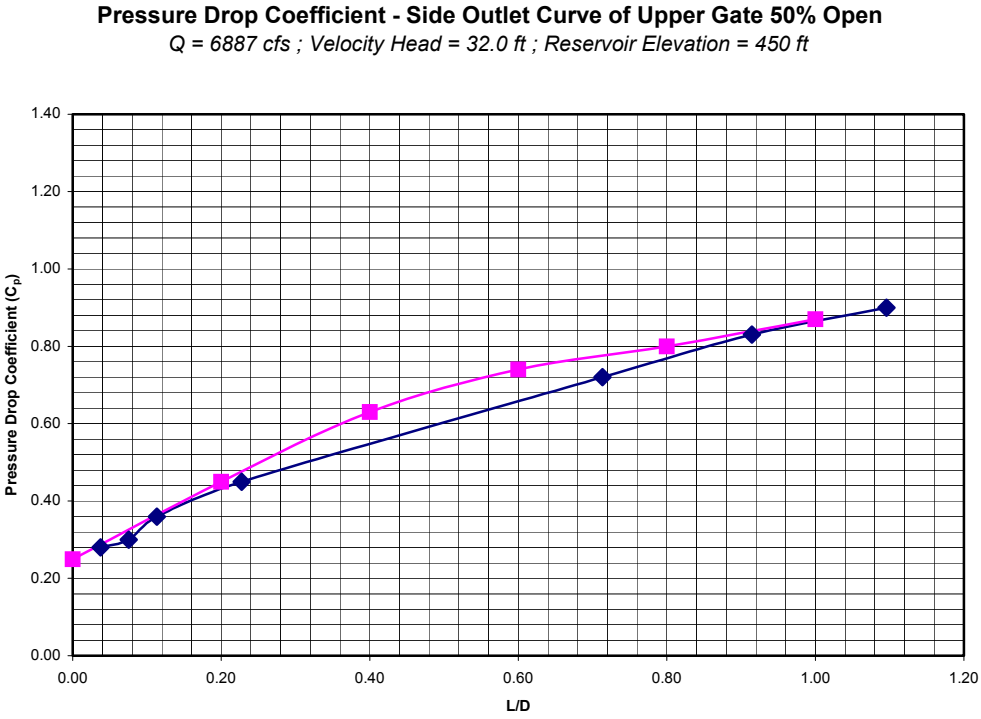

Figure A4: Upper Conduit, side wall piezometers, pressure drop coefficient.

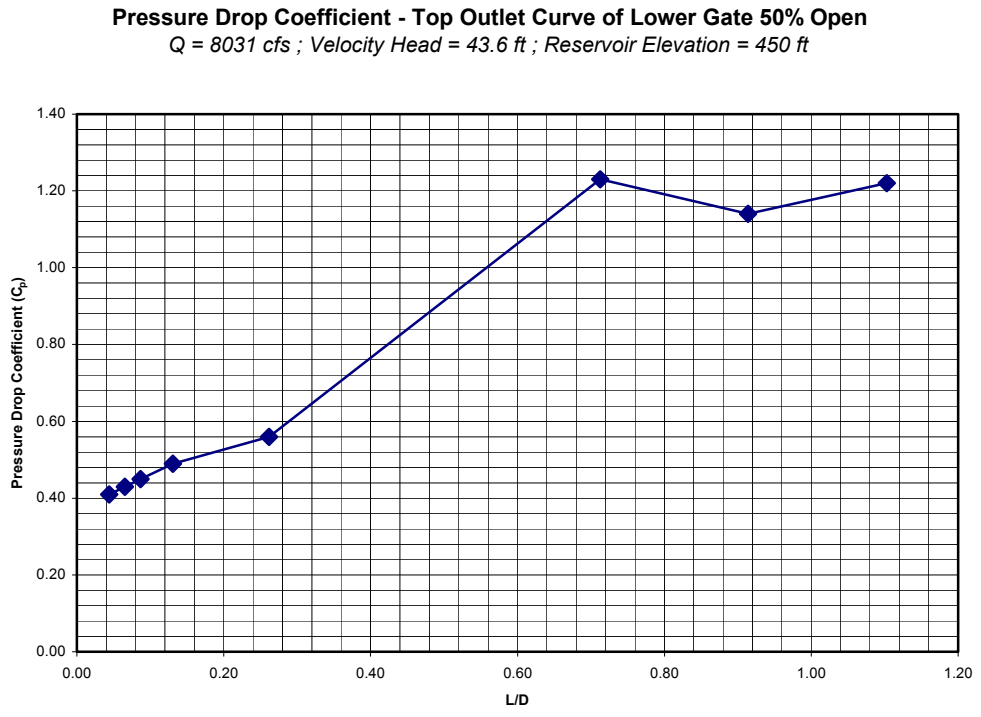

Figure A5: Lower Conduit, top curve piezometers, pressure drop coefficient.

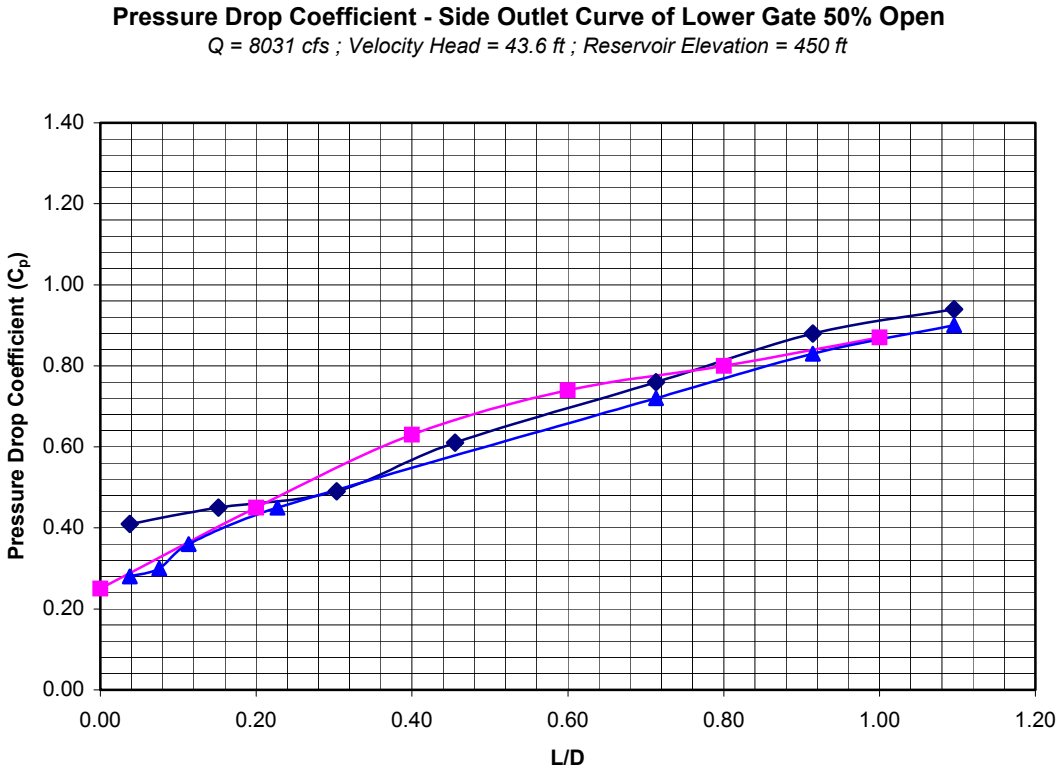

Figure A6: Lower conduit, side curve piezometers, pressure drop coefficient.

This data show pretty good correlation with the COE's Hydraulic Design criteria for the side wall data, however the top centerline data shows a larger pressure drop coefficient, on the order of 1.17 for the top conduit and 1.22 for the lower conduit. These higher pressure drop coefficients definitely are in the range that cavitation could be an issue

Much of the data concerning discharge, both air and water, pressure in the conduit, etc. was not fully completed prior to the review of the gate sizing issue. For this reason, only a few examples of data will be included in this report. Full discharge curves were never completed. Modifications to the area just downstream from the regulating gates were studied. The additions of ramps were tested in the model to improve the appearance of aeration of the jet as well as to see if there was a impact on the pressures in the downstream conduit. Initially it was discovered that the discharge that was measured at the gates was in excess of that predicted by the COE analytically by about 8-10 percent, figure A7. This was prior to the addition of any ramps downstream from the gate. Once the ramps were installed, the discharge reduction that took place was right in line with the analytical predictions, figure A8. The initial difference was probably due to the COE using a inlet loss coefficient of 0.17. While the headloss through the intake hasn't changed, the losses downstream from the gate definitely affect the discharge ratings.

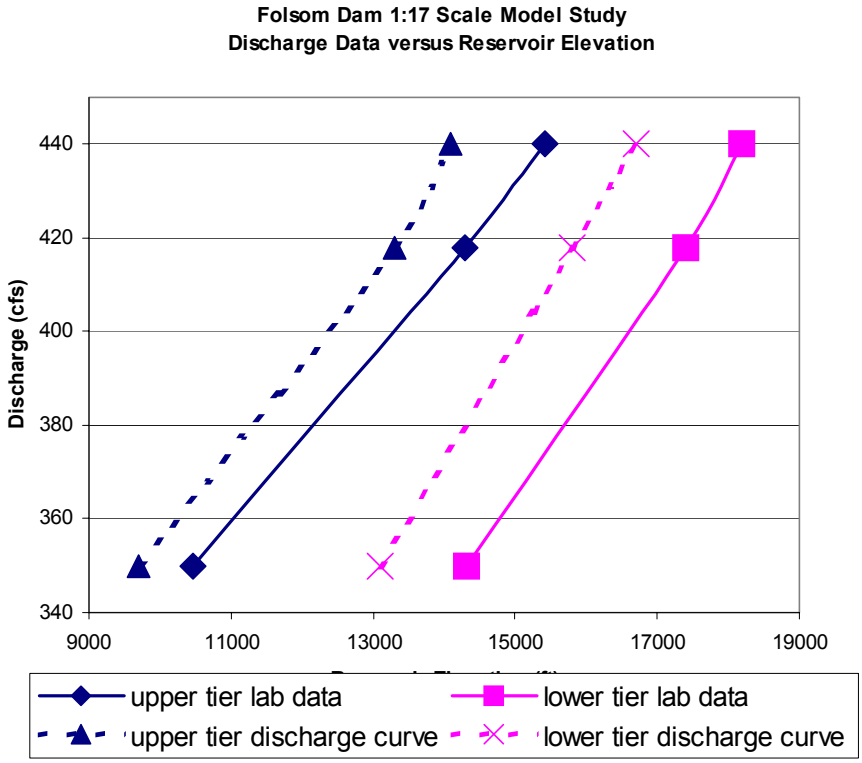

Figure A7: Data showing excess discharge from the model gates at full open position for a variety of reservoirs.

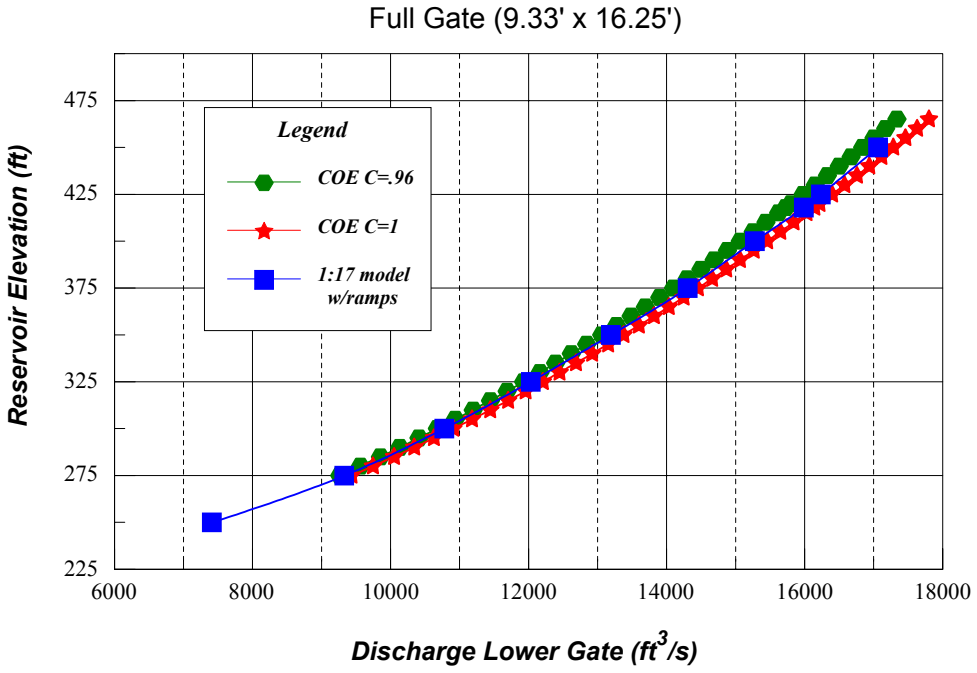

Figure A8: Model data with ramps installed plot right with analytical prediction, between a C=0.96 and 1.0.

A sample of air vent data taken at 400 ft reservoir appears in figures A9-10. These data are presented both in the form of a nondimensionalized flow rate versus gate position, and as air vent discharge versus gate position. The air flow data was not completed prior to redirection of the model study.

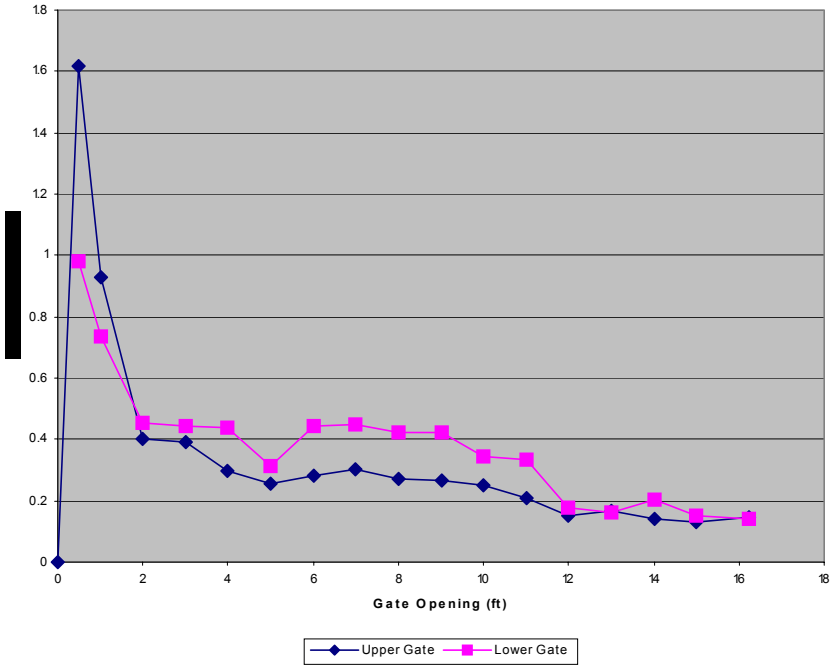

Figure A9: Beta ratio for both gates at a reservoir elevation of 400 ft.

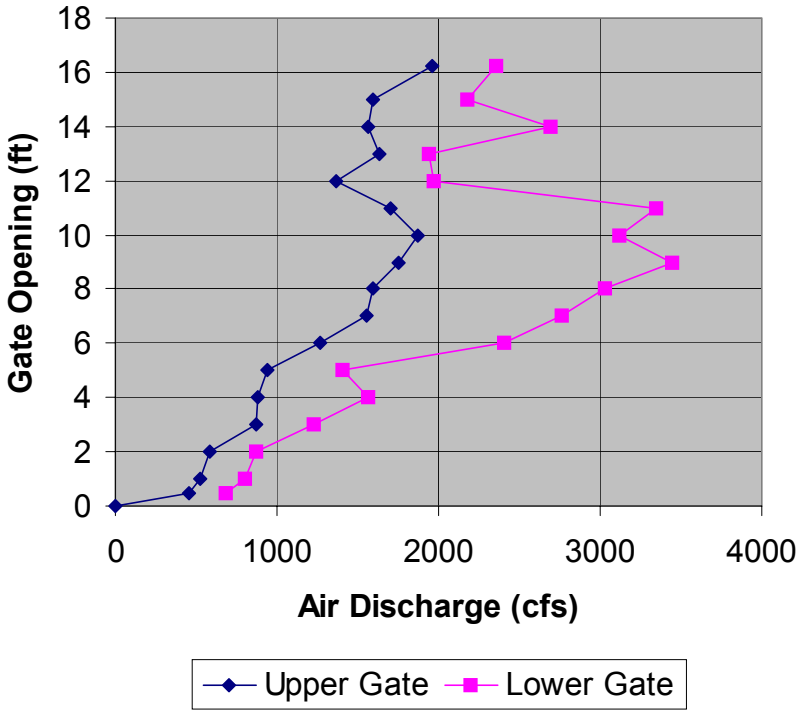

Figure A10: Air flowrates to each gate at a reservoir elevation of 400 ft.

Figures A11 and A12 show pressures along the centerline of the invert, downstream from the gates.

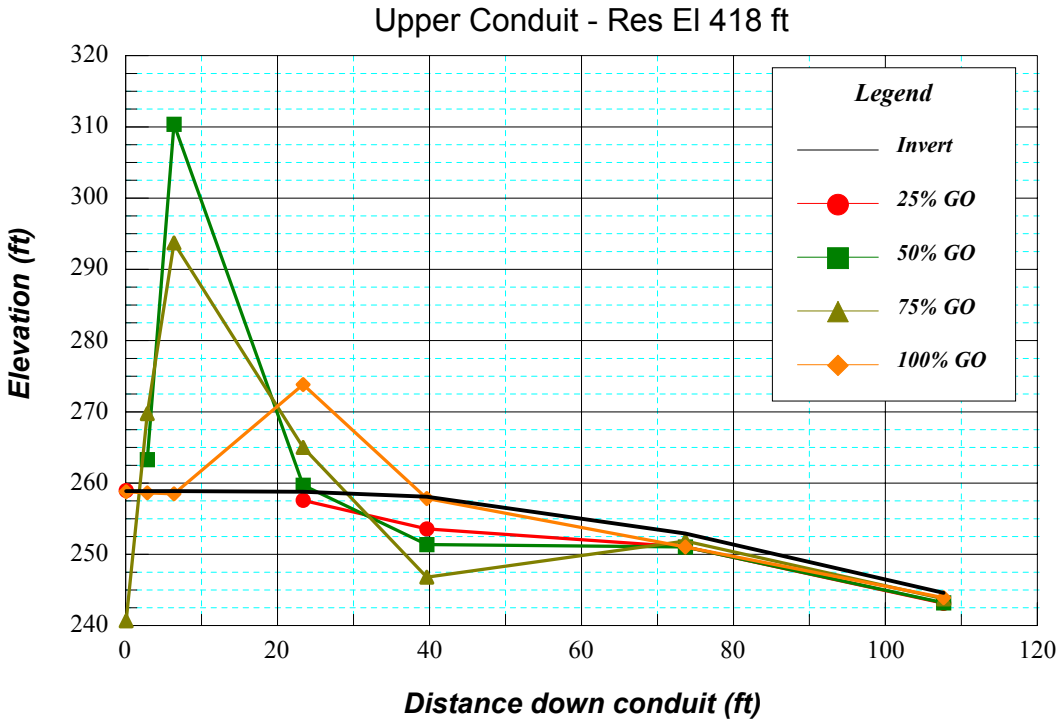

Figure A11: Pressures along the upper conduit invert centerline for various gate openings at 418 ft.

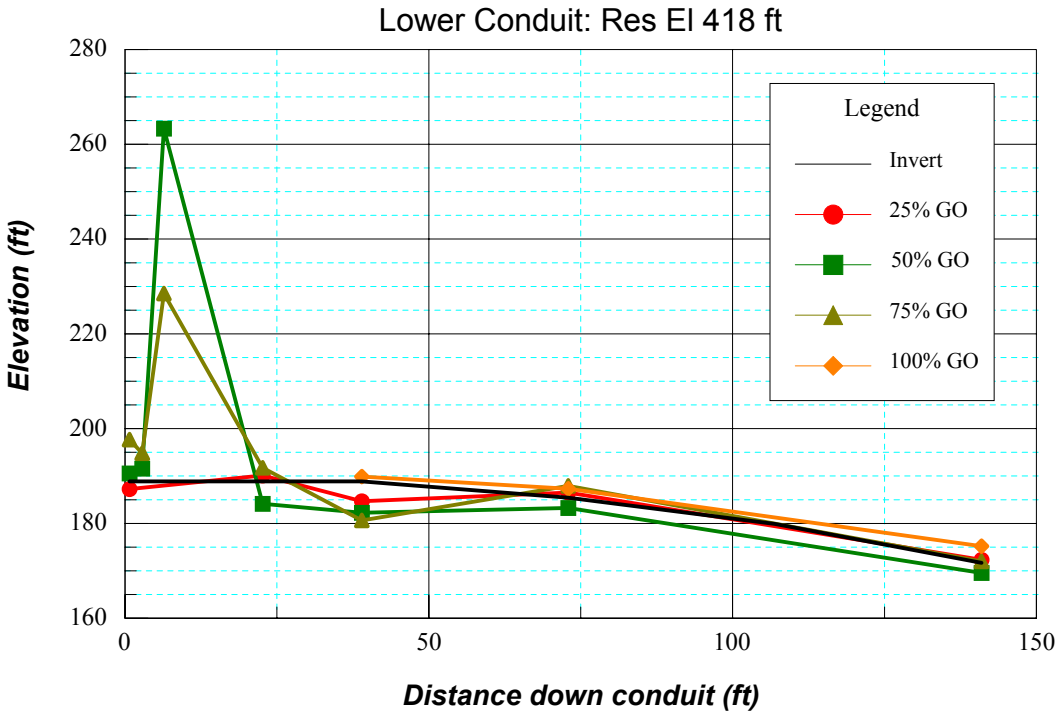

Figure A12: Pressures along the lower conduit invert centerline for various gate openings at 418 ft.

Discussion and Conclusions

A configuration for the outlet works rehabilitation at Folsom Dam was modeled at the Bureau of Reclamation's hydraulic laboratory in Denver, Colorado. A sectional model at a scale of 1:17 was used to observe the operation of 9.33- by 16.25-ft high pressure slide gates in both the upper and lower tiers. A sample of some of the pertinent data has been presented. Many of the same issues were observed in this first model as have been presented in the current design report. While there were some design challenges for gates this large, especially in fabrication and installation, we did not observe any hydraulic features that would preclude using a gate of this size with the head conditions present at Folsom Dam.

APPENDIX B

Quality Control, Instrumentation, Calibrations, and Uncertainty Estimates

QA/QC Plan for 1:17 Hydraulic Model Study of the Folsom Outlet Works Modification

Model Design

Computations involved with the selection of the model scale and critical model elements are performed by the Principal Investigator (PI) and are reviewed by a peer within the Water Resources Research Laboratory. All engineers capable of performing the peer review have at least 10 years experience working with hydraulic scale models. The PI or a technician prepares detailed drawings for use during model construction. If the PI prepares the drawing, the technical details such as dimensions should be checked and initialed by a technician or other aide. If a technician prepares the drawing, the PI indicates checking and approval by initialing the drawings.

Model Construction

Critical Dimensions: Critical model dimensions including all waterways and topography are identified by the PI and monitored by the PI and technicians or other aides during construction. The Principal Craftsman (PC) works with the PI during layout and construction to verify model accuracy using appropriate tools, which may include but are not limited to: levels, theodolite, and total station survey equipment. In the event that any features of the model are built by outside contractors, the PI is responsible for providing clear and detailed drawings and specifications for the feature. The Laboratory Shops foreman will arrange for the contract and the PC will monitor the contract and verify that the feature meets specifications prior to acceptance. Verification of model conformance will be

Non-critical dimensions: Certain dimensions within the model may be deemed non-critical. The tolerances on these dimensions may be large as their accuracy has been identified to be inconsequential. In any event, should a non-critical dimension be discovered to be out of the suggested tolerance appearing on the model design drawings, the PI will approve the variation or require a modification to bring the dimension back within the appropriate tolerance.

Model Testing

The model test plan is developed in the SOW and forms the basis for the agreement to perform the model study. The PI will hold preliminary meetings with the COE and/or their consultants in order to finalize the test plans. The PI will develop a measurement and instrumentation plan that will be approved by the COE and/or their consultants. This plan will provide locations in the model for measurements, identify the sensor, and supply calibration requirements. In addition, calibration records and uncertainty estimates on permanent laboratory equipment which will be used to measure model parameters, i.e. venturi meters, will be provided.

Calibration of sensors will occur prior to installation and will follow manufacturer's instructions

or accepted standard practices. Uncertainty estimates based on calibration records for each sensor will be calculated. Calibration checks or recalibration will follow the manufacturers recommended schedule or upon discovery of an inconsistency or apparent problem with the data.

All data will be documented and kept in a project book. In addition, photos and video will supplement written documentation. At the conclusion of the testing, results will be reviewed in a meeting with the COE and their consultants and final documentation will be generated. This document will be transferred on compact disk to the COE.

Statement of Quality Control

Model design and drawings were prepared by K. Warren Frizell, Bureau of Reclamation, D-8560. Periodic checking was performed by Robert Einhellig. The design was carried out based on extensive discussions and meetings with the COE, Sacramento District and their consultants. Mutual agreements on items such as model scale were achieved prior to design. Model construction was carried out under the supervision of K. Warren Frizell. The Principal Craftsmen were Neil Armstrong and Jason Black. In addition, much of the acrylic work was contracted to AIA Plastics. Important dimensions and elevations were verified throughout the construction process. Contracted plastic work was measured and reworked where necessary in order to provide proper tolerances. During the data collection phase, K. Warren Frizell and Connie DeMoyer collected the model data. In addition to cross-checking the raw data, on almost a weekly basis, data was distributed to the COE and their consultants for review. The documentation has received extensive peer review by the COE and their consultants prior to its finalization.

K. Warren Frizell
Research Hydraulic Engineer
Principal Investigator
Bureau of Reclamation
Technical Service Center D-8560
Denver, Colorado

Instrumentation Plan and Calibrations

Pressures within the model were measured using piezometer taps (0.0625 in diameter), connected to water column manometers or to pressure transducers. The pressure transducer used to measure reservoir elevation and also indicate head drops in the intake curves was a Sensotec Model GM, ReadOut S/N 419180, transducer Model A5/882-15 S/N 387547, range 0-10 psi. This transducer was calibrated using a Druck DPI 610 portable pressure calibrator. This device allows calibration over a wide series of pressure ranges with an accuracy of 0.025% F.S. The Sensotec was calibrated initially, pretest, and then a single point check was completed on 1 month intervals throughout the testing period. The calibration remained very consistent for the entire test period; figure B1 shows the initial calibration.

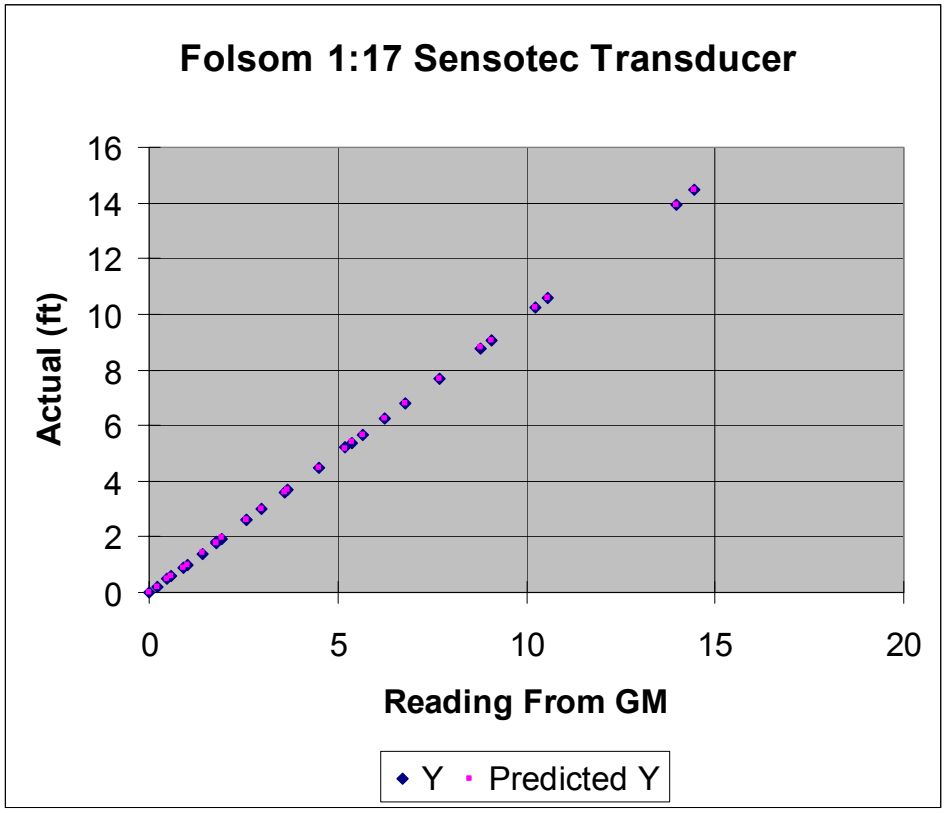

Figure B1: Initial calibration of the Sensotec pressure transducer used to measure and control reservoir elevation.

The scaled output of this transducer was also used as an input to the venturi valve control system in the laboratory to allow automatic adjustment of the flowrate into the model in order to maintain a set reservoir elevation. In the determination of the pressure drop coefficient for the elliptical intakes, this transducer was used to read the differential pressure from the reservoir to the particular piezometer location in question. Figure B2 shows the location of piezometers throughout the acrylic portion of the model. There were 16 piezometer taps located along the top centerline and 16 taps located along the side centerline on both the upper and lower conduit intakes. A more complete analysis of the uncertainty estimate in these measurements appears later in this appendix.

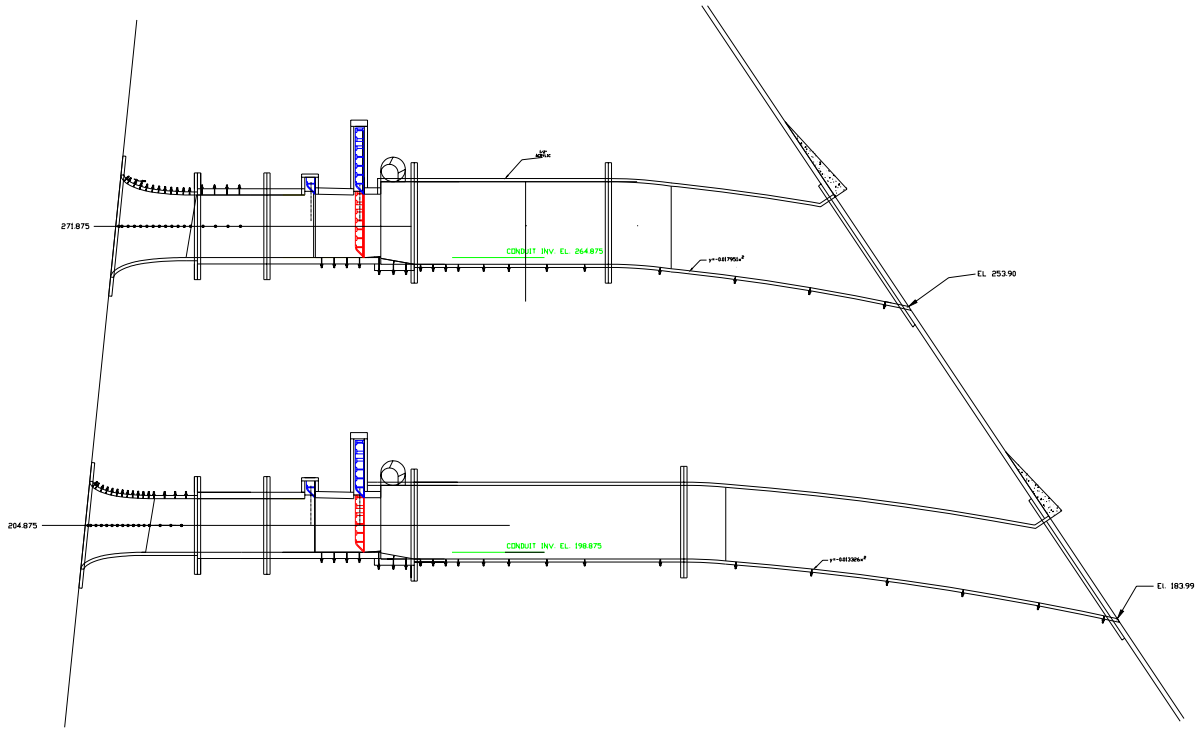

Figure B2: section through the model showing piezometer tap locations on the acrylic sections.

The remaining piezometer taps were connected to water manometers with clear tygon tubing and pressure elevations in feet of water were measured on a scale with division of 0.01 ft.

Gate position was monitored using Celesco string-type position transducers, Model # PT1MA-15-UP-420E-C25. These sensors have a range of 15 inches and provide a 4-20 mA output over this range. A precision resistor was placed across the current loop output that converted the current output to a 1-5 V output. This was done to allow for easier indication at the model. The closed and fully open positions were checked each day of testing and slight adjustments made in order to account for changes in these values if needed. The accuracy of this instrument was ±0.38 in prototype, i.e. a particular gate setting, say a 1 ft opening could be set in the model to an accuracy of 1 ± 0.03 ft.

D P I 610

Standard Specification

Druck

PNEUMATIC CALIBRATOR DPI 610PC

Pressure/vacuum pump
-22 inHg to 300 psi capability

Volume adjuster
Fine pressure adjustment

Release valve
Vent and controlled release

Pressure port
$^1/_8$ NPT (female)

Media
Dry, non-corrosive, non-conductive gasses compatible with 316 stainless steel Hastelloy C276, BUNA-N and nylon.

HYDRAULIC CALIBRATOR DPI 610HC

Priming pump
Feeds from external source

Shut-off valve
Open for system priming

Screw press
0 to 6000 psi capability

Pressure port
$^1/_8$ NPT (female)

Media
Demineralized water and most hydraulic oils

INDICATOR DPI 610I

Release valve
Vent and controlled release

Pressure port
$^1/_8$ NPT (female)

Media
Most common fluids compatible with stainless steel and Hastelloy C276.

PRESSURE RANGES

The DPI 610PC, HC and I include an integral sensor, the range of which should be specified from the list below. Up to 10 remote sensors (option B1) may also be ordered per calibrator.

Pressure Range	Pneumatic DPI 610PC	Hydraulic DPI 610HC	Indicator DPI 610I	Remote Option (B1)	Accuracy % F.S.
1 psi (-1)	G		G	G or D	0.025
2.5 psi (-2.5)	G		G	G or D	0.025
5 psi (-5)	G or A		G or A	G, A or D	0.025
10 psi (-10)	G or A		G or A	G, A or D	0.025
15 psi (-15)	G or A		G or A	G, A or D	0.025
30 psi (-15)	G or A		G or A	G, A or D	0.025
50 psi (-15)	G or A		G or A	G, A or D	0.025
100 psi (-15)	G or A		G or A	G, A or D	0.025
150 psi (-15)	G or A		G or A	G, A or D	0.025
300 psi (-15)	G or A ①		G or A	G, A or D	0.025
500 psi (-15)			G or A	G, A or D	0.025
1000 psi (-15)		G or A	G or A	G or A	0.025
2000 psi		SG or A	SG or A	SG or A	0.025
2500 psi		SG or A	SG or A		0.025
3000 psi		SG or A	SG or A	SG or A④	0.025
5000 psi		SG or A	SG or A③	SG or A③	0.025
6000 psi		SG or A②	SG or A		0.025
10000 psi				SG or A ⑥	0.025

Values in ( ) negative calibration for gauge and differential ranges
A = Absolute, D = Differential (500 psi in pressure), G = Gauge, SG = Sealed Gauge
①, ② and ③ refer to over pressure.

Accuracy is defined as non-linearity, hysteresis and repeatability

Span Shift
0.5%/500 psi of line pressure for differential ranges.

Temperature Effects
±0.002% reading/°F averaged over 15° to 105°F and w.r.t. 68°F.

Remote sensor media
Stainless steel and - compatibility.
Negative Differential: Stainless steel and quartz compatibility.

Overpressure
Safe to 2 x F.S (except ① 500 psi max. ② 9000 psi max. ③ 5000 psi max.
④ 4600 psi max. ⑤ 7250 psi max. ⑥ 13000 psi max).
①, ②, ③, ④, ⑤, and ⑥ refer to pressure range table.

ELECTRICAL INPUTS

Input	Range	Accuracy	Resolution	Remarks
Voltage*	±50Vd.c.	±0.05% Rdg. ±0.004%F.S.	100µV max	Autoranging, > 10MΩ
Current*	±55mA	±0.05% Rdg. ±0.004%F.S.	0.001mA	10 Ω, 50V max.
Temperature	15° to 105°F	±2°F	0.1°F	Case ambient
Switch	Open/Closed			5mA whetting

* Temperature coefficient ±0.004% reading/°F w.r.t. 68°F

ELECTRICAL OUTPUTS

Output	Range	Accuracy	Resolution	Remarks
Voltage	10Vd.c.	±0.1%		Max. load 10mA
	24Vd.c.	±5%		Max. load 26mA
Current*	0 to 24mA	**±0.05%Rdg. ±0.01%F.S.**	0.001mA	

*Temperature coefficient ±0.004% reading/°F w.r.t. 68°F.

SPECIAL FEATURES

Pressure units
25 scale units plus one user defined.

mA step
Continuous cycle at 10 sec intervals.

Function	mA Output						
4 to 20mA linear	4	8	12	16	20		
0 to 20mA linear	0	5	10	15	20		
4 to 20mA flow	4	5	8	13	20		
0 to 20mA flow	0	1.25	5	11.25	20		
4 to 20mA valve	3.8	4	4.2	12	19	20	21

mA ramp
Continuous cycle with configurable end values and 60 sec travel time.

Data log
Multi-parameter with internal memory for 10,000 values. Variable sample period or log on key press.

Snapshot
Paperless notepad. Stores up to 20 complete displays.

Computer interface
RS 232.

Process functions
Tare, max/min, filter, flow, % span.

Language
English, French, German, Italian, Portuguese and Spanish.

Power management
Auto power OFF, auto backlight OFF, battery low indicator and status on key press.

DISPLAY

Panel
2.36 x 2.36 inch graphic LCD with backlight.

Readout
± 99999 capability, 2 readings per second.

ENVIRONMENTAL

Temperature
Operating: 15° to 120°F
Calibrated: 15° to 105°F

Humidity
0 to 90%, non-condensing.

Sealing
Generally to NEMA 12 (IP54).

Conformity
EN61010, EN50081-1, EN50082-1, CE marked.

Physical
6.6 lb, 11.8 x 6.7 x 5.5 inches.

Power supply
Battery powered 6 "C" cells, 65 hours nominal use at 68°F. The unit will operate with 110 Vac 60 Hz and allow battery pack to recharge. When batteries become exhausted, a low battery appears on the display.

AVAILABLE with Signature Calibration
SEE PG. IN-5

Low Range Wet/Wet Differential Pressure Transducers

Models Z and A-5

APPROVED

CE

CENELEC APPROVED

FM APPROVED INTRINSICALLY SAFE AMP

0.5 TO 25 PSID

ACCURACY TO 0.25%

AMPLIFIED OUTPUT AVAILABLE

SENSOTEC's Low Range Wet/Wet Differential pressure transducers utilize a bi-directional design which accepts fluid in both ports to measure full scale differential pressures from 0.5 to 25 psid. Maximum line pressure is 1500 psi as a standard feature and 3000 psi as an option. Standard industrial environments. Impressive accuracies of 0.25% to 0.5% full scale are provided over a wide variety of line pressures. Typical applications include flow measurement, depth sensing, pressure equalization, and liquid level.

Dimensions

Model Z (Order Code AD111)

Model A-5 (Order Code AD112)

Available Ranges
0.5; 1; 2; 5; 10; 15; 25

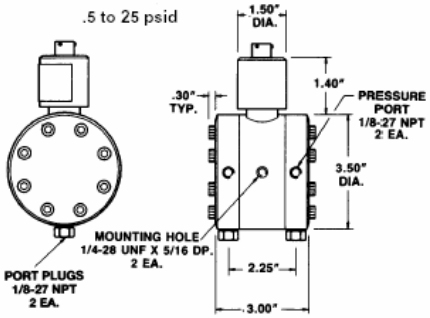

Model Z, or Model A-5

Options (See Appendix)

Temperature compensated 1a; Internal amps 2b, 2c, 2n, 2j; Amp enhancement 3d; Electrical termination 6e, 6f, 6g; Int. shunt cal 8a; Line pressure 25a, 25b; Signature calibration 53e.

Premium Options: 1c, 1d (-10° F to 130° F); 2q; 3a, 3c; 5c; 6b, 6c, 6i, 6j; 25c (≥5 psid); 26a, 26c

Accessories: Mating connectors and connector/cable assemblies; Pressure port adapters

1-800-848-6564 SENSOTEC www.sensotec.com

Single-Channel Signal Conditioner/Indicators

Models GM, GM-A and HM

LARGE 0.56" READOUT

20000 COUNT RESOLUTION

4 1/2 DIGIT LED DISPLAY

SHORT CIRCUIT PROTECTED

Shown with accessory AA924 bench mount bracket

Model GM-A (Order Code AE216)

The GM-A is a low cost digital readout that works with amplified (0-5V or 4-20ma) transducers or transmitters. This unit supplies power to the sensors. For use with two wire current transducers, contact factory. (Separate power supply required for 3-wire use.)

Model GM (Order Code AE213)

The GM is a versatile full function signal conditioner, amplifier and power supply that works with unamplified mv/v transducers. It also provides shunt calibration (R-cal) which enables the system to be set up without using an expensive primary stimulus (done at no extra charge at the factory if the readout and transducer are purchased at the same time). A full range of options like peak/hold, track/hold and dual limits are available.

Model HM (Order Code AE218)

The HM offers all of the standard features of the GM plus a microprocessor based factory programming capability. Linearization can improve the accuracy of a particular transducer. The HM also allows for special application programming which may be required for certain applications. (i.e. can make an accelerometer read out in degrees in order to use it as an inclinometer.) The HM features auto zero, RS-232, and tare capability.

ELECTRICAL	# Characters Displayed	4 1/2
	Power Requirements Standard	115 VAC
	Optional	12 VDC, 220 VAC
	Conversions per Second	3
	Scaling Method	Potentiometer
	Polarity Indication	Yes
	Decimal Point Selection	Jumper (non-solder)
	Display Size	0.56"
	Overrange Indication	Flashing Display
	Resolution	1/20000
	Digital Display	LED
ENVIRONMENTAL	Temperature, Storage	-20°F to 200°F
	Temperature, Operating	32°F to 130°F
PHYSICAL	Weight	2 1/4 lbs.
	Mounting*	Bench, Rack or Panel
	Case Size, Standard	1/8 DIN
	Case Material	Noryl plastic

* Panel mount included with unit.

	INPUT ACCEPTED					EXCITATION PROVIDED		
	.5 mV/V to 5 mV/V	5 mV/V to 50 mV/V	0-2V	0-5V	4-20mA	5V (±2.5V)	10V (±5V)	±15V
GM-A	NA	NA	x	•	x	NA	NA	•
GM	•	x	x	x	o	•	•	NA
HM	•	x	x	x	o	•	•	NA

• = Standard
x = Standard variable, customer's choice
o = Optional
NA = Not Available

SENSOTEC 1-800-848-6564 www.sensotec.com

PT1A

- Short to Medium Range
- Compact Size • OEM Applications
- Precision Potentiometric Output

CE

Specification Summary:

GENERAL

Full Stroke Ranges ..... 0-2 to 0-50 inches, see ① next page
Output Signal ..... voltage divider (potentiometer)
Accuracy ..... ± 0.25 to 0.10% full stroke, see ②
Repeatability ..... ± 0.02% full stroke
Resolution ..... essentially infinite
Measuring Cable ..... 0.019-in. dia. nylon-coated stainless steel
Enclosure Material ..... ABS plastic and black anodized aluminum
Sensor ..... plastic-hybrid precision potentiometer
Weight ..... 1 lb., max.

ELECTRICAL

Input Resistance ..... 500, 1K, 5K, 10K ohms (± 10%) or adj. bridge, see ④
Power Rating, Watts ..... 2.0 at 70°F (derated to 0 @ 250°F)
Recommended Maximum Input Voltage ..... 30 V(AC or DC)
Output Signal Change Over Measurement Range ..... 94% ±4% of input voltage

ENVIRONMENTAL

Enclosure Design ..... NEMA 4, IP67
Operating Temperature ..... -40° to 200°F
Vibration ..... up to 10 G's to 2000 Hz maximum

The PT1A is perfect where space and money are limited. The PT1A is part of Celesco's compact line of cable-extension transducers. Using a high cycle plastic-hybrid potentiometer, the PT1A provides a precision *voltage divider* position feedback signal for full-scale measurement ranges from 2 to 50 inches.

The PT1A has many features to offer: 500 to 10K ohm potentiometer selection, adjustable bridge circuit, up to 4 different measuring cable exits and 2 types of electrical connections.

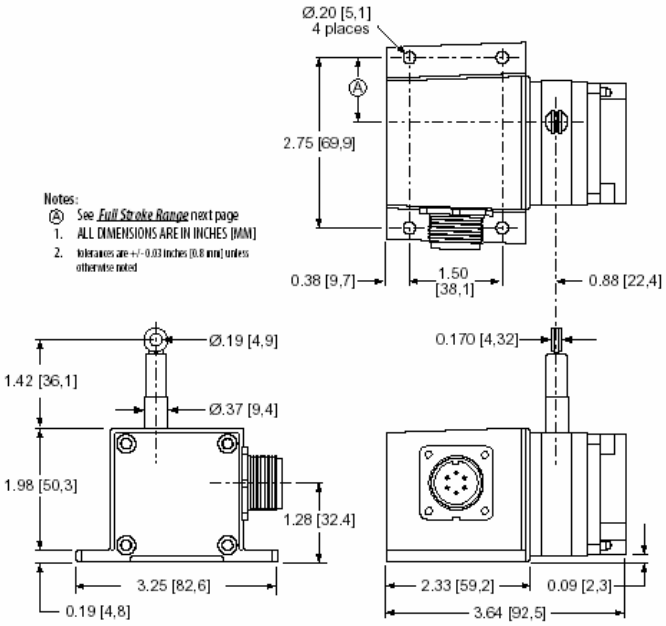

Electrical Output Signal:

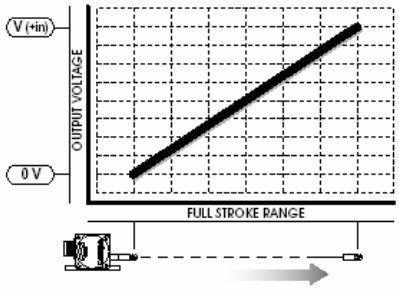

celesco
Celesco Transducer Products, Inc.
20630 Plummer Street • Chatsworth, CA • 91311
tel: (800) 423-5483 • (818) 701-2750 • fax: (818) 701-2799
www.celesco.com • info@celesco.com

General-Purpose Air Velocity Transducers

NEW

Models with Remote Electronics add "-R" Suffix

MADE IN USA · 1 YEAR WARRANTY · CE

FMA-900 Series
$822
Basic Unit

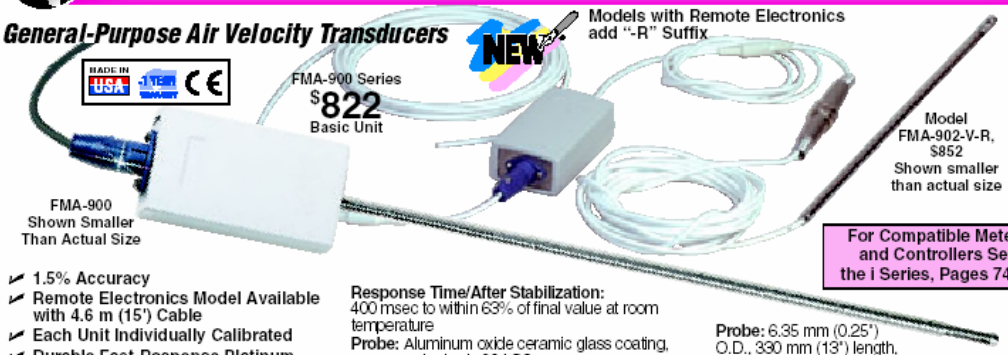

FMA-900
Shown Smaller
Than Actual Size

Model
FMA-902-V-R,
$852
Shown smaller
than actual size

For Compatible Meters and Controllers See the i Series, Pages 74-75

- 1.5% Accuracy
- Remote Electronics Model Available with 4.6 m (15') Cable
- Each Unit Individually Calibrated
- Durable Fast-Response Platinum Sensors
- Compact Solid-State Electronics
- Directly Monitors True Air Mass Velocity
- Linear 0-5 Vdc or 4-20 mA Output
- 400 msec Response Time
- Economical Insertion Design

The unique FMA-900 air velocity transducer utilizes both a velocity sensor and a temperature sensor to accurately measure air velocity (in SFPM, standard feet per minute). The built-in temperature sensor automatically corrects the flowrate for temperature variations. Both sensors are rugged glass-coated platinum resistance detectors (RTDs). The circuit heats the velocity sensor to a constant temperature differential above ambient temperature and measures the cooling effect of the air flow. This design provides excellent low velocity sensitivity and high accuracy. The FMA-900 also features negligible pressure drop.

To obtain mass flowrate in SCFM (standard cubic feet/minute), the SFPM velocity indicated by the FMA-900 is multiplied by the cross-sectional area of the pipe or duct in square feet. A traverse across the pipe or duct can be performed to determine the mounting location for average velocity indication. The FMA-900 can be mounted in pipes (down to 25 mm [1"] size) with the use of OMEGA® SSLK compression fittings (**SSLK-14-14, $8.50 ea**). Teflon® ferrules are required. (model **T-FER-1/4, $40/10 pack**).

Each unit is individually calibrated in OMEGA's NIST-traceable wind tunnel.

Suggested power supply; **FPW-15, $75 ea.**

Specifications

Accuracy: 1.5% FS @ room temp. Add ±0.5% of reading from 0 to 50°C (32° to 122°F); add 1% FS below 1000 SFPM
Repeatability: ±0.2% FS
Initial Stabilization Time in Flow: 40 sec
Response Time/After Stabilization: 400 msec to within 63% of final value at room temperature
Probe: Aluminum oxide ceramic glass coating, epoxy; probe body 304 SS
Probe Temperature: -40 to 121°C (-40 to 250°F)
Probe Pressure: 150 psig max.
Electronics Temperature: 0 to 50°C (32 to 122°F), operating; 0 to 70°C (32 to 158°F), storage
Operating Relative Humidity: less than 80% RH, without condensation
Ambient Temp Compensation: about 5 min for 11°C (20°F) temp change
Outputs: 0 to 5 Vdc or 4 to 20 mA
Voltage Load Resistance: 250 ohms minimum
Current Loop Resistance: 0 ohms min. to 400 ohms max.; 4 wire
Power: 15 to 24 Vdc, 300 mA (0 to 100 and 0 to 200 SFPM only); 15 to 18 Vdc, 300 mA (all other ranges)
Accessories: Mating connector pre-wired to 15' shielded cable (with built-in ferrite core) included
Dimensions:
Case: 89 H x 51 W x 31.8 mm D (3.5 H x 2 W x 1.25" D)
Probe: 6.35 mm (0.25") O.D., 330 mm (13") length, optional 95.25 mm O.D. (3.75") available
Weight: 160 g (5.6 oz)

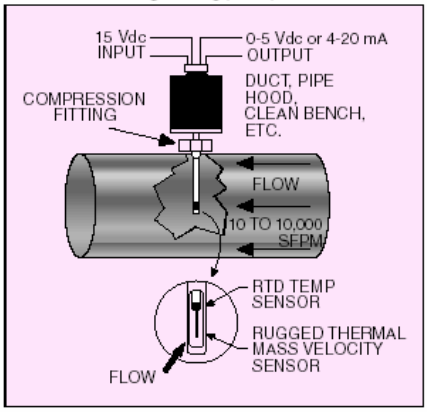

Replacement mating connector, Model No. FMA-3CON, $25.

IN STOCK FOR FAST DELIVERY!

To Order *(Specify Model Number)*

Model No. 0-5 V Output	Price	Model No. 4-20 mA Output	Price	Range
FMA-900-V	$822	FMA-900-I	$882	0-100 SFPM
FMA-901-V	822	FMA-901-I	882	0-200 SFPM
FMA-902-V	822	FMA-902-I	882	0-500 SFPM
FMA-903-V	822	FMA-903-I	882	0-1000 SFPM
FMA-904-V	822	FMA-904-I	882	0-2000 SFPM
FMA-905-V	822	FMA-905-I	882	0-5000 SFPM
FMA-906-V	822	FMA-906-I	882	0-10,000 SFPM

Comes with 4 point certificate of compliance, mating connector pre-wired to 4.7 m (15') shielded cable and complete operator's manual. To order with 95 mm (3.75") probe instead of standard 330 mm (13") probe, add suffix "-S" to model number and add $30 to price.
To order models with remote electronics add suffix "-R" to model number and $30 to price.
Ordering Example: FMA-904-I, probe with 4-20 mA output, 0-2000 SFPM range, $882.

For the complete selection of Flow & Level Instrumentation products, shop online at
omegaFlow.info

Specifications 2635

CHARGE INPUT:
Via 10-32 NF and BNC coaxial socket
Max. Input: ~10^5 pC
SENSITIVITY CONDITIONING:
3 digit dial-in of transducer sensitivity from 0.1 to 10.99 pC/ms^{-2}
AMPLIFIER SENSITIVITY:
0.01 mV to 10 V/pC corresponding to −40 to +80 dB with transducer capacitance of 1 nF
CALIBRATED OUTPUT RATINGS:
Selectable in 10 dB steps
Acceleration: 0.1 mV to 1 V/ms^{-2}
Velocity: 10 mV to 100 V/ms^{-1}
Displacement: 0.1 mV to 10 V/mm
SIGNAL OUTPUT:
Via 10-32 NF and BNC coaxial socket
Max. Output: 8 V (8 mA) peak
Output Impedance: <1 Ω
DC Offset: <±50 mV
FREQUENCY RANGE:
Acceleration*: Switchable 0.2 or 2 Hz to 100 kHz
Velocity: Switchable 1 or 10 Hz to 10 kHz
Displacement: Switchable 1 or 10 Hz to 1 kHz
−10% limits quoted — see Fig. 3
LOW-PASS FILTER:
Switchable −10% limits of 100 Hz, 1 kHz, 3 kHz, 10 kHz, 30 kHz and >100 kHz with attenuation slope of 40 dB/decade
INHERENT NOISE (2 Hz to 22 kHz):
5×10^{-3} pC referred to input with maximum sensitivity and 1 nF transducer capacitance
TEST OSCILLATOR:
159 Hz (ω = 1000 rad/s) sinusoid, factory preset for test level of 1 V
OVERLOAD INDICATOR:
Overload LED lights when input or output of amplifier is overloaded by signals of too high a peak level
RISE TIME: ~2.5 V/µs

Power Supply

Int. Battery: Three 1.5 V alkaline cells, IEC Type LR20, provide approximately 100 hours use
Ext. Source: +6 to +28 V (55 mA) single or ±14 V (14 mA) dual polarity DC

Environmental Conditions

Humidity: 0 to 90% RH (non-condensing). For use in high humidities a 3 W heater may be fitted on special order

* The acceleration mode 0.2 and 2 Hz -10% limits correspond to 0.1 and 1 Hz -3 dB limits

Dimensions and Weight

Height: 132.6 mm (5.2")
Width: 69.5 mm (2.7")
Depth: 200 mm (7.9")
Weight: 1.45 kg (3.2 lb) including batteries

Note: All values are typical at 25°C (77°F), unless measurement uncertainty is specified. All uncertainty values are specified at 2σ (i.e. expanded uncertainty using a coverage factor of 2)

COMPLIANCE WITH STANDARDS:

CE	CE-mark indicates compliance with: EMC Directive.
Safety	IEC 348: Safety Requirements for Electronic Measuring Apparatus.
EMC Emission	EN 50081–1: Generic emission standard. Part 1: Residential, commercial and light industry. EN 50081–2: Generic emission standard. Part 2: Industrial environment. CISPR 22: Radio disturbance characteristics of information technology equipment. Class B Limits. FCC Class B limits.
EMC Immunity	EN 50082–1: Generic immunity standard. Part 1: Residential, commercial and light industry. EN 50082–2: Generic immunity standard. Part 2: Industrial environment. Note 1: The above is guaranteed using accessories listed in this Product Data sheet only. Note 2: See "EMC Conditions".
Temperature	IEC 68–2–1 & IEC 68–2–2: Environmental Testing. Cold and Dry Heat. Operating Temperature: −10 to +55°C (+14 to +131°F) IEC 68–2–14: Change of Temperature: −10 to +55°C (+14 to +131°F) (3°C/min).
Humidity	IEC 68–2–3: Damp heat: 90% RH (non-condensing at 40°C (104°F))
Mechanical	Non-operating: IEC 68–2–6: Vibration: 0.3 mm, 20 m/s^2, 10–500 Hz
Enclosure	IEC 529: Protection provided by enclosures: IP20

EMC Conditions

Susceptibility to disturbances specified in EN 50082–2.
All measurements made at 25°C (77°F) with max. gain, Acceleration: 0.2 Hz, Upper Freq. Limit: 100 kHz and 1 nF termination

RADIATED RF: 3 to 10 V/m 1 kHz 80% AM
Overload can occur. This is indicated by the overload LED on the front panel.
CONDUCTED RF (referred to input): 3 to 10 V 1 kHz 80% AM. Max. 316 fC

Ordering Information

Type 2635 Charge Amplifier
Includes the following accessories:
3×QB 0004: 1.5 V alkaline cell, IEC Type LR20 ("D" size)
JP 0703: 7-pin DIN plug
2×SC 0418: Overlay
YM 0420: Cover for microdot input socket
DT 0074: Cover for BNC input socket

Optional Accessories

QB 0008: Rechargeable NiCd Cells, IEC Type R20 ("D" size)
ZG 0283: Battery Charger

Brüel & Kjær reserves the right to change specifications and accessories without notice

Brüel & Kjær

HEADQUARTERS: DK-2850 Nærum · Denmark · Telephone: +4545800500 · Fax: +4545801405 · http://www.bksv.com · e-mail: info@bksv.com
Australia (02)9450-2066 · Austria 0043-1-8657400 · Brazil (011)5182-8166 · Canada (514)695-8225 · China (86) 1068029906
Czech Republic 02-67021100 · Finland (0)9-755 950 · France (01)69907100 · Germany 06103/733 5-0 · Hong Kong 25487486 · Hungary (1)2158305
Ireland (01)803 7600 · Italy 02 57 68061 · Japan 03-3779-8671 · Republic of Korea (02)3473-0605 · Netherlands (31) 318 559290 · Norway 66771 155
Poland (22)8589392 · Portugal (1)4711453 · Singapore (65) 377-4512 · Slovak Republic 42125443 0701 · Spain (91)6590820 · Sweden (08)4498600
Switzerland (01) 880 70 35 · Taiwan (02)7139303 · United Kingdom (0)1438 739 000 · USA 800 332 2040
Local representatives and service organisations worldwide

BP 0099–15

WaveBook™ Series

Specifications & Ordering Information

General Specifications

Warm-up: 30 minutes to rated specifications
Environment
  Operating: 0° to 50°C, 0° to 95% RH, non-condensing
  Storage: -20° to 70°C
Power Consumption
  /516E: 1.8A max @ 15 VDC
  /516A & /512A: 1.4A max @ 15 VDC
Input Power Range: 10 to 30 VDC
Vibration: MIL STD 810E
PC Communication
  /516E: 10/100baseT Ethernet
  /512A and /516A: Enhanced Parallel Port (EPP)
Channel Capacity
  /516A & /512A: 8 built-in voltage channels, expandable up to 72 channels using WBK options.
  /516E: 8 built-in voltage channels, expandable to 72 channels with WBK options. Also can accommodate up to 3 additional WaveBook/516A, /512A, or WBK40 series options (any combination). Each /516A or /512A can be expanded up to 72 channels. Maximum WBK41 capacity is 224 TC input channels, 4 analog output channels, 272 digital I/O channels, and 6 counter/timer channels (see WBK40 on p. 63 for details).
Dimensions
  /516E: 285 mm W x 220 mm D x 70 mm H (11" x 8.5" x 2.70")
  /516A & /512A: 285 mm W x 220 mm D x 45 mm H (11" x 8.5" x 1.75")
Weight
  /516E: 1.9 kg (4.2 lbs)
  /516A & /512A: 1.5 kg (3.3 lbs)

Analog Inputs (18° to 28°C)

Channels: 8 differential, expandable up to 72 differential
Connector: BNC
Resolution
  /516A & /516E: 16 bit
  /512A: 12 bit
Ranges: Unipolar/bipolar operation is software selectable via sequencer
  Unipolar*: 0 to +10V, 0 to +4V, 0 to +2V
  Bipolar: ±10, ±5V, ±2V, ±1V
Maximum Overvoltage: ±35 VDC
Input Bandwidth: DC to 500 kHz
Input Impedance
  Single-Ended: 5M Ohm in parallel with 30 pF
  Differential: 10M Ohm in parallel with 30 pF
Accuracy
  /516A & /516E:
    ±2 to ±10V: ±0.012% of reading; 0.006% of range
    ±1V: ±0.018% of reading; 0.008% of range
  /512A: ±0.03% of reading; 0.006% of range
Input Noise
  /516A & /516E: <2 LSB (RMS)
  /512A: <1 LSB (RMS)
Total Harmonic Distortion: -84 dB typ
Signal to Noise and Distortion: -74 dB typ
CMRR: 80 dB typ; 70 dB min; DC to 20 kHz

Anti-Alias Filter*

Type: 5-pole Butterworth; 20 kHz low pass software enabled

* No unipolar mode or anti-alias filter with WBK11A, WBK12A, or WBK13A installed

Triggering

Channel 1 Analog & Pulse Trigger
  Input Signal Range: -10 to +10V
  Bandwidth: 1 MHz
  Latency: 300 ns
Multi-Channel Analog Trigger (up to 72 channels):
  Range: Selectable per channel to input range
  Latency: 2 µs/channel, plus 4 µs maximum
TTL Trigger
  Input Signal Range: 0 to 5V
  Input Characteristics: TTL-compatible with 10K Ohm pull-up resistor
  Latency: 300 ns
Software Trigger
  Latency: 100 µs typical
Pulse Trigger Input
  Input Signal Range: ±5V
  Input Characteristics: 75 Ohm
  Input Protection: ±10V maximum
  Minimum Pulse Width: 100 ns
  Maximum Pulse Width: 0.8 sec
  Latency: 300 ns

External Clock

Connector: Available on DB25 digital input
Input Signal Range: 5V TTL compatible
Input Characteristics: 50K Ohms pull up (to +5V) in parallel with 50 pF
Input Protection: Zener clamped -0.7 to +5V
Delay: 200 ns
Signal Slew Rate Requirement: 20V/µs minimum
Rate: Up to 1 MHz
Divisor Ratio: Divide by 1 through 255, selectable
Clock Counter Accuracy: <0.02% error
Clock Counter Range: 0.01 Hz to 100 kHz

Sequencer

Operation: Programmable for channel, gain, and for unipolar/bipolar range in random order
Depth: 128 location
Channel-to-Channel Rate: 1 µs to 1.1 µs/channel, all channels equal
Maximum Repeat Rate: 1 MHz
Minimum Repeat Rate: 100 seconds per scan
Expansion Channel Sample Rate: Same as on-board channels, 1 to 1.1 µs, fixed

High-Speed Digital Inputs/General-Purpose Outputs

Connector: DB25 Female
Configuration: 16 TTL-compatible pins, selectable for input or output
Input Characteristics: TTL-compatible
Output Characteristics: ALS TTL output in series with 33 Ohms
Output Updates: Outputs may be changed via program control
Input/Output Protection: Diode clamped to ground and +5V

Ordering Information

Description	Part No.
16-bit Ethernet, 1-MHz portable data acquisition system includes WaveView, WaveCal, eZ-PostView; LabVIEW & Windows® drivers; and AC adapter	WaveBook/516E
16-bit parallel, 1-MHz portable data acquisition system includes WaveView, WaveCal, eZ-PostView; LabVIEW & Windows® drivers; and AC adapter	WaveBook/516A
12-bit parallel, 1-MHz portable data acquisition system includes WaveView, WaveCal, eZ-PostView; LabVIEW & Windows® drivers; and AC adapter	WaveBook/512A

Accessories

Fastener-panel kit for WBK series (see p. 146)	262-0801
Fastener-panel handle (see p. 146)	HA-111
Optional hardcopy manual set (2); includes program mer's manual, and WBK option cards & modules user's manual	489-0900

Cables

Ethernet patch cable, 1.5 ft.	CA-242
Ethernet patch cable, 7 ft.	CA-242-7
DB25 male to DB25 female parallel cable, 2 ft.	CA-35-2
SYNC cable, 1 ft.	CA-74-1
SYNC cable, 5 ft.	CA-74-5
5-pin male DIN to 5-pin male DIN	CA-115
5-pin DIN to automobile cigarette lighter power cable, 8 ft.	CA-116
DB25 to external clock BNC	CA-178
CE Compliant Cables	
1 male BNC to male BNC	CA-150-1
8 male BNC to male BNC	CA-150-8

Software

Icon-based data acquisition, graphics, control, and analysis software with WaveBook driver	DASYLab
Real-time vibration analysis and recording software for the ZonicBook and WaveBook	eZ-Analyst
ActiveX/COM-based applications program interface	DaqCOM
DaqCOM with network support	DaqCOM/NET
Data acquisition grid control for Visual Basic	DaqCOM/OCX
Post-acquisition time-domain analysis software for data acquired from the WaveBook	eZ-TimeView
Post-acquisition frequency-domain analysis software for data acquired from the WaveBook	eZ-FrequencyView
Reciprocating equipment post-acquisition analysis software for the ZonicBook	eZ-Rotate

Related Products

Hardware	
WBK Options	p. 42
DBK30A	p. 174
DBK34A	p. 176
DBK70	p. 192
Software	
WaveView	p. 32
eZ-Analyst	p. 74
eZ-Rotate	p. 77
DaqCOM	p. 221
DASYLab	p. 224
eZ-TimeView	p. 229
eZ-FrequencyView	p. 230

Uncertainty in the Pressure Drop Coefficient - C_p

The pressure drop coefficient is used to evaluate the hydraulics of intakes, in particular loss characteristics. This coefficient is defined in the Corps of Engineers Hydraulic Design Criteria by:

$$C_p = \frac{\Delta H}{\left(\frac{\overline{V}^2}{2g}\right)} \qquad (1)$$

where ΔH is the difference between the reservoir elevation and the pressure head at the point in question, and $\overline{V}$ is the mean velocity in the conduit downstream from the inlet. The ΔH term is determined by differencing two pressure measurements made with a pressure transducer. The velocity is calculated based on the measured discharge to the model and the measured area of the conduit. We will begin by estimating the uncertainty in each measured quantity.

Mean Velocity $\overline{V}$:

Q_m is the discharge measured by the laboratory system of calibrated venturi meters. The differential pressure across the venturi is measured with a mercury manometer and scale (accuracy 0.001 ft). Calibration of the venturi meters is carried out periodically using a weight tank apparatus. This system measures the mass of water over a measured time period and fits the coefficients in a regression equation based on measured mercury differentials. The details of the calibration as well as supporting data are kept in Reclamation's hydraulic laboratory files, F-198. Based on the most recent calibrations, the uncertainty in the discharge value for the venturi meters in question is always within 0.25-percent.

The area was determined by measurement of the height and width of the conduit using inside calipers and a scale with graduations of 0.01 ft yielding an accuracy of ±0.005 ft. The section was measured upon delivery. The width was W=6.685 in and the height, h=9.880 in.

The equation for the velocity is then given by:

$$\overline{V} = \frac{Q_m}{Wh} \qquad (2)$$

The uncertainty in the mean velocity is then given by the partial differential equation:

$$\delta_{\overline{V}} = \delta_{Q_m} \frac{\partial \overline{V}}{\partial Q_m} + \delta_h \frac{\partial \overline{V}}{\partial h} + \delta_W \frac{\partial \overline{V}}{\partial W} \qquad (3)$$

We can convert the partial differential equation into an approximation by replacing the δ's with the uncertainties in each measured value, w. The best estimate of uncertainty can now be

generated by using the uncertainty in each of the measured values.

$$w_{\overline{V}} = \sqrt{\left\{\left(w_{Q_m}\frac{\partial \overline{V}}{\partial Q_m}\right)^2 + \left(w_h\frac{\partial \overline{V}}{\partial h}\right)^2 + \left(w_W\frac{\partial \overline{V}}{\partial W}\right)^2\right\}} \qquad (4)$$

First for a sample point, compute $\overline{V}$:

$$\overline{V} = \frac{4.896}{0.549 * 0.823} = 10.836\ ft/s$$

$$\frac{\partial \overline{V}}{\partial Q_m} = \frac{1}{hW}\ , \qquad \left(w_{Q_m}\frac{\partial \overline{V}}{\partial Q_m}\right) = \left(0.0122\left|\frac{1}{6.585/12 * 9.880/12}\right|\right) = 0.0270$$

$$\frac{\partial \overline{V}}{\partial h} = \frac{-Q_m}{h^2 W}\ , \qquad \left(w_h\frac{\partial \overline{V}}{\partial h}\right) = \left(0.005\left|\frac{-4.896}{0.549 * 0.823^2}\right|\right) = 0.0658$$

$$\frac{\partial \overline{V}}{\partial W} = \frac{-Q_m}{W^2 h}\ , \qquad \left(w_W\frac{\partial \overline{V}}{\partial W}\right) = \left(0.005\left|\frac{-4.896}{0.823 * 0.549^2}\right|\right) = 0.0987$$

So substituting into equation 4:

$$w_{\overline{V}} = 0.1217$$

The uncertainty in the model measurement can then be written as V_m=10.836± 0.122 ft/s or converting into prototype units: V_p= 44.7 ± 0.50 ft/s. We can now estimate the uncertainty in the velocity head generated by this velocity for use in calculation of the pressure drop coefficient, $H_v=V^2/2g$.

$$\delta_{H_v} = \delta_{\overline{V}}\frac{\partial H_v}{\partial \overline{V}}\ . \qquad (5)$$

The best estimate for the uncertainty in H_v is given in Equation 6.

$$w_{H_v} = \sqrt{\left(w_{\overline{V}}\frac{\partial H_v}{\partial \overline{V}}\right)^2} \qquad (6)$$

So first compute the value of H_v=1.823 ft. Then making the appropriate substitutions,

$$\frac{\partial H_v}{\partial \overline{V}} = \frac{2\overline{V}}{2g}, \qquad \left(w_{\overline{V}}\frac{\partial H_v}{\partial \overline{V}}\right) = \left(0.122\left|\frac{10.836}{32.2}\right|\right) = 0.041$$

Substituting into Equation 6 gives:

$$w_{H_v} = 0.041 ft$$

The uncertainty in the velocity head in the model can then be written as H_{vm}= 1.823 ± 0.041 ft, or converting into prototype units: H_{vp}= 31.0 ± 0.7 ft. We can now look at the pressure drop coefficient C_p,

$$C_p = \frac{\left(H_{res} - H_{tap}\right)}{H_v} \qquad (7)$$

Using the same methodology, the uncertainty in the pressure drop coefficient can be written as:

$$\delta_{C_p} = \delta_{H_{res}} \frac{\partial C_p}{\partial H_{res}} + \delta_{H_{tap}} \frac{\partial C_p}{\partial H_{tap}} + \delta_{H_v} \frac{\partial C_p}{\partial H_v} \qquad (8).$$

The best estimate of the uncertainty in C_p then becomes:

$$w_{C_p} = \sqrt{\left\{\left(w_{H_{res}} \frac{\partial C_p}{\partial H_{res}}\right)^2 + \left(w_{H_{tap}} \frac{\partial C_p}{\partial H_{tap}}\right)^2 + \left(w_{H_v} \frac{\partial C_p}{\partial H_v}\right)^2\right\}} \qquad (9).$$

Computing a value for C_p=1.042, and using the standard error from the transducer calibration of 0.007, we can make the appropriate substitutions:

$$\frac{\partial C_p}{\partial H_{res}} = \frac{1}{H_v}, \qquad \left(w_{H_{res}} \frac{\partial C_p}{\partial H_{res}}\right) = \left(0.007\left|\frac{1}{1.823}\right|\right) = 0.0038$$

$$\frac{\partial C_p}{\partial H_{tap}} = -\frac{1}{H_v}, \qquad \left(w_{H_{tap}} \frac{\partial C_p}{\partial H_{tap}}\right) = \left(-0.007\left|\frac{1}{1.823}\right|\right) = -0.0038$$

$$\frac{\partial C_p}{\partial H_v} = \frac{-(H_{res} - H_{tap})}{H_v{}^2}, \qquad \left(w_{H_v} \frac{\partial C_p}{\partial H_v}\right) = \left(0.041\left|\frac{-(8.33 - 6.43)}{1.823^2}\right|\right) = 0.0234$$

$$w_{C_p} = 0.024.$$

Since this coefficient is a dimensionless parameter, both model and prototype values are the same, and can be written in the form, C_p= 1.04 ± 0.02.

The uncertainty values for C_p are not constant for a given C_p, but vary with the actual values of velocity and heads used to generate the coefficient. The lower discharge and head quantities yield slightly higher uncertainties in the final quantity than if you use the maximum flow and head conditions that are available. A low discharge was used in the above example so this uncertainty result is the maximum value for the data we collected.

The same quantity was measured in the 1:36 model, using fewer piezometer taps at the critical locations (maximum C_p). The measurement techniques were different, although standard water manometers were used. The pressure drop coefficient (Eq. 7) was determined by first indirectly measuring the velocity head. Due to the inability to separately measure each individual conduit

flow in this model, a different approach to determine the velocity head was used. A piezometer ring was installed on each conduit downstream from the intake in the constant area conduit section and upstream from the gate structure. The mean pressure at this location consists of the velocity head with any head losses up to this point, realizing that some pressure recovery will also take place. Due to the relatively low headloss design that is in place, we assumed that the pressure at the ring was all velocity head. Using this method to calculate velocity and computing a discharge from this value compared well with the total laboratory discharge measured by the venturi system. The individual velocities varied up to about ±3.5 percent but when summed, the total discharge was within 1 percent of the laboratory discharge for all the conditions tested.

Determining the uncertainty in the velocity head measurement is then:

$$H_v = \frac{V^2}{2g} = \left(H_{res} - H_{ring}\right)$$

$$\delta_{H_v} = \delta_{H_{res}} \frac{\partial H_v}{\partial H_{res}} + \delta_{H_{ring}} \frac{\partial H_v}{\partial H_{ring}} \qquad (10)$$

approximating equation 10 with the measurement uncertainties of each quantity,

$$w_{H_v} = \sqrt{\left(w_{H_{res}} \frac{\partial H_v}{\partial H_{res}}\right)^2 + \left(w_{H_{ring}} \frac{\partial H_v}{\partial H_{ring}}\right)^2} \qquad (11)$$

Substituting in some actual values, H_v= 417.3-223.8=193.5 ft. The manometer boards have gradations of 0.01 ft, so the readings are accurate to 0.005 ft (model), or 0.085 ft prototype. Substituting into equation 11, w_{Hv} = 0.1202 ft. This would give H_v = 193.5 ± 0.12 ft. The larger uncertainty however is whether the method of determining the actual velocity head by this manner is correct, we estimated the error to be ±3.5 percent to this value, resulting in H_v = 193.5 ± 6.8 ft. Now we can see how this error propagates into the pressure drop coefficient.

Following the same logic as equations 7-9, and substituting in the appropriate values, C_p=1.02:

$$\frac{\partial C_p}{\partial H_{res}} = \frac{1}{H_v}, \qquad \left(w_{H_{res}} \frac{\partial C_p}{\partial H_{res}}\right) = \left(0.085\left|\frac{1}{193.5}\right|\right) = 0.0004$$

$$\frac{\partial C_p}{\partial H_{tap}} = -\frac{1}{H_v}, \qquad \left(w_{H_{tap}} \frac{\partial C_p}{\partial H_{tap}}\right) = \left(-0.085\left|\frac{1}{193.5}\right|\right) = -0.0004$$

$$\frac{\partial C_p}{\partial H_v} = \frac{-(H_{res} - H_{tap})}{H_v{}^2}, \qquad \left(w_{H_v} \frac{\partial C_p}{\partial H_v}\right) = \left((6.8)\left|\frac{-(417.3 - 281.1)}{193.5^2}\right|\right) = 0.0247$$

$$w_{C_p} = 0.025.$$

Since this coefficient is a dimensionless parameter, both model and prototype values are the same, and can be written in the form, $C_p = 1.02 \pm 0.03$. The level of uncertainty is a couple of percent greater in the 1:36 model, largely due to the uncertainty level in the determination of the velocity and resulting velocity head. For the location computed in the above example, the pressure coefficient in the 1:17 model varies from 1.02 to 1.06 (1.04 ± 0.02), and in the 1:36 model it varies from 0.99 to 1.05 (1.02 ± 0.03).

APPENDIX C

Input File for Flow-3D

```
Folsom - normal upper 9x14 intake
 13080, for a velocity of 100.1 ft/s
 $xput
     trest=9.,twfin=2.,deltr=0.00000001,
     epsadj=1.,
     omega=1.3,
     con=0.45,
     lpr=1,itb=1,ifvis=4,
     gz=-32.14,ipdis=1,
     nmat=1,ifpk=1,
     iorder=3,ifenrg=0,ifrho=0,iqsr=1,
     pltdt=0.50,sprtdt=0.05,HPLTDT=0.1,
   iadix=1, iadiy=1, iadiz=1,iqsr=1,
   itrst=1, isolid=0,
 $end
 $limits
     irpr=1,jbkpr=1,ktpr=1,
     itmax=1000,
 $end
 $props
     rhof=1.937,mu1=2.25E-05,
   units='lbm',
 $end
 $scalar
 $end
 $bcdata
   wr=2,
   wl=5, wf=5, wbk=5, wb=2, wt=2,
   ipbctp(1)=0,ipbctp(3)=0,ipbctp(4)=0,
   flhtl=465., flhtf=465., flhtbk=465.,
 $end
 $mesh
   nxcelt=80,
     px(1)=24.,
     px(2)=52.125,
     px(3)=136.5,
     px(4)=149.,
   nycelt=48,
     py(1)=462.5,
     py(2)=537.5,
   nzcelt=168,
     pz(1)=210.,
     pz(2)=244.875,
     pz(3)=298.875,
     pz(4)=479.,
 $end
 $bcdata
   wl=9,   wr=9,   wf=9,   wbk=9,   wb=9,   wt=9,
   flhtl=465.,   flhtf=465.,   flhtbk=465.,
 $end
  $mesh
      nxcelt=136,
        px(1)=36.5,
```

```
      px(2)=142.75,
     nycelt=56,
      py(1)=478.125,
      py(2)=521.875,
     nzcelt=68,
      pz(1)=244.875,
      pz(2)=298.875,
$end



$obs
      avrck=2.,
      nobs=3,
        iob(1)=1,igen(1)=3,
        iob(2)=2,xl(2)=120.,zl(2)=290.,
        iob(3)=3,xl(3)=135.,zh(3)=280.,zl(3)=260.,QSROBS(1,3)=-25335.96,
$end
$fl
   presi=0.0,nfls=1,flht=465.,fzh(1)=465.,
$end
$bf
 nbafs=3,
 bzl(1)=400.,bx(1)=40.,
 bzl(2)=400.,by(2)=525.,
 bzl(3)=400.,by(3)=475.,
$end
$temp
$end
$grafic
    wintl(1)='Top probe 1',xloc(1)=109.5507, yloc(1)=500., zloc(1)=281.4288167,
    wintl(2)='Top probe 2',xloc(2)=110.9507, yloc(2)=500., zloc(2)=280.6936,
    wintl(3)='Top probe 3',xloc(3)=113.7507, yloc(3)=500., zloc(3)=279.8057417,
    wintl(4)='Top probe 4',xloc(4)=116.5507, yloc(4)=500., zloc(4)=279.3424417,
    wintl(5)='Top probe 5',xloc(5)=119.3507, yloc(5)=500., zloc(5)=279.0733417,
    wintl(6)='Top probe 6',xloc(6)=122.1507, yloc(6)=500., zloc(6)=278.925625,
    wintl(7)='Top probe 7',xloc(7)=124.9507, yloc(7)=500., zloc(7)=278.8751417,
    wintl(8)='Top probe 8',xloc(8)=130.5507, yloc(8)=500., zloc(8)=278.875,
    wintl(9)='Side probe 9',xloc(9)=113.666,     yloc(9)= 494.1204, zloc(9)=271.875,
    wintl(10)='Side probe 10',xloc(10)=116.2417, yloc(10)=495.32, zloc(10)=271.875,remark='minused 0.02 from
each top yloc',
    wintl(11)='Side probe 11',xloc(11)=118.6533, yloc(11)=495.3397, zloc(11)=271.875,
    wintl(12)='Side probe 12',xloc(12)=121.08,   yloc(12)=495.3614, zloc(12)=271.875,
    wintl(13)='Side probe 13',xloc(13)=123.512,  yloc(13)=495.3427, zloc(13)=271.875,
    wintl(14)='Side probe 14',xloc(14)=125.912,  yloc(14)=495.3429, zloc(14)=271.875,
    wintl(15)='Side probe 15',xloc(15)=129.5117, yloc(15)=495.3429, zloc(15)=271.875,
    wintl(16)='Side probe 16',xloc(16)=134.3114, yloc(16)=495.3429, zloc(16)=271.875,
    wintl(17)='Reservoir Ref at 82,487,246',xloc(17)=82., yloc(17)=487., zloc(17)=246.,
$end
$parts
$end
```

APPENDIX D

Supplemental Testing of End-of-conduit Dentates

Background

As a result of computer modeling performed by Erik Bollaert, there was some interest in seeing if there could be additional jet breakup and spreading by adding ramps or dentates to the ends of the conduit sections. Two configurations were tested. The first featured 46-inch-high ramp sections. The upper conduit had two ramps, basically 1/3 the width of the outlet located along the outside walls and the lower conduit had a single ramp 1/3 the width of the conduit, centered (figure D-1a&b)

Figure D-1a. Upper conduit end ramp/dentates (46-inch high)

Figure D-1b. Lower conduit ramp/dentate, 46-inch high.

These ramps were tested at reservoir elevation 418 ft, and 100-percent gate openings. Photographs and dynamic pressures were recorded for each conduit. These large ramp heights were very effective in spreading the jet laterally, especially for the upper outlet, figure D-2. The single ramp in the lower conduit was somewhat effective when considering the lower fall height to the tailwater, D-3.

Figure D-2. Spread of the upper conduit jet. Width at the tailwater interface is approximately 80 to 85 ft. Note appearance that conduit may be full or choked at the downstream end.

Figure D-3. Spread of jet from lower conduit. Width of jet at tailwater interface is about 35 to 40 ft.

The dynamic pressure extremes were reduced considerably over the recommended design with no outlet end dentates, however the size of the dentates is considerable and does greatly impact the flow in the conduits – especially the upper conduit. Air is essentially cut off from entering the downstream end of the conduit due to the large sectional profile of the end ramps. We therefore modified the height of the ramps, reducing them to 24-inch high in the upper conduit and removing them totally from the lower conduit. This improved flow conditions in the conduits themselves; however there was much less spreading of the jet (figures D-4 and D-5) and in return did not significantly reduce the pressure magnitudes (figures D-6).

a) close up of small ramps

b) Jet spread is now less than 50 ft.

Figure D4. Upper conduit, small end ramps (2 ft high).

Figure D5. Lower conduit, no exit ramps. Note very small lateral spread of the jet.

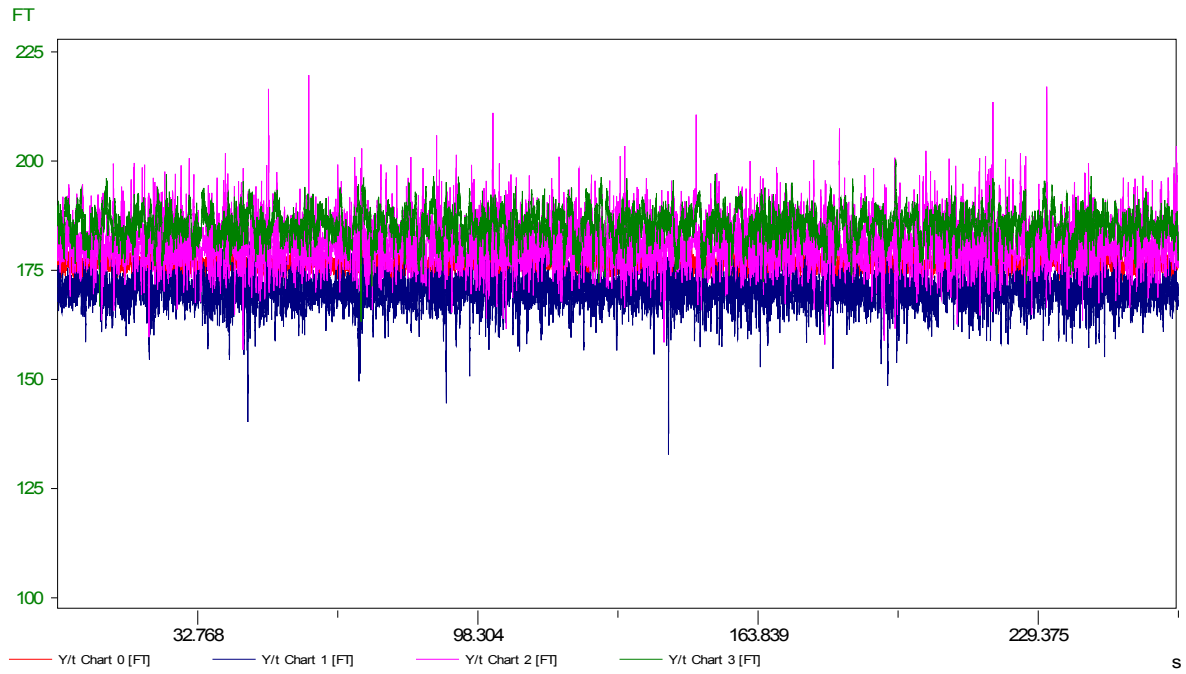

a) Upper outlet with small exit ramps, 100% open with reservoir at 418 ft, pressures shown are in ft of water elevation

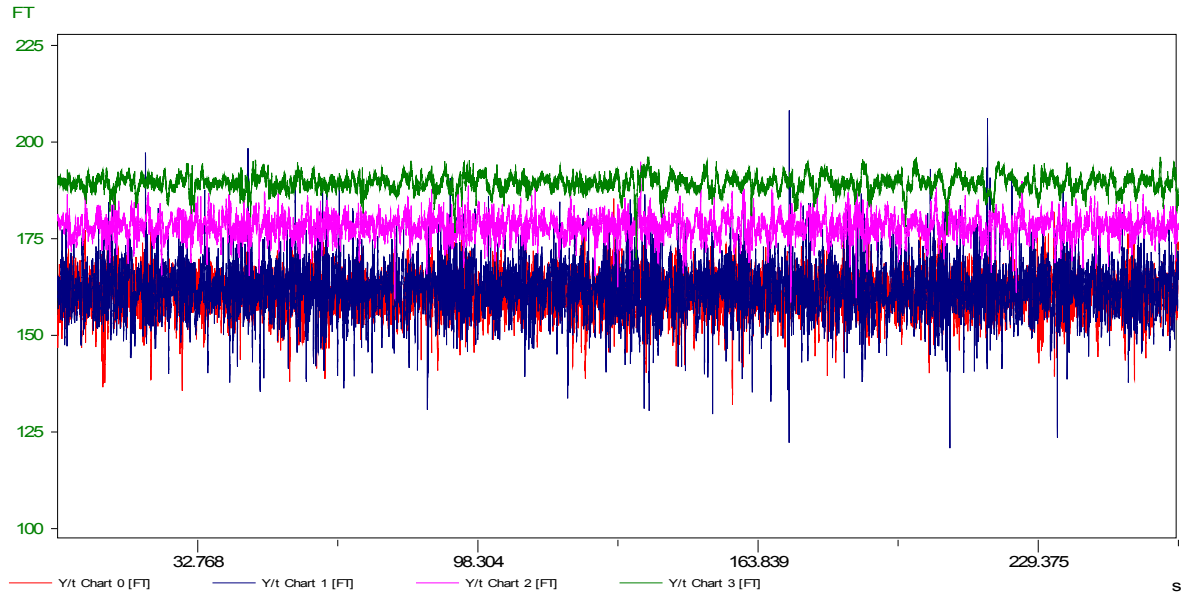

b) Lower outlet, no ramps, 100% open with reservoir at 418 ft, pressures shown are in ft of water elevation.

Figure D6. Chart 0, Chart 1, Chart 2, and Chart 3 are at stations 13+01, 13+51, 14+01, and 14+51 respectively. These are scaled prototype runs of just over 18 minutes. Tailwater set at 180 ft at the endsill.